Harshit Kumar Jayant

Harshit Kumar Jayant PhD Thesis.pdf

Delhi Technological University

Document Details

Submission ID
trn:oid:::27535:99818124

Submission Date
Jun 8, 2025, 9:54 AM GMT+5:30

Download Date
Jun 8, 2025, 10:04 AM GMT+5:30

File Name
Harshit Kumar Jayant PhD Thesis.pdf

File Size
7.6 MB

121 Pages

25,987 Words

140,037 Characters

6% Overall Similarity

The combined total of all matches, including overlapping sources, for each database.

Filtered from the Report

- Bibliography
- Small Matches (less than 10 words)

Exclusions

- 3 Excluded Sources
- 9 Excluded Matches

Match Groups

117 Not Cited or Quoted 5%
Matches with neither in-text citation nor quotation marks

12 Missing Quotations 1%
Matches that are still very similar to source material

0 Missing Citation 0%
Matches that have quotation marks, but no in-text citation

0 Cited and Quoted 0%
Matches with in-text citation present, but no quotation marks

Top Sources

2% Internet sources
3% Publications
4% Submitted works (Student Papers)

Integrity Flags

0 Integrity Flags for Review

No suspicious text manipulations found.

Our system's algorithms look deeply at a document for any inconsistencies that would set it apart from a normal submission. If we notice something strange, we flag it for you to review.

A Flag is not necessarily an indicator of a problem. However, we'd recommend you focus your attention there for further review.

Match Groups

- 117 Not Cited or Quoted 5%
  Matches with neither in-text citation nor quotation marks
- 12 Missing Quotations 1%
  Matches that are still very similar to source material
- 0 Missing Citation 0%
  Matches that have quotation marks, but no in-text citation
- 0 Cited and Quoted 0%
  Matches with in-text citation present, but no quotation marks

Top Sources

- 2% Internet sources
- 3% Publications
- 4% Submitted works (Student Papers)

Top Sources

The sources with the highest number of matches within the submission. Overlapping sources will not be displayed.

1	Publication	
Amir Ghaderi, Mehdi Dasineh, Francesco Aristodemo, Costanza Aricò. "Numerical...		<1%
2	Internet	
www.researchgate.net		<1%
3	Internet	
riunet.upv.es		<1%
4	Submitted works	
Institute of Aeronautical Engineering (IARE) on 2023-02-17		<1%
5	Internet	
doaj.org		<1%
6	Submitted works	
Middle East Technical University on 2024-05-31		<1%
7	Publication	
Saber Ebrahimiyan, Hooman Hajikandi, Mahmood Shafai Bejestan, Saeed Jamali, ...		<1%
8	Submitted works	
Universidad Politécnica de Cartagena on 2018-11-13		<1%
9	Publication	
Pagliara, Stefano, and Michele Palermo. "Hydraulic jumps on rough and smooth b...		<1%
10	Publication	
Rasoul Daneshfaraz, Reza Norouzi, Parisa Ebadzadeh, Silvia Di Francesco, John Pa...		<1%

11 Publication
Umut Türker, Manousos Valyrakis. "Hydraulic jump on rough beds: conceptual m... <1%

12 Submitted works
University of Strathclyde on 2018-04-16 <1%

13 Publication
Simsek, Çagdas. "Forced Hydraulic Jump on Artificially Roughened Beds.", Middle ... <1%

14 Internet
iwrj.sku.ac.ir <1%

15 Submitted works
The Hong Kong Polytechnic University on 2012-04-13 <1%

16 Submitted works
University of Newcastle upon Tyne on 2016-08-11 <1%

17 Internet
www.freepatentsonline.com <1%

18 Publication
Mohamed F. Sauida. "Simulation of relative energy loss downstream of multi-gat... <1%

19 Publication
Osama Saleh, Suzan Abdalla, Eman Elnikhely. "Effect of different screen areas on ... <1%

20 Submitted works
Aligarh Muslim University, Aligarh on 2024-03-09 <1%

21 Publication
Murzyn, F.. "Free-surface fluctuations in hydraulic jumps: Experimental observati... <1%

22 Submitted works
University of Surrey on 2016-11-22 <1%

23 Internet
open.metu.edu.tr <1%

24 Publication
"Computational Fluid Dynamics", Springer Science and Business Media LLC, 2009 <1%

25 Publication

Hamed Azimi, Saeid Shabanlou, Saeid Kardar. "Characteristics of Hydraulic Jump i... <1%

26 Submitted works

University of Technology on 2017-09-26 <1%

27 Internet

www.norsarinnovation.com <1%

28 Submitted works

Indian Institute of Technology Guwahati on 2025-01-06 <1%

29 Internet

ci.lib.ncsu.edu <1%

30 Publication

Anand Kumar Patel, Pankaj Mishra. "CFD Analysis of Geothermal Heat Exchanger ... <1%

31 Publication

Jun Li, Ibrahim Yavuz, Ismail B. Celik, Steven E. Guffey. "A Numerical Study of Wor... <1%

32 Submitted works

Liverpool John Moores University on 2023-03-28 <1%

33 Submitted works

National University of Singapore on 2016-01-14 <1%

34 Submitted works

Queensland University of Technology on 2023-10-26 <1%

35 Submitted works

University of Edinburgh on 2023-04-11 <1%

36 Submitted works

University of Leeds on 2022-04-27 <1%

37 Submitted works

University of New South Wales on 2017-05-19 <1%

38 Submitted works

Indian Institute of Technology, Madras on 2015-06-15 <1%

39 Publication
Mehdi Dasineh, Amir Ghaderi, Mohammad Bagherzadeh, Mohammad Ahmadi, Al... <1%

40 Submitted works
The Robert Gordon University on 2019-08-10 <1%

41 Submitted works
Universiti Sains Malaysia on 2012-02-20 <1%

42 Internet
rucore.libraries.rutgers.edu <1%

43 Internet
unsworks.unsw.edu.au <1%

44 Internet
www.vaia.com <1%

45 Submitted works
Aligarh Muslim University, Aligarh on 2024-08-12 <1%

46 Submitted works
Cranfield University on 2017-09-04 <1%

47 Publication
Hossam Mohamed Ali Ahmed, Mohamed El Gendy, Ahmed Mohamed Hassan Mir... <1%

48 Publication
Ming-Jyh Chern, Sam Syamsuri. "Effect of Corrugated Bed on Hydraulic Jump Char... <1%

49 Submitted works
NIT Imphal on 2021-01-29 <1%

50 Submitted works
University of British Columbia on 2005-03-17 <1%

51 Submitted works
University of Stellenbosch, South Africa on 2010-11-04 <1%

52 Internet
caballerojose.com <1%

53 Internet

www.hindawi.com <1%

54 Publication

Abbaspour, A.. "Effect of sinusoidal corrugated bed on hydraulic jump characteris... <1%

55 Publication

Abdel-Azim Negm. "Hydraulic jumps at positive and negative steps on sloping flo... <1%

56 Submitted works

Cranfield University on 2012-05-17 <1%

57 Submitted works

Cranfield University on 2024-03-24 <1%

58 Publication

M. A. R. Sharif, K. K. Mothe. "Evaluation of Turbulence Models in the Prediction of ... <1%

59 Publication

Mahdi N. Mahyari, Hasan Karimi, Hasan Naseh, Mehran Mirshams. "Numerical an... <1%

60 Publication

Nahid Pourabdollah, Manouchehr Heidarpour, Jahangir Abedi Koupai. "Character... <1%

61 Publication

Nallamuthu Rajaratnam. "The Hydraulic Jump as a Well Jet", Journal of the Hydra... <1%

62 Publication

Sanjay Singh Rathore, Suresh Kant Verma. "Numerical investigation on the effica... <1%

63 Submitted works

Universitat Politècnica de València on 2022-04-12 <1%

64 Submitted works

University Tun Hussein Onn Malaysia on 2013-06-24 <1%

65 Submitted works

University of Exeter on 2016-04-28 <1%

66 Submitted works

University of Leeds on 2016-11-28 <1%

67 Submitted works
University of Liverpool on 2023-05-14 <1%

68 Submitted works
University of Newcastle on 2010-08-19 <1%

69 Submitted works
University of Portsmouth on 2024-05-02 <1%

70 Submitted works
University of Rijeka on 2017-11-02 <1%

71 Submitted works
University of Strathclyde on 2018-03-26 <1%

72 Submitted works
University of Technology on 2016-09-04 <1%

73 Internet
dergipark.org.tr <1%

74 Internet
lib.buet.ac.bd:8080 <1%

75 Internet
patents.google.com <1%

76 Submitted works
Adnan Menderes Üniversitesi on 2019-07-12 <1%

77 Submitted works
Aligarh Muslim University, Aligarh on 2023-11-22 <1%

78 Submitted works
Auston Institute of Management and Technology on 2010-09-29 <1%

79 Publication
Diana De Padova, Michele Mossa. "Hydraulic Jump: A Brief History and Research C... <1%

80 Publication
Gilang Idfi, Umboro Lasminto, Anak Agung Gde Kartika. "Experimental Study of E... <1%

81 Submitted works
Institute of Technology, Nirma University on 2015-10-04 <1%

82 Publication
Juan Francisco Macián Pérez. "Numerical and physical modelling approaches to t... <1%

83 Publication
Mahmoud Debabeche, Sonia Cherhabil, Amin Hafnaoui, Bachir Achour. "Hydrauli... <1%

84 Publication
Mohsen NASRABADI, Mohammad Hossein OMID, Javad FARHOUDI. "Submerged ... <1%

85 Publication
Nasrin Hassanpour, Ali Hosseinzadeh Dalir, Davod Farsadizadeh, Carlo Gualtieri. "... <1%

86 Publication
Razavinia, Nasimalsadat. "Low Grade to High Grade Energy Conversion: An Appro... <1%

87 Publication
S. A. Ead, N. Rajaratnam. "Hydraulic Jumps on Corrugated Beds", Journal of Hydra... <1%

88 Publication
S. H. Chan. "Transport Phenomena In Combustion, Volume 1 - Proceedings of the ... <1%

89 Publication
Stefano Pagliara, Ilaria Lotti, Michele Palermo. "Hydraulic jump on rough bed of s... <1%

90 Submitted works
The University of Manchester on 2016-09-05 <1%

91 Submitted works
Tikrit University on 2025-02-05 <1%

92 Publication
Topics in Mining Metallurgy and Materials Engineering, 2015. <1%

93 Submitted works
University of Greenwich on 2023-03-03 <1%

94 Submitted works
University of Salford on 2020-05-21 <1%

95 Submitted works
University of Surrey on 2014-05-27 <1%

96 Submitted works
University of Surrey on 2022-05-09 <1%

97 Submitted works
University of Sydney on 2017-11-02 <1%

98 Internet
archive.org <1%

99 Internet
ir.lib.uwo.ca <1%

100 Internet
madison-proceedings.com <1%

101 Internet
mts.intechopen.com <1%

102 Internet
www.science.gov <1%

CHAPTER 1

INTRODUCTION

1.1 General

Hydraulic structures can experience failure for many reasons, and comprehending these factors is of utmost importance to ensure the efficient design and maintenance of such structures (Novak et al. 2017) [1]. The report of Federal Emergency Management Agency (FEMA) published in 2017 [2], listed several common causes for the failure of hydraulic structures. Among these causes, one notable factor is the development of piping and internal soil erosion in embankment dams. It should be noted that erosion and scour are of primary concern for hydraulic engineers when designing hydraulic structures. When water is released from the upstream of a hydraulic structure to the downstream, the potential head of water is converted into kinetic energy. This increase in kinetic energy can result in erosion of the downstream bed and potentially lead to piping underneath the hydraulic structure. Ultimately, this can cause the failure of the hydraulic structure. To address the abovementioned issues, hydraulic engineers apply a technique wherein they strategically design the stilling basins located downstream of the hydraulic structure. This is achieved through the implementation of energy dissipator structures.

Figure 1.1 depicts a stilling basin located downstream of the dam. This structure, built in Jhon Martin, United States, is positioned at the foundation of the spillway to effectively minimize the excess kinetic energy of flowing water by creating a hydraulic jump within the basin. The flow passing over the crest of the spillway undergoes a transition from supercritical to subcritical flow when it reaches the dam toe and meets the normal flow in the downstream side. This transition leads to the hydraulic jump. It is important that the design of the stilling basin promotes the occurrence of a hydraulic jump in its reach so as not to damage the channel located behind the basin. To accomplish this, it is crucial that the post jump depth obtained from the sequent depth relation precisely matches the tail water depth. A stilling basin is composed of a concrete apron and several additional structures, including an end sill, chute blocks, and baffle blocks. Peterka (1958) [3] laid the groundwork and offered valuable insights into the mechanics and principles behind hydraulic jumps in stilling basins. In addition, Bureau of Indian Standards Code 4997 (1968) [4] offers valuable guidance on the design of hydraulic jump stilling basins. These basins play a crucial role in safely dissipating the energy of flowing water, commonly located downstream of dams, weirs, and spillways. This standard applies to rectangular stilling basins and suggests conducting model testing for designs with falls exceeding 15 m or discharge intensities surpassing 30 m^3/s.

Hager in 1988 [5] emphasised knowledge regarding hydraulic jumps in sloping channels. Underlined their properties and behaviour as a key factor in the development of efficiency dissipation structures for hydraulic engineering applications. This understanding plays a significant role in the design of effective stilling basins, which are commonly used at the bottom of spillways. According to

Chow (1959) [6], it is commonly observed that stilling basins are not built in such a way that a free hydraulic jump is fully restrained by the length on a particular apron. This is primarily due to the high cost associated with constructing such a basin. Hence, it is common practice to install accessories in the basin to regulate the jump. The primary objective of implementing such a control mechanism is to effectively decrease the distance covered during a jump, consequently leading to a reduction in the dimensions and expenses associated with the stilling basin. The evolution of hydraulic jump chambers (HJCs) or stilling basins can be traced back to the initial designs proposed by Wiggert in 1971[7]. Subsequent modifications were made by Sarikelle and Simon (1980) [8], Wiggert and Erfle (1972) [9]. In their study, Korom et al. (1990) [10] undertook a comprehensive investigation focused on model studies aimed at identifying the most effective design for HJCs (Hydraulic Jump Chambers). The conducted studies encompassed the construction of models of HJCs, wherein different arrangements of baffle blocks were implemented. The primary objective was to evaluate the performance of these models in terms of velocity reduction.

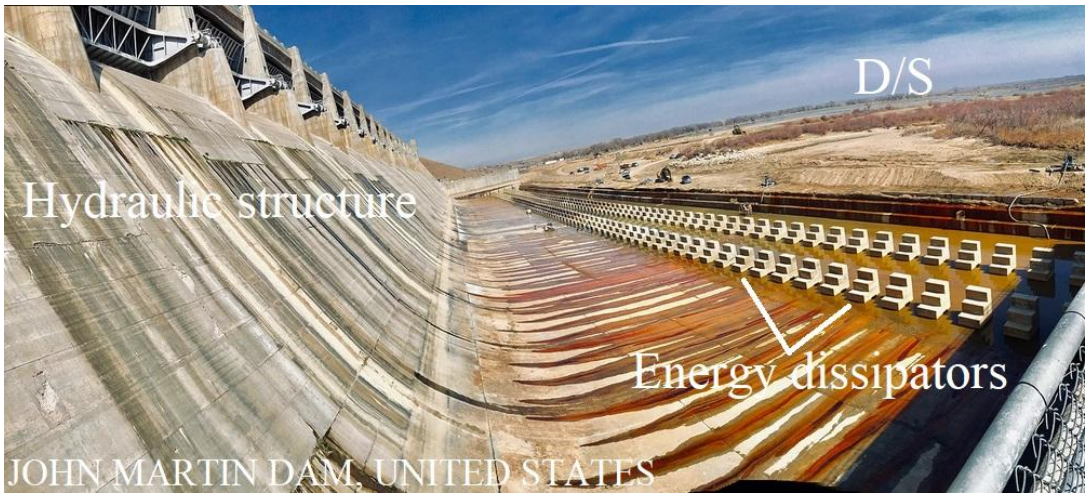

Figure 1.1 Stilling basin downstream of the dam, Jhon Martin, United States

1.2 Hydraulic jump

In a study conducted by Chow (1959) [6], the hydraulic jump phenomenon was examined. This phenomenon is commonly observed in open-channel flow situations, such as the flow of water in rivers, channels, and spillways. The observed phenomenon exhibits a notable decline in the rate of fluid motion and a sudden elevation in the level of water over a comparatively limited span. In their study, Knight and Shiono (1996) [11] examined the flow dynamics in natural rivers, specifically focussing on the occurrence of hydraulic jumps caused by natural obstacles. The authors delved into the mechanisms and processes involved in the formation of these hydraulic jumps, shedding light on their significance in understanding the overall flow behaviour in natural river systems. The formation of hydraulic jumps in natural streams is primarily attributed to the presence of natural obstacles. The hydraulic jump phenomenon was achieved by constructing artificial obstacles in the flow path when natural obstacles were not present. The implications of such factors have been found to have a positive impact on the overall health and well-being of aquatic species and

their habitats. Figure 1.2 depicts the hydraulic jump phenomenon, which occurs downstream of a hydraulic structure. In his seminal work, Rajaratnam (1967) [12] undertook a comprehensive investigation into classical jumps, delving into the intricate dynamics of velocity profiles and the dissipation of energy. Moreover, the scholarly works of McCorquodale (1986) [13] and Hager (1992) [14] have contributed to the advancement of knowledge regarding hydraulic jump characteristics. These studies have delved into various aspects such as the relationships between sequent depths and the efficiency of energy dissipation. In their recent publication, Padova and Mossa (2021) [15] provided a thorough examination of the historical progression and advancement of studies pertaining to hydraulic jumps, with a specific focus on energy dissipation and the design of stilling basins.

Figure 1.2 Phenomenon of hydraulic jump occurring downstream of the Hira Kund dam, Odisha, India

1.2.1 Practical applications of hydraulic jump

The utilization of hydraulics jumps as a means to reduce energy and velocity downstream of a dam or chute, with the aim of mitigating and managing erosion of the channel bed, was examined by Hager (1992) [14]. Hydraulic jumps, a phenomenon extensively studied by Chanson (2004) [16], play a crucial role in flood management strategies. These jumps are employed to effectively control and mitigate the impact of floodwaters. For pollution control purposes, aeration of water is commonly employed in natural channels.

1.2.2 Classical theory of hydraulic jumps

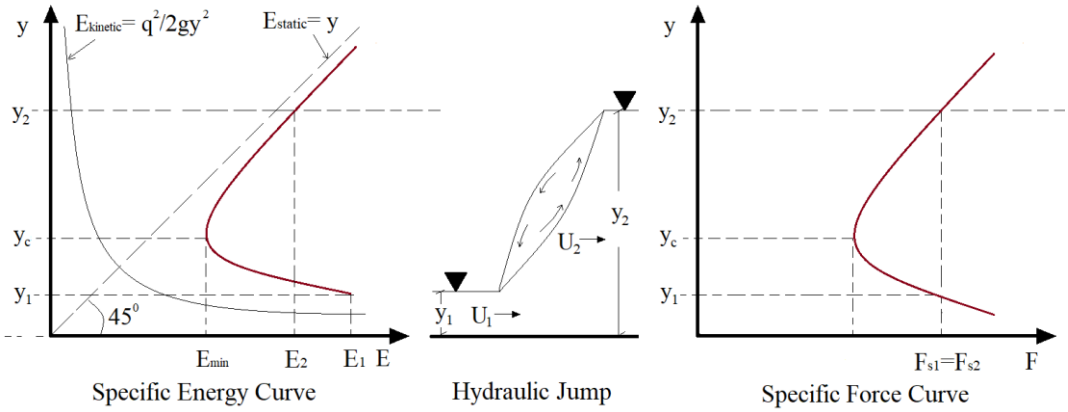

Figure 1.3 Definition sketch of specific energy, hydraulic jump and specific force curve [21]

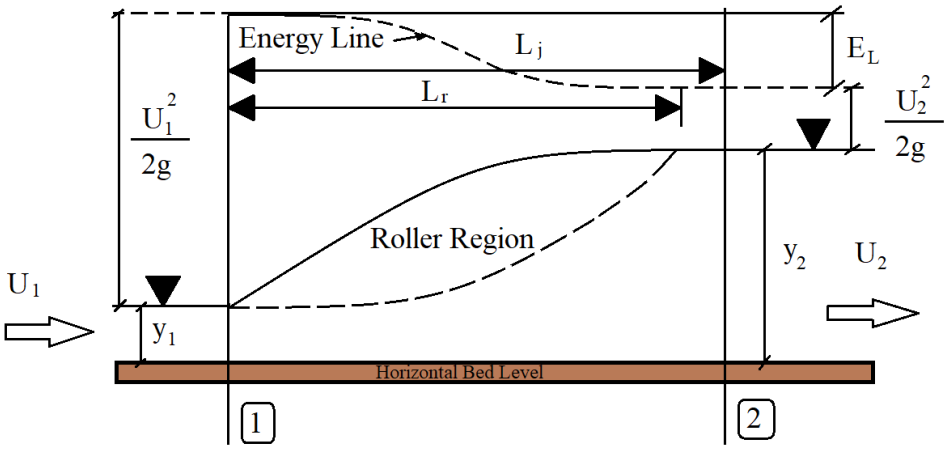

Figure 1.4 Definition sketch of hydraulic jump showing relevant parameters

Specific-energy, hydraulic jump, and specific force diagrams are discussed on Figure 1.3. It means that the given specific energy is the lowest at some accurate point. As shown also in Figure 1.3, the water depth y_c in open channel that relates to the minimum specific energy is defined as the critical depth. The water depth y_c in open channel, which corresponds to the minimum specific energy as depicted in Figure 1.3, is specified as the critical depth. The pre-jump depth y_1 is termed as initial depth of water whereas the post-jump depth y_2 is called the sequent depth or conjugate depth of jump. Figure 1.4 depicts the schematic diagram of the hydraulic jump phenomenon, illustrating the various parameters associated with it. Rajaratnam (1967) [12] defined the length of a jump (L_j), the range measured as a distance from the toe to the place practically to where the level of water settles, and the mean elevation of water attains its peak. However, it should be noted that this definition can be

ambiguous. The length of the roller (L_r) is a very significant factor in studies carried out on hydraulic jumps as it profoundly affects energy dissipation, flow stabilization and the design of hydraulic systems in general. The length of a roller, as defined by Murzyn and Chanson (2009) [17], is the stretch over which the mean free surface level advances monotonically. Additionally, numerical study conducted by Ghaderi et al. (2021) [18] gives a precise illustration of the exact position where the gap from the take-off point to the initial point of the positive forward movement is known as the roller length of jump.

1.2.3 Types of flows

Henderson (1966) [19] and Chanson (2004) [16] classified the flow on the basis of critical depth (y_c) and the actual depth (y) of water in an open channel. When (y)>(y_c), flow referred to as tranquil or subcritical, for (y)=(y_c) flow referred to as critical and for (y_c) > (y) flow referred to as torrential or supercritical flow.

1.2.4 Hydraulic jump in a horizontal rectangular channel

The analysis of hydraulic jumps typically involves examining the depth of flow prior to and following the jump. Hager (1992) [14] discussed that the Froude number plays a crucial role in determining the flow conditions that result in a hydraulic jump and the equations that govern the classical jump involve the correlation between the tailwater depth and the length of the roller.

The energy equation is not applicable for analysing hydraulic jump due to significant energy loss and limited understanding of the exact amount of energy loss associated with the phenomenon. The classical theory of hydraulic jump utilises the momentum principal hydraulic jump le to analyse hydraulic jumps. Figure 1.5 depicts the specific section of the that is being analysed as the control volume.

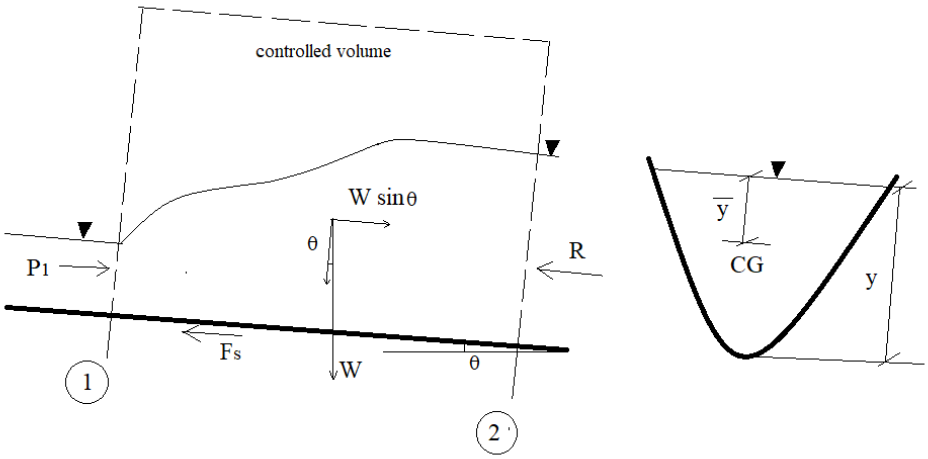

Figure 1.5 Sketch showing controlled volume of fluid

In studying hydraulic jump, one assumes that there is flow uniformity with hydrostatic pressure in the initial phases of the jump as well as of the final phases of jump. The relative loss as a result of friction on the channel floor is assumed to be

small relative to the length of the jump so as to be neglected. Additionally, it is assumed that the channel floor is horizontal in order to eliminate the weight component of the water mass that makes up the jump.

The jump that occurs in most water exercises can be explained with the help of three fundamental equations of mass, momentum and energy conservations.

Continuity:

The relationship between velocities and cross-sectional area and volume flow rate Q can be expressed as follows:

$$A = \frac{Q}{U} \tag{1}$$

Momentum:

With the application of momentum principle to the control volume (in Figure 1.5):

Net pressure force = Rate of change of momentum

$$P_1 - R - F_s + W sin\,\theta = M_2 - M_1 \tag{2}$$

P_1, R is the pressure force at the control surface at section 1 and 2 respectively.

F_s= Shear force acting on the control surface in near the channel bed.

M_1 and M_2 is the longitudinal momentum flux at the beginning and at the ending of the control volume.

The rectangular channel is assumed to be horizontal and frictionless, with a unit width. Equation (2) can be expressed as:

$$p_1 A_1 - p_2 A_2 = \rho Q\,(U_2 - U_1) \tag{3}$$

The average pressure can be determined by calculating the pressure at the centroid, denoted as $\bar{p}$ and may be written as $\rho g \overline{y}$, where $\overline{y}$ represents the depth of the centroid below the surface.

On expansion of equation (3),

$$\rho g \overline{y}_1 A_1 - \rho g \overline{y}_2 A_2 = \rho\, Q\, (\frac{1}{A_2} - \frac{1}{A_1}) \tag{4}$$

Assuming unit width of the channel (b=1) and substituting $\overline{y}$= (1/ 2) y, A = y, $Q = q$ in above equation

$$\frac{y_1^2 - y_2^2}{2} = \frac{q^2}{g}\left(\frac{1}{y_1} - \frac{1}{y_2}\right) \tag{5}$$

$$\frac{1}{2} * \frac{y_2}{y_1} * \left(1 + \frac{y_2}{y_1}\right) = \frac{q^2}{g y_1^3} \tag{6}$$

On replacing the $\left(\frac{q^2}{gy_1^3} = \frac{U^2}{gy_1}\right)$ with Fr_1^2 (The dimensionless Froude number, denoted as Fr_1, plays a significant role in open channel flows. This is known as the inertial force to gravity force ratio).

$$\frac{y_2}{y_1} = \left(\frac{1}{2}\right) * \left[-1 + \sqrt{(1 + 8 * Fr_1^2)}\right] \quad (7)$$

According to Tokyay (2005) [20], equation (7) for a horizontal, frictionless and rectangular channel is referred to as the Belanger momentum equation.

Energy:

With the application of energy equation to control volume (in Figure 1.5).

$$E_1 - E_2 = \left(y_1 + \frac{q^2}{2gy_1^2}\right) - \left(y_2 + \frac{q^2}{2gy_2^2}\right) \quad (8)$$

On simplifying the above equation

$$E_L = (y_2 - y_1)^3 / 4y_1y_2 \quad (9)$$

1.2.5 Classification of Jumps

Figure 1.6 illustrates the categorisation of jumps based on Froude number. The occurrence of hydraulic jump is influenced by various factors like bed roughness. Subramanya (2009) [21] discussed the five types of jumps.

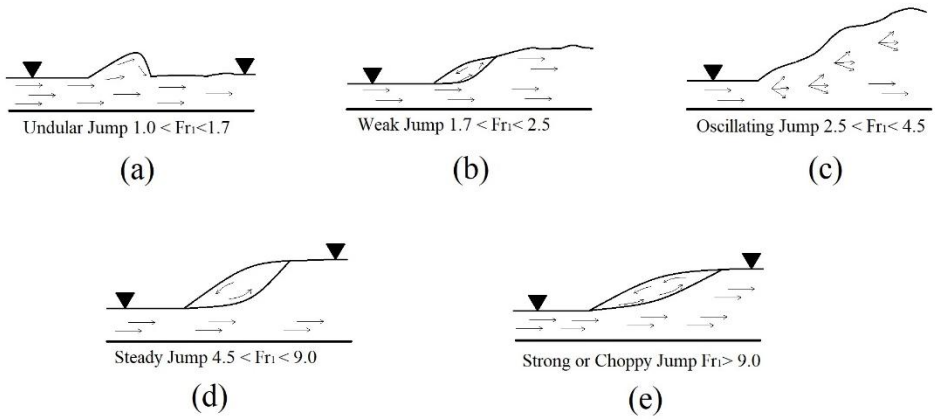

Figure 1.6 Classification of jump based on Froude Number [21]

The Undular Hydraulic Jump, characterised by a Froude Number ranging from 1 to 1.7, exhibits irregularities in its formation and is not well-defined. Turbulences can be observed in the water particles during this phenomenon. A weak jump occurs in a situation where the velocity of water is relatively small, and such jump occurs prevails when the Froude number is equal to between 1.7 and 2.5. The oscillating hydraulic jump is formed if an oscillating jet becomes a super critical state where the particles contained in the flow oscillate either in a clockwise or an

anticlockwise manner. This type of jump happens when Froude number falls in the range of 2.5 and 4.5. Another familiar type of jump is steady jump in which the particle migrates in one direction with high turbulence and such type of jump is born when the Froude number ranges approximately 4.5 to 9. The case of strong hydraulic jump take place when Froud number is greater 9, from this point the turbulence is higher and water surface elevation is high as compared to steady jump.

Further, Subramanya (2009) [21] discussed types of jumps based on location of jump. Figure 1.7 illustrate the types of jumps based on location of jump. Jump can be defined as free, free repelled and submerged based on tail water depth (y_t) and normal depth (y_1). When tailwater depth equals to the normal depth of water it is referred as free jump. When tailwater depth remains lower than the normal depth it is referred as free repelled jump and for tail water depth greater than the normal depth it is referred as submerged hydraulic jump.

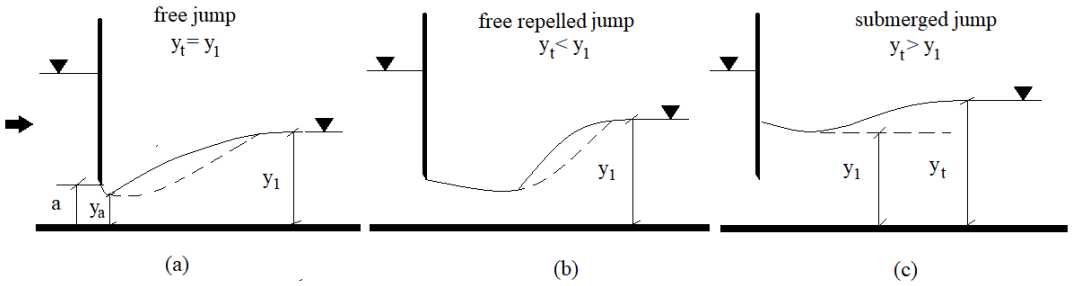

Figure 1.7 Sketch showing different types of hydraulic jump based on depth [21]

1.3 Computational Fluid Dynamics

Computational Fluid Dynamics (CFD) implements numerical methods and algorithms based on the concepts of fluid mechanics for solving the problems of fluid flow. John von Neumann played a remarkable role in development of algorithms. John D. Anderson (1995) [22] covered the fundamentals of CFD, including numerical methods, grid generation, and applications. Required surface description in terms of its boundary conditions and use when analysing the interaction between liquids and gases in the CFD models. This technique helps design teams reduce the risk of design failures, optimize engineering designs, and gain a competitive market edge. CFD models are based on the Navier-Stokes equations and are solved iteratively either in steady-state or transient modes.

1.3.1 Multiphase models

H.K. Versteeg and W. Malalasekera (2007) [23] provided an introduction of the finite volume method which is the pivotal for the realization of the Volume of Fluid (VOF) in CFD. It also explains the basic of the VOF method and focuses on the steps of develop of the method which are interfacial capturing, estimation of volume fraction and, surface tension forces. The VOF model is a computational multiphase technique for tracking the volume fraction of each fluid in every cell, accurately

representing fluid behaviour and interactions (Canonsburg, 2013) [24]. Its primary goal is to capture the interface shape and dynamics between immiscible fluids, efficiently addressing problems like free-surface flows and surface tension effects. The Eulerian model considers each phase as an overlapping continuous medium; the conservation equations of the sub-phases are solved and precise interaction between phases –momentum, mass, and energy exchanges are accounted for. This method suits systems where both phases significantly occupy the computational domain and interact strongly. The Mixture Model considers the multiphase flow as a single entity, where a single set of momentum equations is solved for the entire mixture and velocities between the phases are taken into account. It simplifies the multiphase flow problem by assuming local equilibrium between phases, making it computationally less intensive than the full Eulerian model.

1.3.2 Turbulence models in computational fluid dynamics (CFD)

The RANS (Reynolds-averaged Navier-Stokes) method is widely used in the field of CFD for the prediction of turbulent flow regimes. RANS that govern fluid motion are time averaged which implies the study focuses on the average flow parameters velocity, pressure etc. Wilcox (2006) [25] discussed different types of turbulence models that is utilized in CFD such as k-ε and k-ω.

Due of its wide range of applications, the k-ε model is widely applied for RANS simulations. It evaluates the value turbulent kinetic energy, k and its rate of dissipation, ε, hence the two model equations. This model is based on the assumption that turbulent eddies die out via viscous diffusion and turbulent transport, where the decay is proportional to the rate of dissipation of kinetic energy. The k-ε model is commonly used to solve complex fluid dynamics problems by resolving two distinct equations throughout the simulation. Its performance is comparable to experimental results and other models like the k-ε model. Additionally, it uses a scalable wall-function to enhance solver efficiency and shows increased robustness with fine meshes. This model is commonly used for cost-effective turbulent flow simulations and does not require geometry-specific parameters.

The k-ω model, a variant of the k-ε model, focuses on the specific dissipation rate of turbulent kinetic energy, making it more suitable for near-wall flows. This tends to include computation of the transport variable k, turbulence kinetic energy and turbulence dissipation rate. The k-ω model often outperforms the k-ε model in certain scenarios. The software may also offer near-wall treatment solutions and address low Reynolds number problems. This model's advantage lies in its use of the ε-equation alongside the ω-equation, facilitating more accurate numerical simulations.

The Reynolds Stress Model (RSM) is a computational approach that calculates the Reynolds stresses directly, which are the key factors causing turbulence anisotropy. Although the computational cost of this model is higher than that of eddy viscosity models, it provides improved accuracy for more complex flows. Spalart Allmaras turbulence model is a turbulence model that was developed by Spalart and Allmaras and is one of the most commonly used models in CFD. This one-equation model is suitable for high Reynolds number flows, as it solves for the eddy viscosity.

Numerous methods are utilized in the discipline, such as Large Eddy Simulation (LES), Direct Numerical Simulation (DNS), and Detached Eddy Simulation (DES). LES is commonly used to simulate turbulent flows by directly resolving large-scale eddies. On the other hand, a Sub Grid Scale (SGS) model is used to close the equations for smaller scale eddies. Unlike approaches based on rheological models for flows, including all of the turbulence in the geometrical grid, LES is convenient for the design of complex turbulent flows which exhibit a large range of scales, from the large systems down to the smallest vortices. DNS, or Direct Numerical Simulation, is a computational method that simulates turbulent flows by numerically solving the Navier-Stokes equations, eliminating the need for turbulence modelling. This technique allows for precise simulation across various scales, from large structures to minute eddies, without requiring sub grid-scale models. DNS is considered the most accurate technique for turbulent flow simulation, capturing all intricate flow field details, including small-scale features not accurately represented by traditional turbulence models. The DES model integrates aspects of RANS and LES models, facilitating a seamless transition from RANS to LES in regions with well-resolved turbulence. This approach is particularly effective for flows featuring separation and recirculation.

The detailed discussion on transport equations involved in above discussed models are done in Chapter 3 of the present thesis.

1.4 Need of the study

At present, the comprehension towards the utilization of CFD in the area of hydraulic engineering is somewhat vague. The need of the study is to offer valuable insights to field engineers on the design of hydraulic energy dissipators using computational fluid dynamics (CFD) modelling. The aim is to provide these insights in a cost-effective manner. Additionally, it has been determined that the hydraulic jump is the primary phenomenon for energy dissipation in the discipline of hydraulic engineering. However, it is worth noting that this topic has not been extensively studied using Computation Fluid Dynamics. The following are a list of novel and rarely studied gaps in the field of Computational Fluid Dynamics and the Hydraulic Jump phenomenon.

Although a lot of research has been done on hydraulic jumps, there are still major gaps specifically in learning how strips of roughness on the bed affect hydraulic jumps. Research on roughness so far usually covers general impacts but does not look at how the shape, size and alignment of roughness elements in stilling basins influence water flow. The behaviour of various strip macroroughness shapes, in particular triangular, trapezoidal, semicircular and novel forms, has not been thoroughly analysed together with their aspect ratios. Further, no studies have thoroughly investigated the role of the layout and positioning of roughness within stilling basin type hydraulic jumps. These problems are compounded, since past numerical studies often fail to consider how different boundaries affect the action of hydraulic jumps over rough areas and how this affects the flow, energy loss and computer calculations. In addition, not much is known about the influence of boundary conditions on successful convergence, the quality of results and how long the simulation takes. The absence of

clear evaluation methods decreases how dependable and effective CFD models are for hydraulic jump research, mostly in cases of complex configurations or rapid turbulence. Dealing with these overlooked items is crucial for making advanced and affordable numerical frameworks for stilling basin design. It is because of these vital parts that we need to use a combined approach of studying different geometries and using advanced computer modelling to improve energy management and flow control in hydraulic structures. Motivated by these gaps, the present study employs high-resolution Computational Fluid Dynamics (CFD) simulations using ANSYS Fluent with the Volume of Fluid (VOF) method and multiple turbulence models to evaluate hydraulic jump characteristics over smooth and artificially roughened beds. Through mesh sensitivity analysis and model validation against experimental data, the study aims to provide detailed insights into optimizing roughness configurations for enhanced energy dissipation and flow stability, thereby supporting the design of more efficient and cost-effective stilling basins

1.5 Objective of the study

The objective of this study is to investigate the characteristics of hydraulic jumps over smooth and macrorough beds in a prismatic rectangular channel located downstream of a hydraulic structure operated by a sluice gate. The following objectives are set to numerically study the hydraulic jump characteristics under varying channel conditions. The present study aims to investigate multiple aspects of hydraulic jump behaviour under different conditions. Specifically, it focuses on studying the effect of various flume configurations on the characteristics of classical hydraulic jump. Additionally, it examines the effect of various artificial strip macroroughness on the characteristics of free and submerged hydraulic jump. Further, the study explores the influence of the height to base width ratio of macroroughness and their possible arrangement on free and submerged hydraulic jump characteristics. Lastly, it investigates the effect of the height to wavelength ratio of macroroughness on free and submerged hydraulic jump characteristics.

1.6 Outline of thesis

The present thesis is structured into five chapters, each addressing a specific aspect of the study. CHAPTER 1 gives a brief introduction to the hydraulic jump phenomenon, numerical modelling techniques, the necessity of the study, its objectives, and the overall scope of the present work. CHAPTER 2 provides knowledge regarding numerical and experimental investigations of hydraulic jumps over both smooth and macrorough beds, drawing upon existing literature. CHAPTER 3 elaborates on the approach utilized for the current study, detailing the methodology and the process through which the numerical models are validated. CHAPTER 4 presents the results and discussions arising from the numerical simulation of the hydraulic jump phenomenon under various conditions. Finally, CHAPTER 5 summarizes the conclusions drawn from the present study and outlines the scope for future research work in this domain.

CHAPTER 2

LITERATURE REVIEW

2.1 General

Over the years, a substantial body of literature has accumulated on the subject of hydraulic jump analysis, encompassing theoretical, experimental, and numerical investigations. These studies have significantly advanced our understanding of the complex fluid mechanics involved in hydraulic jumps, particularly in terms of energy dissipation, flow regime transitions, air entrainment, turbulence characteristics, and the influence of channel geometry. This section aims to synthesize the current state of knowledge by examining representative studies across these domains, highlighting key developments, identifying existing knowledge gaps, and outlining opportunities for future research in hydraulic jump phenomena.

2.2 Hydraulic jump in prismatic rectangular channel with smooth bed

Rajaratnam (1967) [12] offered exhaustive insight of many different kinds of hydraulic jumps such as the classical hydraulic jump, submerged jump, forced jump, jump in sloping channel, pre-entrained jump and jump in non-rectangular channel, jump in conduit, jump in non-prismatic channel, and jump in stratified flow. He used Prandtl type pitot tube to measure the forward velocity and from the observations, the velocity profile of a hydraulic jump was found to be of plane turbulent wall jet. He emphasized the importance of taking into account the longitudinal velocity gradient and the bed shear stress distribution in the jump region.

Hager and Bretz (1986) [28] analysed the important hydraulic flow characteristics described in hydraulic jumps that take place at both positive and negative steps in a rectangular, horizontal, and prismatic channel. They paid more attention to these factors with a view of establishing the correlation between length of jump and these phenomena. They stated that the shape of the step was not crucial as it depends on the transition from supercritical to subcritical flow at the step. Consequently, the sequent depth ratio was highly dependent on the height of the steps as well as the approaching Froude number. Moreover, the evaluation indicated that the degree of the tailwater depth was nearly six times more variable in the case of the negative step than the flow depth. Hydraulic jumps taking place at negative steps are characterized by a higher dynamic in the adjustment of the depth of the tailwater and the Froude numbers in which efficiency might be maximized. Therefore, the tested hydraulic jump over positive steps proved to be more stable as compared with that over negative step.

Hager (1988) [5] examined the hydraulic jump in a rectangular channel of invariably varying width. He contemplated a steep slope at the channel bottom in the upstream portion of the canal and a lower slope toward the downstream portion. He divided various jump types (A, B, C, D) on the basis of hydraulic jump with sloping as well as level part of the channel. He worked out several equations for finding sequent depth ratio, roller length and the initial Froude number and relative static head regain. The equations were ideal for the need of designing. Further, it expanded on the hydraulic jump and how it is useful in controlling the energy dissipation of the flow as

one of the critical avenues for controlling flow and eradicating erosion in stilling basins. It was also identified that the work done in the case of the formation of a hydraulic jump in the classical way had the highest efficiency.

97 Long, Rajaratnam, et al. (1991) [30] investigated the hydraulic jump in a horizontal rectangular flume of width 0.47m, height 0.52m and length 7.5m. They used Froude numbers between 4 and 9 in their study. They developed the replica of flow regime near the wall by employing high speed photographic technique, where they took about 2000 frames/s. Jump was subsequently disaggregated into several parts based on inlet Froude numbers as well as timing partitions. In the multiple graphs they drew the changes taking place in the surroundings of the vortices. These multiple graphs denote the locations and sizes of these vortexes based on the extruded analogy of the vortex dominated zone and correlate to the change in Froude numbers. They said that it is crucial to shed light on the vortex pattern of hydraulic jump especially in these tremendously huge structures. Besides providing a complete picture of vortex action inside them, a precise description of such action is useful when it comes to making more accurate predictions of jump behaviour and developing the most effective hydraulic structures.

The above studies collectively emphasize that hydraulic jumps are complex, multi-type phenomena influenced by channel geometry, slope, step configuration, and Froude number. The Froude number emerges as a key parameter affecting sequent depth, roller length, and energy dissipation. Internal flow structures like velocity profiles, shear stress, and vortex patterns are crucial for understanding jump behaviour, highlighting the need for experimental techniques such as Pitot tubes and high-speed photography. These studies also show that positive step jumps offer better stability than negative ones. Overall, an integrated analytical and experimental approach is essential for effective hydraulic jump design in open channel systems.

Rajaratnam (1995) [31] investigated several methods of quantifying hydraulic jumps. Such techniques included direct methods, which engaged tools like velocity probes and pressure transducers, and indirect methods that embraced methods like flow visualization and the surface profiles. It features not only measurement approaches and problems and limitations related to it but also shows how flow conditions, channel geometry, or turbulence might influence hydraulic jump measurements.

Wu and Rajaratnam (1996) [33] explored the behaviour of the hydraulic jump from the wall jet flow structure to the semilogarithmic velocity profiles of open channel flow. They tested in a parallel flow channel with a flat, slippery bottom and transparent sidewalls with Froude numbers from 3.87 to 10.48. They observed the velocity profile at first moment seemed to behave like wall jet with maximum at the bed level. They concluded that during transition from hydraulic jump to open channel flow, the bed shear stress was decreased along with other velocities. The minimum bed shear stress declines with an increase in Froude number and becomes near zero at a certain Froude number which suggests the possibility of flow separation from the bed. About the centreline there is dissipation of energy which dissipates the flow intensity until it gets into the intensity of the open channel flow. They further pointed out that the length of the transition zone was roughly ten times the tailwater depth. The extent of this transition region was found to be adequately characterized by the Froude number and the depth of the tailwater.

Chanson and Gualtieri (2008) [37] conducted experiments in two geometrically similar channels with a scaling ratio of 2:1 to study how air entrainment scales. They observed void fraction distributions and bubble count rates, which followed a diffusion model in the larger channel but showed scale effects in the smaller one. Lower Reynolds numbers in the smaller channel resulted in greater air detrainment, leading to less overall aeration. They revealed that dynamic similarity in hydraulic jumps was affected by multiple parameters, such as Froude, Reynolds, and Morton numbers, making it difficult to perfectly model air entrainment at different scales. The small-scale models may underestimate air entrainment characteristics, providing insight into the limitations of physical modelling in hydraulic engineering. The smaller hydraulic jumps possessing lower air entrainment and higher air detrainment phenomenon showed overall lower aeration of the jump roller in comparison with the larger hydraulic jumps. The measurements of the dimensionless bubble count rates were significantly lower in the smaller channel particularly in the mixing layer. The also identified an advective-diffusion shear layer in hydraulic jumps, but for Reynolds numbers below a critical value, air entrainment was weak, and detrainment processes dominated. The inability to achieve dynamic similarity due to differences in Reynolds and Morton numbers highlights challenges in scaling hydraulic jumps and maintaining accurate modelling of air entrainment processes across different model sizes.

Murzyn and Chanson (2009) [17] primarily focused on experimental studies of hydraulic jumps with Froude numbers ranging from 3.1 to 8.5. They examine the chaotic motions between large-scale eddies and the free surface and the application of acoustic displacement sensors and phase-detection probes for free-surface oscillations and two-phase flow characteristics. They observed free-surface fluctuations increases with the Froude number, especially in the roller region of the jump. The turbulent fluctuation levels peaked in the first half of the roller, with the peak increasing with larger Froude numbers. For instance, the maximum fluctuation was reported about 1.5 times the inflow depth for a Froude number of 8.5. They found acoustic displacement meters to be an effective tool for measuring free-surface dynamics in hydraulic jumps, with their time-averaged readings closely corresponding to the division of the flow domain between the isolated turbulent shear layer and the upper free-surface layer.

hachereau and Chanson (2011) [42] investigated the morphology of free-surface oscillations and air-water gas-liquid interfacial characteristics in a hydraulic jump roller. They carried out investigations in a horizontal rectangular channel for comparatively low Froude number. They normally employed non-intrusive Acoustic Displacement Meters (ADM) for the real-time measurement of free-surface fluctuations. Also, they used several numbers of Acoustic Doppler Velocimeters (ADVs) to show the turbulence mechanisms of the hydraulic jumps with great accuracy. They determined that the mean free surface profile had a clear configuration in agreement with the visual and photorealistic parameters. The violent character of the fluctuations which formed hydraulic jumps with certain fluids was reported to be anisotropic, especially in the neighbourhood of the free-surface. They identified that the amplitude of turbulence fluctuations strongly dependent on the Froude number of the incoming flow.

Xiang, Cheung, et al. (2014) [50] proposed a comprehensive numerical modelling approach to simulate the complex flow dynamics in hydraulic jumps, focusing on air entrainment and bubbly flow. They combined a Volume-of-Fluid (VOF) approach with the Multiple-Size-Group (MUSIG) model, using an Eulerian–Eulerian multi-fluid framework to enables simulation of air and water interaction, including the entrainment of air bubbles at the jump toe and their dispersion in the flow. They reported that model predicted the location and rate of air entrainment accurately, aligning well with experimental data from previous studies. Also model effectively captured the flow patterns in jet region, shear layer, and recirculation region. regions, particularly the velocity profiles and turbulent roller formation. They reported that bubbles accumulate in the recirculation region, and their size reduces downstream due to breakage by turbulence. Despite its accuracy, the model showed limitations, especially in predicting downstream bubble frequency and velocity near the free surface.

Chanson and Shi (2015) [53] presented a comprehensive analysis of the current obstacles and notable progress in hydraulic engineering, with a specific focus on the environmental aspect using experimental and analytical methods. They introduced more varied aspects and including elaborate features of water pertaining to water systems, temporal and spatial scales, water-solid, water-air, and water-biological life. They emphasized the need to create technical solutions for overcoming of the tackling hydraulic problems in the environment.

Bayon-Barrachina and Lopez-Jimenez (2015) [55] put forward a computational fluid dynamics (CFD) model that utilises the Open FOAM platform to design hydraulic jumps taking place in horizontal, smooth and rectangular prismatic channels in 3D manner. They used three turbulence models including the standard k-ε, RNG k-ε and the SST k-ω to encounter the turbulences. They used the Volume of Fluid (VOF) model to represent the interface between two immiscible fluids. They realised that through integrating the CFD modelling method in simulating hydraulic jumps, that the basic hydraulic jump parameter inclusive of water surface profile, sequent depth ratio and length of jump have been determined with a very good accuracy of more than 98 percent.

Kim, Choi, et al. (2015) [56] studied the hydraulic parameters of hydraulic jump using a fixed weir and a sluice gate-type movable weir in a rectangular channel. They used energy dissipators in the downstream of the hydraulic structure in order to sink high rates of kinetic energy and protect the channel bed. They reported that by placing energy dissipators at the sluice gate, energy dissipation can be reduced by more than 52% compared to those without energy dissipators. It was also ascertained that the hydraulic jump lengths of sluice gate type movable weir and fixed weir are of equal length. Movable weirs of sluice gate type can establish flow regions of high velocity and can experience bed scouring. They developed an improved design of movable weirs based on improvements in the design criteria for riverbed protection.

Luo (2015) [57] examined the hydrodynamic characteristics of a submerged hydraulic jump. He employed numerical, experimental, and analytical approach to probe three features including the fluid depth, the turbulent primary velocity, the shear stress and turbulent kinetic energy. He provided such alternatives

in mathematical representation for factors such as water depth, primary turbulent velocity, the shear stress as well as the kinetic energy of turbulence for both fixed and movable beds. He identified three eddy zones, influenced by forward and backward velocities, scoured holes, and adverse pressure gradients which significantly affect the flow structure in submerged hydraulic jumps. Also, he suggested that numerical models using standard k-ε turbulence models need adjustments for certain parameters, particularly in higher Froude number inflows.

The advancements in the study of hydraulic jumps through experimental, analytical, and numerical methods present compelling arguments for an integrated approach to understanding complex flow phenomena. Experimental investigations, such as those by Rajaratnam and Wu & Rajaratnam, provide direct insights into velocity fields, pressure changes, and wall jet behaviour using sophisticated tools like velocity probes and pressure transducers, while indirect techniques help visualize surface and flow structures. Researchers like Chanson and Gualtieri extended this understanding by focusing on air–water interactions, where parameters like the Morton number and void fraction play crucial roles in determining entrainment and turbulence behaviour. The use of advanced instruments such as ADM and ADV enhances the accuracy of turbulence and surface fluctuation measurements. Complementing physical observations, numerical studies employing CFD tools and multiphase models like VOF and various turbulence closures simulate intricate flow dynamics including jet evolution and bubble transport. These combined efforts argue strongly for a hybrid approach, as neither experimental nor numerical methods alone can fully capture the multifaceted processes of energy dissipation, flow transition, and erosion potential associated with hydraulic jumps.

Wang and Chanson (2016) [58] understood the scale effects of hydraulic jumps, particularly in down-scaled physical models, as well as the behaviour of free-surface dynamics, air entrainment, and turbulence. They conducted experiments on hydraulic jumps with various Froude and Reynolds numbers, investigating their effects on parameters such as surface deformation, bubble-turbulence interactions, and air entrainment rates. They concluded that while self-similar behaviours exist for certain flow properties, many key turbulent and air entrainment processes are scale-dependent. Full-scale conditions are necessary to accurately capture these effects, particularly for bubble dynamics and turbulence intensity.

Hafnaoui, Carvalho, et al. (2016) [60] performed an experimental investigation to model the jump in a sloping rectangular channel. They managed to produce a MATLAB model operating under the Saint-Venant equations and the TVD MacCormack explicit scheme which was used to predict the location of hydraulic jumps both in rectangular and triangular channels. Beyond that, they obtained correlations to express the errors in hydraulic jump positions; they illustrated the dependence of predictions on both slope and Froude number changes. Both of them stressed that the availability of the model for the prediction of sediment discharge is valuable, however, adjustments for the slope and downstream conditions are critical for accurate calculations especially for slopped triangular channels.

73 Sauida (2016) [61] employed Artificial Neural Networks and multiple linear regression model for predicting length of submerged hydraulic jumps

downstream of multi-vent regulators. They discovered that Artificial Neural Networks had a slightly higher coefficient of determination and so predicted more accurately than the multiple linear regression model models with 12% improvement. The ANN model results in improved modelling of the length of the hydraulic jump as the influence of the gate operation changes from case to case.

Valero, Viti, et al., (2018) [65] provided a theoretically elaborate account of prior studies performed in the context of hydraulic jump phenomenon with specific focus on experimental analysis data. They pointed out some ambiguity in the modelling technique due to occurrence of highly turbulent flow features in hydraulic jump flow that cause bubble formation. In their opinion, regarding the scope of the study in the established experimental framework, the assessment of the spread of the liquid phase and the formation of bubbles by PIV and ADV instruments was inadequate. The same would extend to the geometry employed in the numerical modelling where the impacts of scale or inflow-outflow flow rate fluctuations are also manageable.

Salmasi and Samadi, (2018) [68] investigated the flow behaviour, energy loss/dissipation and other hydraulic phenomena occurring over stepped spillways thru the Ansys Fluent computational models. They described a step spillway case, where they used the k-ε turbulence model, as well as the Volume of fluid (VOF) model in order to assess the scale of turbulence as well as the associated interface. The discrepancy between two groups of data indicated that the numerical model possessed an acceptable level of capability in foreseeing flow characteristics and energy loss, and most of the potential errors seemed to be falling within 3 to 6%.

Jesudhas, Balachandar, et al. (2018) [69] conducted an ideal a classical hydraulic jump with maximum inlet Froud number of 8.5 using a DES complemented with VOF for the free-surface capturing, allowing a better insight into the dynamics of turbulence in a hydraulic jump. This was important in offering information on the turbulence characteristics and flow structure of the hydraulic jump that lacked representation in prior experiments. They are some features such as the enlargement of the shear layer. They compared their deterministic and stochastic simulation results with the experimental results concerning mean flow profiles and free surface profiles, velocity fields and turbulence characteristics, and got fairly good correlations.

Al-Hashimi, Saeed, et al. (2019) [70] presented the results of in-depth investigation of turbulent characteristics of a classical hydraulic jump created with minimum Froude number of inlet flow is 8.5. To simulate the hydraulic jump, they used a unsteady three dimensional DES model in combination with the VOF approach for surface capture. They said that in the area of their investigations concerning the wall jet flow and the interaction between the roller area they used such values to compare the simulation data obtained with the experimental data taken. In the course they noticed that the flowing shear layered continues to amplify while implying to the free surface and the free surface is marked by features, which include rupture and very violent oscillations. Their results emphasized the fact that there should exist a mesh resolution capable of capturing details of the complex bubbly flows solution which is computationally intensive particularly at a higher Froude number.

Yildiz, Marti, et al. (2020) [73] examined the location of hydraulic jump occurring in a rectangular channel after a sluice gate. The flow conditions were simulated by them using Fluent software. As observed from the simulation they noted that the values arrived at by this method complied with the experimental findings. They also discovered that direction of the jump varies with the discharge, hydraulic geometry of the flume, and position of the step.

Jesudhas, Balachandar, et al. (2020) [74] focused on the results of the study regarding the phenomenon of Symmetric Submerged Spatial Hydraulic Jumps (SSHJ). They employed three-dimensional, unsteady detached eddy simulations coupled with Volume of Fluid multiphase method as a tool for the flow surface modelling. They identified that the jump roller is relatively thicker all across the channel conveyance but thinner in the middle part of the flume which may lead to increased scour near the walls. Localization highlighted temporal oscillations at the outlet of the conduit. The following are the criteria for identifying vortices; The formation of series of rectangular vortex rings at the exit of the wall jet inside the conduit. These rings got distorted and broken down into the above-said smaller vortex structures existing in the system because of pressure differences in velocities. This made it clear that the prime cause of turbulence in the SSHJ flow field was the dimensional shear layer arising out of the expanding wall jet. The different rollers or structure of beds cause the disintegration of the eddies into little eddies or the increase in the dissipation of energy of turbulence.

Macián-Pérez, Bayón, et al. (2020) [75] performed a numerical analysis on change in energy in case of the hydraulic jump in a rectangular channel. For a particular initial Froude number, they used the standard large scale CFD solvers of Open FOAM and FLOW-3D to study the phenomenon more elaboratively. In order to check the effectiveness of the results to a real building they compared between the physical simulation results to the results got through the simulation software. They addressed themselves with such aspects like the shape of the free surface, length of the roller system, effectiveness of a jump, distribution of velocities and pressure fluctuations. They pointed out that the obtained simulation result is qualitatively close to the experimental result and also acknowledged the fact that there is a quantitative difference in velocity distribution and pressure fluctuation. Their finding thus indicates that CFD codes were perceived to be useful in the design of energy dissipater hydraulic structures. Consequently, the sequent depth values estimated by Open FOAM were fairly accurate regarding their estimation being more than 97% accurate. Similarly, other software failed to show acceptable performance expect FLOW-3D which had accuracy above 94.2% for the same factors.

Hien and Duc (2020) [77] investigated the hydraulic characteristics of the Ngan Truoi construction encompassing the spillway, channel chute, stilling basin. They noticed when using several tools that include the computational fluid dynamics and some physical models. They employed RANS and LES turbulence models. From this they were able to deduce that the RANS model was able to provide better results in predicting the water level, velocity and pressure distribution than LES. They emphasised the importance of a model that would define air entrainment in order to have a better compatibility with the numerical model of the rapid flow of water over

the structure. Among the works of greatest interest, the mesh size of 0.1 m provides the best fit to the numerical simulations with physical measurements.

Nandi, Das, et al. (2020) [79] provided a set of numerical data that was expected to describe the formation of a hydraulic jump in a rectangular channel in which the bottom slope is low. They also used MacCormack scheme for the solution of differential equations of the Saint-Venant type in one dimension only. They did twenty laboratory experiments in an attempt to tune the numerical model. These experiments entail characterization of the upstream Froude numbers in the range of 2.17 to 7.0 and were conducted for three bed inclinations of 0, 0. 02174 and 0. 0475. They noted that there was close correlation between the hydraulic jump experimental data and the simulated hydraulic jump profiles. However, when slopes were not horizontal, the location of the jump was farther downstream than position established in the experiment. This was especially so when the Froude numbers were high as was suggested in the subsequent experiment presented in this study.

Hafnaoui and Debabeche (2021) [83] evaluated Iber software's effectiveness in simulating the location and movement of hydraulic jumps in rectangular channels. They focused on different Froude numbers and sill heights to observe the hydraulic jump's behaviour in rectangular channels. Their simulations closely matched experimental results, particularly for certain Froude numbers. Therefore, they found Iber software valuable for flood risk management and protecting hydraulic structures from erosion.

Gualtieri and Chanson (2021) [84] discussed the complexities of modelling air-water interactions and the need for ongoing improvements in both physical and numerical approaches, including further validation and overcoming scale effects. They considered two case studies to demonstrate these modelling approaches. They stated that laboratory-based physical models have been traditionally used to study self-aerated flows. However, they face limitations, such as scale effects, that hinder accurate extrapolation to real-world systems. Whereas, new development in Computational Fluid Dynamics (CFD) has made it possible to examine such flows in details. While CFD can model full-scale scenarios, it requires proper validation against high-quality experimental data to ensure accuracy.

Nasrabadi, Mehri, et al. (2021) [86] predicted submerged hydraulic jump (SHJ) characteristics using machine learning methods. They performed experiments in a rectangular flume measuring 9m long, 0.5m wide, and 0.45m deep with minimum initial Froude numbers of 3.5 and maximum of 11.5, and minimum submergence ratios of 0.1 and maximum of 4. On submerged hydraulic jump characteristics, they used the method called the Developed Group Method of Data Handling and compared with the Group Method of Data Handling model. They trained and tested both models with experimental data to predict relative submergence depth, jump length, and relative energy loss. They reported that the DGMDH model, combining regression and intelligent neural networks, provided more accurate predictions than the GMDH model. Hence, they recommend using DGMDH to estimate submerged hydraulic jump characteristics in hydraulic engineering.

Wuthrich, Shi, et al. (2022) [90] presented hydraulic jumps with low inflow Froude numbers i.e., 2.1 and 2.4, exploring their air-water flow properties under high Reynolds number conditions. They involved experimental tests using dual-tip phase-detection probes and high-speed video cameras for capturing characteristics features such hydraulic jump surface patterns, voids percentage, bubble formation rate, and interfacial velocities. They showed that data from the sidewalls might not accurately reflect the behaviour at the centre, especially regarding air entrainment and flow dynamics, as sidewalls tend to affect flow properties differently. They concluded that hydraulic jumps with low Froude numbers were found to be effective energy dissipators, contributing valuable insights to the design of hydraulic structures for long-term operation.

Wiest, Júnior, et al. (2020) [82] proposed a procedure for initiating an advancing hydraulic jump with a sloping front at specific points on a Creager spillway. They performed experiments using a two-dimensional model of a hydroelectric power plant's spillway and stilling basin. Their experimental results allowed them to develop an equation that accurately predicts the start position of the hydraulic jump. That equation was validated through experimental data and comparisons with previous studies. They found that the jump's position is primarily influenced by the incident Froude number and the submergence factor.

Recent research on hydraulic jumps shows that turbulence, air entrainment, and energy dissipation are strongly influenced by scale, Froude number, slope, and channel geometry. Full-scale models and advanced CFD methods like DES and VOF provide accurate flow predictions. Machine learning and numerical models improve jump location and length estimates, while experiments highlight the importance of turbulence and bubble dynamics. Overall, understanding scale effects, flow conditions, and turbulence modelling is key for reliable hydraulic jump design

2.3 Hydraulic jump in triangular or trapezoidal channels

(Kateb, Debabeche, et al. (2015) [54] investigates the hydraulic jump in a sloped trapezoidal channel through theoretical and experimental methods. They conducted experiments in a trapezoidal channel at five different positive slopes ranging from 0% to 2% for wide range of Froude numbers from 3.5 to 14.5. The experimental data helped refine the theoretical relation. They derived the theoretical relationships or expressions in terms of the inflow Froude number and do sequent depth ratio, channel slope or steepness. They concluded that the sequent depth ratio increases with an increase in the channel slope.

Debabeche, Cherhabil, et al. (2009) [40] used both theoretical and experimental methods to investigate the impact of the channel slope on sequent depth ratio in an open channel triangular channel with six positive slopes of the channel of 0%, 2%, 5%, 10%, 15% and 20%. they developed an expression for inflow Froude number in terms of sequent depth ratio and channel bed slope. From this they obtained an expression which related the sequent depth ratio, as well as the length of the jump, to the channel slope. A correction coefficient was introduced to account for discrepancies between the theoretical and experimental jump volumes. This coefficient was reported invariant and hence not affected by the Froude number and

the channel slope. They confirmed the published data that even the slope of the triangular channel remains affecting the sequent depth ratio of the hydraulic jump.

Hager and Wanoschek (1987) [29] investigated hydraulic jump in a channel of semi triangular cross-section and compared it with a rectangular cross section. They described that the horizontal velocity profiles and the free surface forms are characteristically different in the case of the triangular channel. However, here the sequent depth ratio was observed to be lesser than that identified in the case of the rectangular channel. It was found that the efficiency of energy dissipation in the conical channel was approximately 30% higher in comparison with one realized in a flat channel. Further it was observed that the distance jumped over by the mass was of equal to one half of the length of the rectangular channel. Despite the fact that the triangular channel was 1.39 times shorter than the rectangular one, the volume of the hydraulic jump was 30% more. A wider surface width at the onset of the jump was observed in the triangular channel, and may cause limitation in the available lateral space. The hydraulic jump in the triangular channel was less sensitive to small changes in the discharge but more sensitive to small changes in the tailwater compared to the rectangular channel.

Above studies investigate how channel slope and cross-sectional shape influence hydraulic jump characteristics, particularly the sequent depth ratio, jump length, and energy dissipation. They show that increasing slope generally increases the sequent depth ratio, while channel shape affects velocity profiles, jump length, and energy dissipation efficiency.

2.4 Hydraulic jump in expanding channels

France (1981) [26] examined hydraulic jumps occurring in a rectangular gradually varied channel. In his study he took into consideration the divergence angles of up to 8.7° and no bottom slope. The objective of such jumps was to compare it with the conventional hydraulic jumps that occur in prismatic channels. He derived theoretical equation to compute sequent depth ratio factoring the influence of effective Froude number and side pressure forces. He reported that the parameter was invariant with the angle of divergence but when angle of divergence was increased a lot more fluctuation in the jump stability was experienced. He concludes that energy dissipation in diverging hydraulic jumps is greater than energy dissipation in converging hydraulic jumps and this difference increases with the initial Froude number. Furthermore, the height of the jump was also shorter by up to 40 % when compared to what is referred to as the classical hydraulic jump. Unlike a parallel channel, it is observed that the relative energy loss can increase up to a maximum of about 12%. The overall length of the hydraulic jump that was observed was relatively shorter than the length calculated using the theoretical model. He concluded that, by using diverging rectangular channels, energy can be well discharged through hydraulic jumps.

Alhamid and Negm (1998) [32] proposed an easy mathematical model to predict the sequent depth ratio of hydraulic jumps in abruptly widening rectangular channels. From the collected experimental data and analytical tool, they analysed the cause-effect relationship of different parameters associated with hydraulic jump. They developed an equation based on the application of one-dimensional momentum and continuity equations adjusting the classical Belanger equation by the effects of sudden expansion through Froude number, and finally they mentioned that derived equation

provides the simplest and more effective method to predict sequent depth ratio compared to other models. Despite the fact that the algorithm of its application is very simple, it can be helpful in designing such hydraulic structures as stilling basins. Their results indicate that the new models would be 'design friendly' indicating that design of improved models is highly achievable. The most significant impact was recorded concerning the sudden expansion they realized had a negative impact on stability.

Omid, Esmaeeli Varaki, et al. (2007) [35] proposed a theoretical and experimental investigation of the hydraulic jumps in trapezoidal channels with gradually expanded stilling basins. They were able to advance the basin by enhancing the width of its bed in the stream wise direction. Angles of expansion ranged from 3 to 9 degrees and trials were conducted on three different side slopes. They conducted experiments in a laboratory setting with a channel equipped with adjustable side walls to simulate various angles and side slopes. They measured upstream and downstream depths, jump length, and flow conditions, with Froude numbers ranging from 3 to 10. They have presented a one-dimensional momentum equation, which could be used to predict the sequent depth and energy loss in a trapezoidal channel. They reported the surface profile of the jump was approximated by a quarter-elliptical shape. The stability of the hydraulic jump improves with increased expansion angles, especially at higher Froude numbers. Increasing the expansion angle reduces the sequent depth and jump length while increasing energy loss in the jump. Similarly, decreasing the slope of the basin walls leads to smaller sequent depth but larger jump length and energy loss. Divergence of the basin results in higher energy dissipation compared to hydraulic jumps in rectangular or trapezoidal sections with unchanging dimensions.

Valiani and Caleffi (2011) [43] analysed the conservation of both linear and angular momentum within diverging channel, particularly in turbulent flow conditions, and developed an analytical solution to describe the flow profile and sequent depths in a hydraulic jump. They investigated the interaction stresses between the roller and the mainstream, revealing that these stresses increase sharply at the start of the jump before gradually decreasing, consistent with turbulent jump behaviour. They developed equations for calculating the flow's free surface profile, mainstream and roller thicknesses, and power losses.

Chanson (2012) [46] used field data, including measurements from natural and artificial channels, to test theoretical solutions for dynamics of hydraulic jumps, particularly for irregular channels. He highlighted that the shape of the channel and bed friction significantly impact flow properties. In non-rectangular channels, the effects of flow resistance yield a smaller ratio of conjugate cross-sectional areas for a given Froude number. The reported that field data showed deviations in the Froude number calculation by up to 74% from traditional methods, depending on channel shape and flow resistance.

Esmaeili Varaki, Kasi, et al. (2014) [52] conducted a series of experiments in a flume with various bed slopes and diverging angles to study the parameters of the hydraulic jump including sequent depth, jump length, energy loss at the jump under various Froude numbers. They developed a momentum-based theoretical model to predict the sequent depth ratio and compare it with experimental data. The model assumes parabolic water surface profiles and neglects frictional forces. They showed

that increasing the adverse slope and divergence angle reduces the sequent depth and jump length while increasing energy loss compared to classical hydraulic jumps. The sequent depth decreases by up to 51%, and the jump length by up to 38% and energy loss increases by up to 23% with the highest divergence angle and bed slope.

Hassanpour, Dalir, et al. (2017) [63] performed experiments for hydraulic jumps at the zone of transition from a wide rectangular channel to wider, lozenge-shaped channel with divergence ratios of 0.4, 0.6, 0.8, and 1. They examined the post jump depth, the length of jump, length of roller and by changing the inlet Froud numbers in the range of 6 to 12. They stated that the relative length of hydraulic jump is found to depend on the magnitude of relative Froude number and divergence ratio. However, when the ratio of roughness elements increase, the length of the jump reduced as observed earlier. On the other hand, the further apart is the divergence ratio, the greater is the relative energy loss.

Eshkou, Dehghani, et al. (2018) [66] investigated the characteristic of hydraulic jump in a gradually varied area of channel provided with series of inclined baffle blocks. They said that baffle blocks offer even better jump characteristics than the open diverging channel in the absence of baffle blocks. Furthermore, they also discovered that the manner in which the baffle blocks are arranged systematically in a converging manner towards the flow direction enhances the properties of jumps. They undertook an experiment of the variety of angles that were tried (10, 20, 30, 40, 50, 60, 70, 80) of which the only convergence angle of 30 degrees was able to factor the top-quality results. In this case the average depth of the jump is reduced by approximately 16% and the average length of the jump reduced by approximately 35% on average.

Torkamanzad, Dalir, et al. (2019) [72] discussed how roughness elements and abrupt asymmetrical expansions affected the jump length, sequent depth, energy dissipation and stability of the jump when compared to classical hydraulic jumps in smooth, rectangular channels. They undertook a number of tests in an open and extended channel that included four physical models of different expansion rates. To generate different types of rough bed conditions, they considered two values of heights of element's roughness equal to 1.4 and 2.8 cm. According to the data obtained, the post jump depth and jump length outcomes were decreased with the roughness height increase and the expansion ratio decrease.

Hassanpour, Dalir, et al. (2021) [88] provided an experimental study of pressure variation in spatial hydraulic jump that develops in stilling basins with different expansion ratio. They conducted experiments in a rectangular flume with varying expansion ratios i.e., 0.4, 0.6, 0.8, and 1 to simulate hydraulic jumps. They used pressure transducers to measure pressure fluctuations at 31 points along the centreline of the stilling basin. They observed that pressure fluctuations increased significantly near the hydraulic jump toe and then decayed downstream. The Froude number strongly influenced pressure fluctuations, with larger Froude numbers leading to higher pressure fluctuations. The maximum root means square values vary with different expansion ratios, with the highest observed at an expansion ratio of 0.8.

Hydraulic jumps in diverging channels show reduced sequent depth and jump length but increased energy dissipation compared to classical jumps. Higher divergence angles and Froude numbers amplify these effects. Channel shape and roughness affect stability and energy loss. Adjusted momentum-based models better predict jump behaviour than classical ones. Increased turbulence and pressure fluctuations near the jump require careful design of stilling basins.

2.5 Hydraulic jump over natural & artificial rough channel bed

Hughes and Flack (1984) [27] conducted various experiments in a horizontal rectangular flume with smooth sidewalls to investigate the characteristics of hydraulic jump over rough and impervious beds. They used 5 long test beds, one plain and 2 strip roughened beds and 2 densely packed gravel beds. The maximum relative roughness value was set to 0.9. The researchers recorded flow rate, upstream depth, tailwater depth, and jump length from roughly 200 hydraulic jump observations. They noted that the behaviour of the shear stress and sequent depth ratio over a roughened bed varied with the initial Froude number in different ways. In particular, the shear stress grew with the decrease of the sequent depth ratio when the first Froude number augmented.

Ead and Rajaratnam (2002) [34] studied the dynamics of hydraulic jumps on particular types of channels called corrugated beds, during a series of experiments in the laboratory. They proceeded with experiments at four Froude numbers of 4 to 10 with relative roughness range of 0.25 to 0.50. They pointed out that deep of tail water needed for the formation of jump on corrugated bed was relatively small when compared to the depth needed for the formation of jump in smooth beds. They said that that hydraulic jumps on corrugated beds were almost 50% the length of that in smooth beds and also observed that the shear stress was about 10 times as much in corrugated beds as in smooth beds. Axial velocity profiles in the jump were also compared to the jump in the smooth beds but with some disparity. The boundary layer thickness relative to the length scale of the velocity profile grew faster on corrugated beds compared to smooth beds. They indicated that hydraulic jumps on corrugated beds could be highly effective in dissipating energy, making them an attractive option for energy dissipators under hydraulic structures. However, they suggested further exploration of the effects of corrugation amplitude and wavelength.

Tokyay (2005) [20] investigates the effect of corrugated channel beds on hydraulic jumps characteristics such as jump length, energy dissipation, tailwater depth, and jump location through experimental research. He used two corrugated aluminium sheets with different wave lengths and heights and a rectangular channel of certain dimensions. He disclosed that the depth of the tailwater needed to develop the hydraulic jump on corrugated beds was roughly 20% less than on smooth beds. The recorded height of the jump was approximately 35% lower over corrugated beds than the height over smooth beds. It was found that jumps, made on corrugated beds, exhibit higher energy dissipation, thus making them suitable for energy dissipation. He confirmed that corrugations can be an effective alternative to traditional structures like baffle blocks and sills in stilling basins.

Carollo, Ferro, et al. (2007) [36] investigated hydraulic jump in a rectangular channel. They assessed rough beds in form of artificial and natural stones.

These stones were characterised by different grain size distributions and the grain size values varied between 0.46 to 3.20 cm. They carried out only experimental work to validate the new solution of the momentum equation for the sequent depth ratio and to assess the empirical relation for the roller length. They also discovered that at some Froude number and particle roughness height the sequent depth ratio was less than the sequent depth of a smooth channel bed.

Abbaspour, Hosseinzadeh Dalir, et al. (2009) [38] examined the effect that wave steepness of the corrugated wall had on hydraulic jump features like the location of the free surface, the fluid velocity and the shear stress as well as energy dissipation rates. They varied initial Froude numbers from 3.8 to 8.6 for six different quantities of corrugated beds, where each of those values corresponded with a set wave steepness ranging between 0.286 to 0.625. They noted that the flow and the length of jump are substantially lower over the corrugated bed than in the smooth channel bed. The depth of the tailwater depend on the Froude number although the wave steepness does not have any effects. On the corrugated bed, the normalised boundary layer thickness was found to be 0.57. The stress distribution in the corrugated beds was seen to be about 10 times of smooth beds. They reported that the application of corrugated beds at stilling basins can be useful in the dissipation of hydraulic jump energy.

Abbaspour, Farsadizadeh, et al. (2009) [39] evaluated hydraulic jumps on corrugated beds using computational fluid dynamics (CFD) and turbulence modelling. They used the two-dimensional RANS equations for flow predictions, VOF to capture free surface. They utilized two equation k-ε turbulence models to simulate the turbulent characteristics of the hydraulic jump. They found good agreement between simulated and experimental data with relative errors between 1% and 8.6% for water surface profiles. The jump length predictions had errors ranging from 1% to 12%. The RNG k-ε model provided a slightly better match with experimental data in contrast to the k-ε model (standard). They found corrugations on the bed effective to reduce the length of the hydraulic jump and tailwater, mitigating cavitation risks by keeping crests below the flow.

Elsebaie and Shabayek (2010) [41] investigated hydraulic jump on various shapes of strip corrugation to understand jump characteristics. These shapes comprised of sinusoidal, triangular, and trapezoidal with two side slopes and rectangular. They used variables like sequent depth, length of jump, depth deficit factor, velocity at the different sections of the channel and the bed shear stress. They considered Froude number ranging from 3 to 7, and the relative roughness values of 0.36 and 0.72 in their study. They showed that the amount of jump length for corrugated beds was 50% shorter than of that for the smooth beds. This was due to the fact that, because of the bed's corrugations, the bed shear stress increased. Comparing the integrated bed shear stress on corrugated beds and on smooth beds, the latter was reported to be more than 15 times less than the former. The dimensionless depth deficit, which reflects the difference between classical and corrugated bed jumps, was consistently around 0.37 for all bed shapes. It was ascertained that the shape of the corrugation had a very small effect on the hydraulic jump behaviour in spite of constant amplitude and wavelength of the corrugation. They confirmed that the corrugated beds have ability to dissipate energy below hydraulic structures.

Tokyay, Evcimen, et al. (2011) [44] carried out experiments to study the impact of corrugations and prismatic roughness elements on hydraulic jumps, focusing on characteristics like jump length, tailwater depth, and energy dissipation capacity. They covered the entire basin length and with prismatic roughness elements arranged in either strip or staggered configurations They reported that roughness elements significantly reduced the hydraulic jump length. More specifically, corrugations reduced it by about 35%, strip roughness by 40%, and staggered roughness by 35-55%. Corrugations lowered the tailwater depth by 20%, strip roughness by 5-13%, and staggered roughness by 7-15% compared to a classical hydraulic jump. Roughness elements also improved energy dissipation, with an increase of 3-10% over classical jumps which makes them viable alternatives to traditional stabilization devices like baffle blocks and sills.

Afzal, Bushra, et al (2011) [45] presented a detailed analysis of the flow structure of a turbulent hydraulic jump in the wide channel with a rough bed. They focused on dividing the flow into inner and outer layers and using depth-averaged momentum equations to analyse the jump in case of rough beds. They reported that the bed roughness only passively influences the flow in the outer layer. The jump characteristics such as conjugate depth ratio, length of jump, and length of roller can be universally described by relations that were independent of the bed roughness when expressed in terms of the effective upstream Froude number. They established several new empirical relationships for roughness drag based on relative roughness.

Tokyay and Velioğlu (2012) [47] examined the impact of various components of bed roughness on the properties of jumps. They stabilized jump locations and reduced stilling basin lengths using alternative roughness elements, such as corrugations, strip, staggered roughness elements, and gravels. According to them, corrugations cause a reduction in jump length by between 20% and 25%, gravels by 20%, strip roughness by 30%, and staggered roughness by between 35% and 55% compared to the classical hydraulic jump. Also, Roughness elements increase energy dissipation by 3-15% more than classical jumps, with gravels being the most efficient at inducing energy loss. The roughness types effectively stabilized jump locations, making them viable alternatives to traditional baffle blocks and sills. They suggested that incorporating roughness elements like gravels and corrugations can significantly enhance the performance of hydraulic jumps in terms of reducing jump length and increasing energy dissipation.

Samadi-Boroujeni, Ghazali, et al. (2013) [48] concentrated in order to determine the influence of triangular corrugated beds on the parameters of hydraulic jumps in a rectangular channel. They conducted 42 tests in a 12-meter-long, rectangular flume using six different triangular corrugated bed configurations. The tests were performed for Froude numbers ranging from 6.1 to 13.1. The authors pointed out that corrugated bed minimizes the conjugate depth by 25% and the hydraulic jump length by a 54.7% compared to smooth beds. They observed that the shear stress on the corrugated bed was about 8.5 times more than that of the smooth beds. The relative height and shape of the corrugations has no significant effect on reducing both tailwater depth and jump length, indicating that no specific corrugated configuration could optimize both parameters simultaneously. They suggested that

optimizing both depth reduction and jump length with a single corrugated sheet is not feasible.

Abbaspour, Farsadizadeh, et al. (2013) [49] discussed possible approaches for using soft computational modelling like artificial neural networks and genetic models to predict some features of hydraulic jumps, for instance, the position of the free surface and energy dissipation on corrugated beds. They conducted 123 experiments on hydraulic jumps formed on a corrugated polyethylene bed to gather data. The experimental setup featured various combinations of Froude numbers and bed roughness heights, among other variables. Using these data, they developed models with artificial neural networks and genetic modelling, intending to estimate the jump depth, length and energy dissipation employing Froude number and dimensions of corrugation. Their analysis revealed that the artificial neural networks model provided better accuracy compared to the genetic model, especially in estimating jump characteristics. The artificial neural networks model was able to achieve higher correlation coefficients and lower errors. The genetic model, while practical for producing mathematical relationships, was found to be less precise in comparison.

Ahmed, El Gendy, et al. (2014) [51] focused on how corrugated beds affect the properties of hydraulic jumps specifically for submerged jump. They conducted experiments in a laboratory using a flume with a streamlined-lip gate to develop the required supercritical flow. They used aluminium triangular sheets to create the corrugated bed. The corrugation dimensions were 40 mm in height and width with a side angle of 45°. Thirty overall experimental runs were conducted in total and covering both smooth and corrugated beds with recorded minimum Froude number of 1.68 and a recorded maximum of 9.29. They reported that the relative sequent depth over corrugated beds reduces compared to smooth beds. An optimal spacing of 12 cm between the corrugations resulted in a reduction in sequent depth by approximately 15–17%, depending on the Froude number. The submergence depth reduces by 18–38% over corrugated beds compared to smooth beds. The depth of the water downstream also decreased by up to 15% at the optimal corrugation spacing compared to the smooth bed. It was noted that the bed length was reduced by a maximum of 28% on the corrugated beds. The efficiency of the hydraulic jump increased by up to 50% for corrugated beds compared to smooth beds, with an optimal spacing of 12 cm providing the maximum efficiency.

Mahtab and Sattari (2016) [59] confirmed the M5 Model Tree over rollers length and sequent depth of the smooth and rough beds. The statistical results of the modelled tree on the M5 Model Tree, ANN and the empirical–based equations for sequent depth ratio were then compared. Regarding the plans of inference, they identified that the ratio of complexity level of the sequent depth proposed by the M5 Model Tree is straightforward and accurate.

Abbaspour, Parvini, et al. (2016) [62] gave a realistic model to solve the problem of erosion of beds by the provision of buried plates in the channel bed. They placed buried plates on the range of distances from the apron in the open channel with both slope of the horizontal and reverse bed. They also discovered that through the proper positioning and orientation of the plates, scouring was well controlled and reduced. Besides, while comparing the results obtained in case of a single buried plate

with that of two buried plates, they found that the effectiveness of the two buried plates placed at 30 cm and 45 cm below the non-erodible bed was significantly higher than the single buried plate in reducing the depth of scouring.

Bejestan and Hajibehzad (2018) [64] conducted an experimental study of hydraulic jumps of the B-F type formed on rock cascades. They introduced a new dimensionless parameter with an intention of developing the impacts that are driven by the jump toe as well as the roller length. This is because they identified that when the chute gradient was variable and the stilling basin slope definitive the changes in the quantity of the variable often led to a fall in the sequent depth ratio. Thus, the ratio of sequent depth decreases, when the value of relative roughness increases for the fixed value of variable.

Felder and Chanson, (2018) [67] investigated the motion of the air–water mixture and some general features of the flow in a hydraulic jump over a rough regular bed with large equally spaced protuberances and smooth bed. They considered Froude numbers between 1 and 10.5 to 6.3 in their study. From these observations, they found that bubble count rate and void fraction near the jump toe increased during the first several minutes of the hydraulic jump when macroroughness was applied. In the second half, the cross-sectional area of the bed of the water course increases unevenly and up to a part that was as clear as 50 meters downstream strong indications of turbulence were observed.

Kumar, Kumar, et al. (2019) [71] studied the impact of the roughness heights and slopes on the response of hydraulic jump like sequent depth ratio using laboratory and numerical experiments. They applied Artificial neural network (ANN) as a numerical technique. Two positive bed slopes and crushed, rounded aggregates were used to attain needed roughness at the flume bed. At the same flume condition, they noted that crushed aggregates lower the sequent depth ratio by a factor of 35% in contrast with rounded aggregate. However, it was observed that the sequent depth ratio is approximately 45 percent less as the bed slope is increased.

Studies on hydraulic jumps over rough and corrugated beds commonly highlight improved performance compared to smooth beds. Rough beds effectively reduce the length and depth of hydraulic jumps while enhancing energy dissipation and increasing bed shear stress due to greater turbulence. These modifications lower the tailwater depth required for jump formation and offer a practical alternative to traditional energy dissipation devices like baffle blocks. While the shape of the roughness elements has minimal influence, factors such as spacing, amplitude, and bed slope are more significant in affecting jump characteristics. Some researchers suggest that roughness mainly influences the inner flow layer, and computational models have shown reliable accuracy in simulating hydraulic jump behaviour over rough beds.

Ghaderi, Dasineh, et al. (2020) [76] performed a numerical study of free and submerged hydraulic jump with and over three types of roughness in an open channel. These shapes were triangular, square and semioval in shape. They used these shapes in form of strips which were provided along the width of the flume. In this research, they employed the RNG k-ε turbulence model in order to predict the size of turbulence. They pointed out that among the three types of roughness which have been

tested that the triangular roughness improves the jump characteristics more than the other two.

Mahtabi, Chaplot, et al. (2020) [78] analysed the classification of hydraulic jump over rough beds employing a novel method based on a decision tree. They employed 581 data sets with 280 drawn from the natural rough bed and 301 from the artificial rough bed. That used to analyse these data, they categorized these into four groups that are A, B C and D based on the energy that was lost. They pointed out that a condition signified by the rough bed had large impact to the stability of the bed shear stress which in turn enhance the lost energy every time the initial Froude number was raised.

Macián-Pérez, Vallés-Morán, et al. (2020) [80] analysed the spatial shape of the free surface together with velocity field of a hydraulic jump in a USBR II stilling basin to improve understanding of energy dissipation in these structures. They conducted an experimental campaign using innovative tools like a pitot tube and a time-of-flight camera to measure the free surface profile and the general velocity field of the flow. They discussed the strengths and limitations of the experimental tools. The LIDAR provided accurate free surface measurements despite limitations like splashing, while the Pitot tube had difficulties capturing velocities in highly aerated areas. They demonstrated that the maximum velocity within the hydraulic jump is affected by the energy dissipation devices, which cause the maximum velocity to occur near the channel bottom, unlike classical hydraulic jumps. Finally concluded that the hydraulic jump in the stilling basin was found to have a lower sequent depth ratio and higher energy dissipation efficiency compared to classical jumps.

Nikmehr and Aminpour (2020) [81] applied a 2-phase flow theory, utilizing the FLOW-3D software. They used the VOF (Volume of Fluid) method and RNG turbulence models to simulates hydraulic jumps over rough beds in a rectangular flume. They reported that rough beds significantly affect hydraulic jump characteristics by reducing sequent depth and jump length, and by modifying the velocity distribution. They compared the numerical data against experimental data to verify accuracy, particularly focusing on the water surface profile and discharge measurements and reported that numerically derived hydraulic jump length and roller length closely matched experimental data, with mean errors of 4.8% and 10.85% respectively. Therefore, numerical models like FLOW-3D are effective for simulating hydraulic jumps.

Maleki and Fiorotto (2021) [85] presented a novel method to define hydraulic jump characteristics over rough beds taking into account both the Froude number and bed roughness. They found that approximately 35% reduction in hydraulic jump length when boulders or gravel protect the bed, minimizing erosion and cavitation. Their analysis reveals that the integrated bed shear stress depends on the Froude number.

Turker and Valyrakis (2021) [87] intended to evaluate and measure such effects scientifically in terms of the channel bed roughness on hydraulic jumps. They introduced new definitions and models, particularly for the shear force coefficient and roller length, validating their findings through experiments. They conducted 60

experiments using a flume, roughening the channel bottom with different sizes of sand and gravel to observe how various bed roughness levels influence hydraulic jump characteristics. They found that as bed roughness and flow turbulence increase, the length of the hydraulic jump reduces, with the shear force coefficient directly related to bed roughness. They also noted that for Froude number between 1.1 and 9.8, both shear force coefficient and roller length estimated fairly close to the experimental values.

Ghaderi, Dasineh, et al. (2021) [18] conducted numerical simulations to investigate the flow properties of the submerged jump over macrorough beds specifically in triangular strip macroroughness. They used the FLOW-3D model to explore several parameters, including streamlines and flow patterns, velocity profiles, energy loss, turbulent kinetic energy (TKE), shear Stress. They reported that maximum flow velocity occurs closer to the bed in submerged jumps compared to free jumps over smooth and rough beds. Further, distance between triangular macroroughnesses significantly influences the flow behaviour and triangular macroroughnesses increase bed shear stress and energy loss more than smooth beds. They validated the simulation findings against experimental results with a maximum error of 8.41% and a mean relative error of 4.83%.

Dasineh, Ghaderi, et al. (2021) [89] predicted the properties of jumps on triangular strip rough bed using both soft computing methods and numerical modelling. They utilized Computational Fluid Dynamics (CFD) via the FLOW-3D software to simulate hydraulic jumps on triangular bed roughness under various hydraulic conditions. They reported that the FLOW-3D® model showed a mean relative error of 4.1%, indicating a strong predictive capability. To verify the effectiveness of the CFD model's, they employed three artificial intelligence methods such as Support Vector Machines, Gene Expression Programming, and Random Forest. Among the soft computing methods, SVM was identified as the most accurate, with the lowest root mean square error and highest correlation coefficient. They concluded that hydraulic jumps on rough beds exhibited smaller sequent depths and shorter lengths compared to smooth beds, leading to greater energy dissipation.

Parsamehr, Kuriqi, et al. (2022) [91] conducted a comprehensive experimental investigation on hydraulic jumps occurring downstream of hydraulic structures. They tested various roughness elements on horizontal and adverse bed slope of -1.5% and -2.5% to study their effects on jump properties, such as energy dissipation, post jump depth ratio, and roller length. They found that both increased slope steepness and roughness height enhanced energy dissipation by forming larger size eddies and huge turbulence, significantly reducing the sequent depth ratio. The energy loss with roughness elements ratio of 1.33 on a -2.5% slope was 19.6% higher than that of a classical hydraulic jump. Also, the bed shear coefficient increased by 12.4 times compared to a smooth bed on a -2.5% slope.

Bahmanpouri, Gualtieri, et al. (2023) [92] examined the effects of bed roughness on turbulence properties like intensity, correlation time scales, and advective length scales in a hydraulic jump. They conducted experiments in a rectangular flume where natural river pebbles were placed on the bed for roughness. They captured air-water flow data using phase-detection probes under different

hydraulic jump conditions. They reported that turbulence intensity and the presence of larger eddies were greater on the rough bed, indicating more complex interactions between the air-water flow and bed roughness.

Zaffar and Hassan (2023) [93] used FLOW-3D models to simulate the flow behaviour and hydraulic jumps in wedge-shaped baffle blocks stilling basin. They focused on variables such as ambient surface profiles, length of roller, longitudinal velocity profiles, and turbulent kinetic energies. They reported that the new wedge-shaped baffle blocks stilling basin stabilized the hydraulic jump and shortened the jump lengths compared to traditional USBR-Type III basins. They concluded that the FLOW-3D software successfully simulated and validated the hydraulic behaviour for different stilling basin designs, providing reliable insights into the performance of the new wedge-shaped splitter blocks.

Macián-Pérez, García-Bartual, et al. (2023) [94] investigated the efficiency of stilling basin and more precisely this type of stilling basins that include an abrupt change in the depth through modelling with the help of CFD methods. They analysed six discrete numerical models, each of which they explored with two imaginable relative heights of an abrupt drop. They studied the effect of a decrease in the energy dissipation rate and changes with regard to the dimensions and hydraulic characteristics of the jump. They also looked into the pressures acting on the streambed, and the variation in the pressures. They indicated that the sharp decrease causes low subcritical depths and consequently small basin dimensions and somewhat longer hydraulic jump length. As mentioned earlier it was to the advantage if there was a sudden drop when seeking to control hydraulic jumps in the stilling basin.

The reviewed studies collectively highlight the significant influence of bed roughness, slope, and structural modifications on hydraulic jump characteristics. Numerical models and turbulence models have proven reliable in simulating jump behaviour, closely matching experimental data. Experimental tools, though useful, face limitations in highly aerated regions. Moreover, methods involving artificial intelligence and decision trees have shown promise in predicting jump characteristics with high accuracy. However, several research gaps remain. There is a lack of a unified comparative framework that evaluates various roughness types, slopes, and simulation methods under consistent conditions. Most findings are based on controlled environments with limited field validation, reducing their applicability to real-world scenarios. Additionally, the combined effect of slope and roughness, optimal roughness arrangements, and transitions between free and submerged jumps are not fully explored. Furthermore, while AI has been used for prediction, its application in real-time control and optimization of hydraulic structures remains underutilized. Improved tools and methodologies are needed to address measurement errors in aerated zones and advance the practical understanding of hydraulic jumps.

64

CHAPTER 3

METHODOLOGY

3.1 General

This chapter describes the method that has been used to study the free and submerged hydraulic jumps in a prismatic rectangular channel on smooth and macrorough beds. Figure 3.1 depicts the definition sketch of free and submerged hydraulic jump, along with their associated parameters.

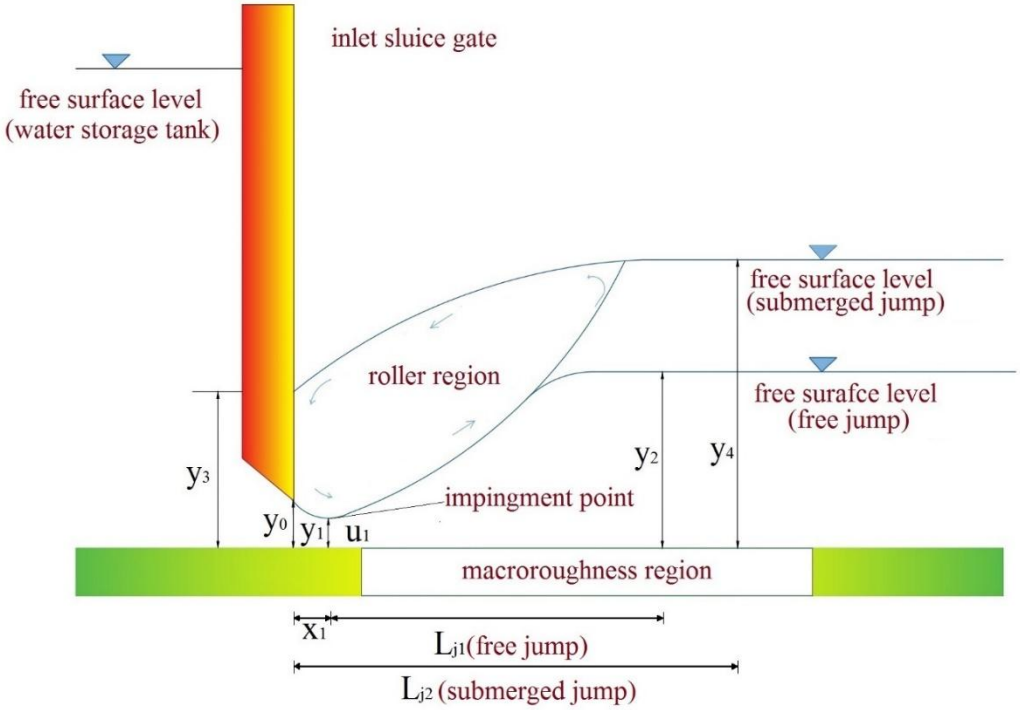

Figure 3.1 Definition sketch of free and submerged hydraulic jump showing relevant parameters

The research work was conducted using numerical simulation and subsequently validated against the physical findings of the present study. It should be noted that the validation was performed for only three specific cases. The initial phase involved conducting physical experimental analysis of hydraulic jump on a smooth bed and two distinct types of artificial macrorough beds, namely triangular and trapezoidal, within a laboratory flume. In addition, numerical simulations were performed using Ansys Fluent R22 software, taking into account the experimental data. The findings of the numerical simulation were compared with experimental findings and previous studies for only three cases. The following sections outline the detailed steps of the experimental and numerical analysis.

3.2 Physical experimental model

In the present work, hydraulic jump phenomenon was studied in an open channel prismatic rectangular flume at Delhi Technological University's hydraulics lab which was 10.0 m long, 0.5 m deep, and 0.5 m wide. Figure 3.2 represents the experimental setup and physical macroroughness prepared with iron material that were positioned across the whole width of the flume up to certain length to create bed macroroughness. For every round of the experiment, the bed macroroughness length was kept constant. On a mild bed slope with varying Fr_1 numbers ranging from 3.5 to 7.0, forty-two runs were conducted. Discharge and velocity were measured with the help of digital discharge meter and digital pitot tube (L-type pitot tube of 6 mm diameter and digital manometer with an accuracy of ±0.5% full scale deflection), respectively. Other relevant measurements such as water depth were done with the help of rail mounted pointer gauges with an accuracy of 0.2 mm. Figure 3.2 represents the experimental setup and physical macroroughness used in experiments. Table 3.1 depicts the parametric variations considered in the present study.

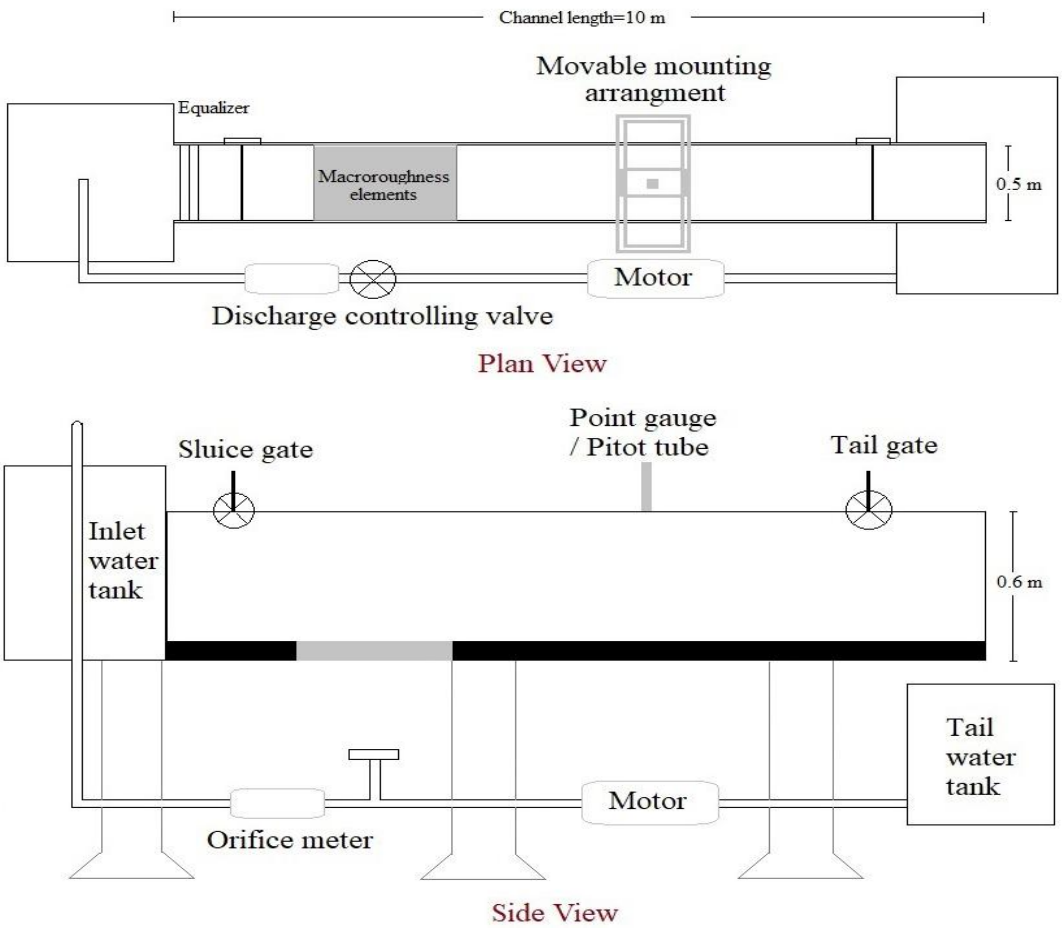

(a)

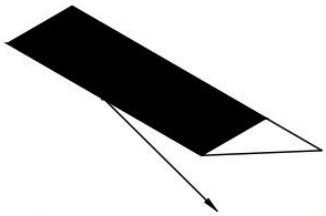

Strip macroroughness

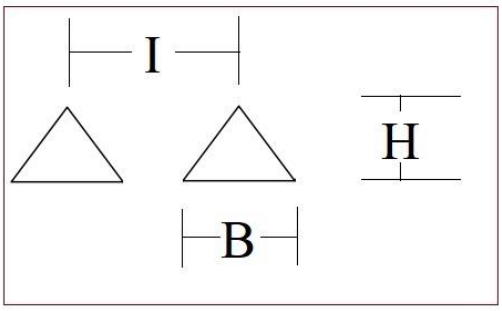

H=0.055 m, B=0.11 m, I=0.22 m

(b)

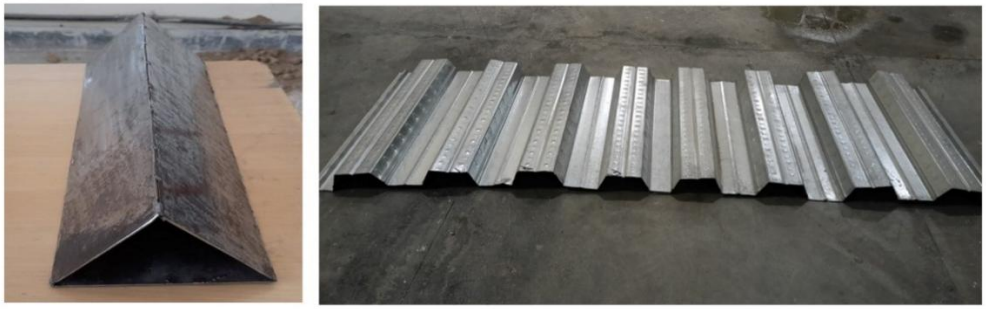

(c)

Figure 3.2 (a) Definition sketch of experimental setup; (b) Definition sketch of strip macroroughness; (c) Physical strip macroroughness elements

Table 3.1 Parametric variations of flow for present study (numerical and experimental)

Bed Type	*Q (l/s)*	y_o *(cm)*	y_1 *(cm)*	*u (m/s)*	Fr_1
Smooth	15-25	2.5-3.0	1.1-1.5	1.24-2.23	3.7-7.0
Rough	15-25	2.5-3.0	1.1-1.5	1.24-2.23	3.7-7.0

3.3 Numerical Simulation

The objective of this study was to employ Computational Fluid Dynamics (CFD) to analyses the hydraulic jump phenomenon in a rectangular open channel, both over smooth and rough beds. The investigation was conducted numerically. Figure 3.3 illustrates the standard procedure employed in numerical simulation.

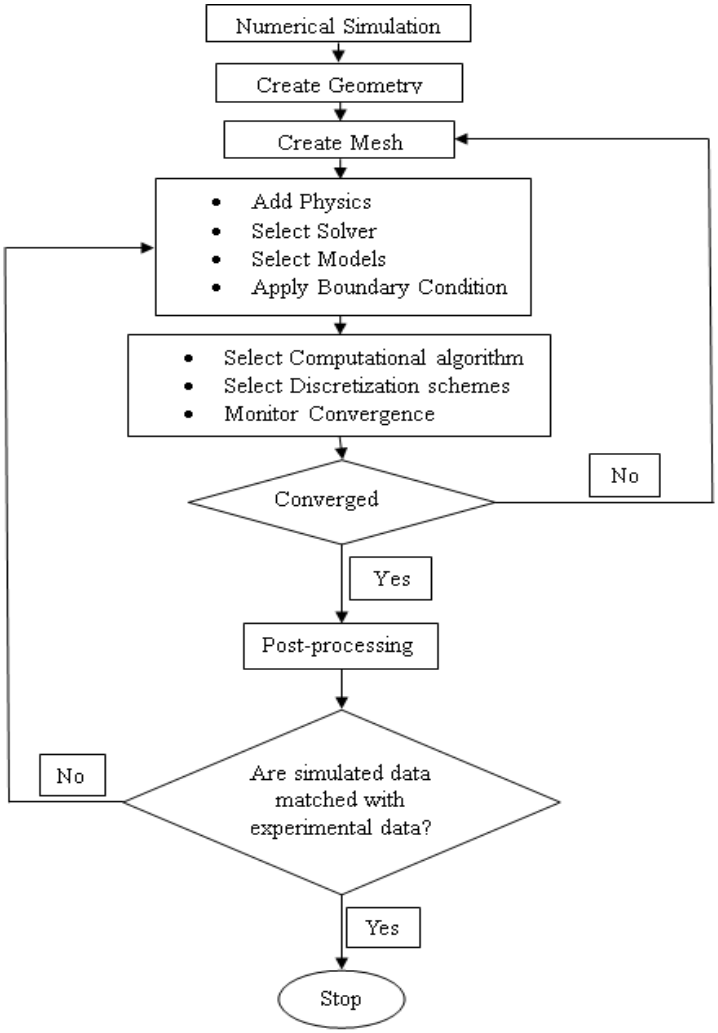

Figure 3.3 Flow chart of adopted methodology for numerical simulation

3.3.1 Governing Flow Equations

The Navier-Stokes equations were historically identified as the momentum equations for a viscous flow. Claude-Louis Navier (1838) [95] first derived the equations from Newtonian mechanics of fluids taking into consideration the forces because of viscosity. However, in the modern context of Computational Fluid Dynamics (CFD) these terms are used to refer to the entire set of flow equations required to be solved for viscous flow. That is as it pertains to continuity, energy, and momentum relations respectively. Consequently, in the CFD literature the phrase

numerical solution to the Navier-Stokes equations is generally understood to mean the numerical solution of the full system of equations. Thus, in the context of CFD literature, 'Navier-Stokes solution' means the solution to the problem of viscous flow wherein the full set of governing equations has been employed.

3.3.2 Navier Stokes Equation

CFD simulation of the fluid flow is based on the Navier-Stokes equations as a primary navigation of the system. Viscous fluid substances can be defined and explained by the set of partial differential equations for their motion. These equations are obtained when applying Newton second law on the fluid flow and considering the forces of viscosity and pressure forces in the fluid.

The continuity equation is as follows;

$$\frac{\partial \rho}{\partial t} + \nabla \cdot (\rho \vec{v}) = 0 \tag{10}$$

The momentum equation is as follows:

$$\frac{\partial}{\partial t}(\rho \vec{v}) + \nabla \cdot (\rho \vec{v} \vec{v}) = -\nabla p + \nabla \cdot (\vec{\tau}) + \rho \vec{g} + \vec{F} \tag{11}$$

Where, ρ is the fluid density, $\vec{v}$ is the velocity vector, p is the static pressure, $\vec{\tau}$ is stress tensor, $\rho \vec{g}$ is the gravitational body force, $\vec{F}$ is the external body force.

Stress tensor, $\vec{\tau}$ is given by

$$\vec{\tau} = \mu \left[(\nabla \vec{v} + \nabla \vec{v}^T) - \frac{2}{3} \nabla \cdot \vec{v} I \right] \tag{12}$$

3.3.3 Volume of Fluid (VOF) Model

The VOF model is utilized to monitor the volume fraction and even predict the extent of each fluid contained in each computational cell. The most important goal to achieve is to accurately represent the geometry and behaviour of the interface between two nonmixing fluids. The method is very efficient for the problems which relate to the interaction between the phases, for example, the flows of free surfaces and the impact of surface tension forces.

Earlier works of Bayon-Barrachina and Lopez-Jimenez (2015) [55] & Ghaderi et al. (2021) [18] used computational fluid dynamics (CFD) technique to track the free surface of the flow. This was made possible through a complicated method known as the volume of fluid (VOF) model to make the animations. In this study, the VOF model has been used as it helps in tracking the volumetric ratio of interface in two-phase gas/liquid applications. In this case, water is a liquid while air on the other hand is a gas. On this basis, the physical classification of matter is made.

Canonsburg (2013 [24] discussed the basic definition and governing equations of Volume of Fluid (VOF) model. Model employs a volume fraction α_q to represent the fraction of a cell that is filled with the q^{th} fluid. In a two-phase system,

the volume fraction α_q of fluid 1, such as water, is defined as follows: In a two-phase system, the volume fraction α_q of fluid 1, such as water, is defined as follows:

- The value of α_q=0 is relevant to that cell in which there is only the second type of fluid, for instance, air.
- α_q=1 corresponds to a cell containing only fluid 1.
- 0<α_q<1 corresponds to a cell containing the interface between the two fluids.

Volume Fraction Equation:

Transitions between the phases occur based on the solution to an equation of continuity associated with the volume fraction of one or more phases. Performance of the model for the q^{th} phase can be described by the following equation:

The equation for the q^{th} phase takes the following form:

$$\frac{1}{\rho_q}\left[\frac{\partial}{\partial t}(\alpha_q\rho_q) + \nabla\cdot(\alpha_q\rho_q v_q) = S_{\alpha q} + \sum_{p=1}^{n}(\dot{m}_{pq} - \dot{m}_{qp})\right] \quad (13)$$

Where $\dot{m}_{pq}$ is the mass transfer from phase q to phase p and $\dot{m}_{qp}$ is the phase p to phase q. The source term $S_{\alpha q}$ is zero by default.

The equation of volume fraction of the primary phase will not be solved for this case. However, the volume fraction of the primary phases will be estimated a priori according to the following constraint:

$$\sum_{q=1}^{n}\alpha_q = 1 \quad (14)$$

Volume fraction equation may be solved either numerically explicitly incorporating time as a variable or using it for iterative computations.

Implicit Time Discretization:

It should be mentioned that in employing the implicit methods the future state of the system is found by solving a system of equations. These methods are usually stable, thereby allowing more forecasts to be made using larger steps than are possible with explicit methods. However, these tasks are computationally more intensive mainly because of the importance given to iterative solvers.

Explicit Time Discretization:

In explicit time discretization one determines the state of the system at the next time step merely utilizing the information of the current time step. What is more,

the implementation of this method is usually easier, and the computational complexity per time step is less. However, to have a stable solution, it is required to take small time steps especially in the problems, which involve high velocities and large gradients.

That is, whether one uses explicit or implicit time discretization depends on the specific requirement of the problem as it pertains to stability, accuracy and computational expense. It is suggested to employ explicit methods if the size of time steps is small because the methods are rather simple and fast. However, implicit methods are more appropriate for use when larger time steps are needed or the system of equations is stiff.

Momentum Equation:

The momentum equation of the VOF model is for the whole mixture and includes contributions coming from both phases:

$$\frac{\partial(\rho\vec{u})}{\partial t} + \nabla\cdot(\rho\vec{u}\vec{u}) = -\nabla p + \nabla\cdot\tau + F \tag{15}$$

where:

- ρ is the density of the mixture, calculated as $\rho = \alpha\rho_1 + (1-\alpha)\rho_2$, where ρ_1 and ρ_2 are the densities of fluids 1 and 2, respectively.
- p is the pressure.
- τ is the stress tensor, incorporating the effects of viscosity, calculated as $\tau = \mu\left(\nabla u + \nabla u^{T}\right)$, where μ is the dynamic viscosity of the mixture.
- F includes body forces such as gravity and surface tension.

Energy Equation:

The energy equation, also shared among the phases, is shown below;

$$\frac{\partial}{\partial t}(\rho E) + \nabla\cdot(\vec{u}(\rho E + p)) = \nabla(k_{eff}\nabla T) + S_h \tag{16}$$

The VOF model treats energy, E, and temperature, T, as a mass-averaged variables.

The parameters, ρ and k_{eff} are all per phase. The source term S_h which resides on the right-hand side includes the effects due to radiation as well as any other volumetric heath source, as well as any other volumetric heat source.

The simulation of multiphase flows in Ansys Fluent requires careful consideration of surface tension and wall adhesion. These parameters are particularly important when dealing with immiscible fluids. For the water-air interface, the Surface Tension Coefficient was set to 0.072 N/m. To accurately model the effect of open channel flow, the Open channel sub-VOF model was selected. The above model covers

for the situation that arises due to the existence of free surface between the fluid in motion and the fluid on top of the former.

3.3.4 Turbulence models

To study the hydraulic jump characteristics using CFD it has become imperative to simulate the flow using right techniques. That is why RANS equation is obtained from the Navier-Stokes equation. Here the velocity and pressure fields are described simply as the meantime and adding a fluctuating term (Gualtieri and Chanson 2021) [84].

Turbulence modelling is the most demanding tool in Fluent software for the simulation of fluids and it is used particularly when the turbulent flow is disturbed and chaotic. There are two commonly used turbulence models: These models are split into the zero-equation model and the two equation models. Zero equation model is regarded to be the simplest form of the turbulence modelling as a matter of fact. It is known by the names of Algebra of Mixing, Algebraic Model, or Mixing Length Model. This model is based on log laws and can be used for the simplest and highly deterministic turbulent, thus it is applied when the nature of the flow is rather evident. There is no other transport equations solved for turbulence quantities. Two Equation Models are well acclaimed and widely used for variety of turbulent flows. These models incorporate two extra transport equations to consider the impact of turbulence: There are common variables such as the turbulence kinetic energy (k) and another for the turbulence dissipation rate (ε) or specific turbulence dissipation rate (ω). Ansys Fluent offers two commonly used two-equation models: two models, of which the first is known as the k-ε model and the second as the k-ω model.

Lu et al. (2022) [96] in their study devoted to the sensitivity analysis of the mesh and turbulence using the Ansys Fluent software. They concentrated on a nuclear fuel bundle in a standard pressure flume and explored how the decision of the meshing technique and the turbulence models can influence the results of velocity profile predictions. Such factors are known to have a very close and direct relationship to such outcomes and their discoveries supported this fact.

According to Bayon-Barrachina and Lopez-Jimenez (2015) [55], the RNG k-ε model gives better result in analyzing hydraulic jumps than other models consisting of SST k-ε and standard k-ε. Nikmehr and Aminpour (2020) [81] checked the reliability of the RNG k-ε model by conducting numerical simulation of hydraulic jumps over trapezoidal rough beds. Further numerical analyses of hydraulic jumps in macrorough bed conditions carried out by Ghaderi et al. (2021) [18] suggest that the RNG k-ε model is rather similar to the standard k-ε model, although there are some differences. Canonsburg (2013) [24] suggest that this model provides better modelling of whirling. The present study compared standard k-ε, RNG k-ε, Realizable k-ε, and SST k-ω turbulence models to get the best turbulence model.

Transport Equation for the Standard k-ε model:

$$\frac{\partial}{\partial t}(\rho k) + \frac{\partial}{\partial x_i}(\rho k u_i) = \frac{\partial}{\partial x_j}\left[\left(\mu + \frac{\mu_t}{\sigma_k}\right)\frac{\partial k}{\partial x_i}\right] + G_k + G_b - \rho\varepsilon - Y_M + S_k \qquad (17)$$

$$\frac{\partial}{\partial t}(\rho\varepsilon) + \frac{\partial}{\partial x_i}(\rho\varepsilon u_i) = \frac{\partial}{\partial x_j}\left[\left(\mu + \frac{\mu_t}{\sigma_\varepsilon}\right)\frac{\partial \varepsilon}{\partial x_i}\right] + C_{1_\varepsilon}\frac{\varepsilon}{k}\left(G_k + C_{3_\varepsilon}G_b\right) - C_{2_\varepsilon}\rho\frac{\varepsilon^2}{k} + S_\varepsilon \quad (18)$$

$$\mu_t = C_\mu \frac{\rho k^2}{\varepsilon} \quad (19)$$

$C_\mu, C_{1_\varepsilon}, C_{2_\varepsilon}, \sigma_k, \sigma_\varepsilon$ are the model parameters of RNG k -ε turbulence model; these constants have following values: 09, 1. 44, 1. 92, 1. 0 & 1. 3, respectively.

Transport Equation for the RNG k-ε model:

$$\frac{\partial}{\partial t}(\rho k) + \frac{\partial}{\partial x_i}(\rho k u_i) = \frac{\partial}{\partial x_j}\left[\alpha_k \mu_{eff}\frac{\partial k}{\partial x_i}\right] + G_k + G_b - \rho\varepsilon - Y_M + S_k \quad (20)$$

$$\frac{\partial}{\partial t}(\rho\varepsilon) + \frac{\partial}{\partial x_i}(\rho\varepsilon u_i) = \frac{\partial}{\partial x_j}\left[\alpha_k \mu_{eff}\frac{\partial \varepsilon}{\partial x_i}\right] + C_{1_\varepsilon}\frac{\varepsilon}{k}\left(G_k + C_{3_\varepsilon}G_b\right) - C_{2_\varepsilon}\rho\frac{\varepsilon^2}{k} - R_\varepsilon + S_\varepsilon \quad (21)$$

$$\mu_t = C_\mu \frac{\rho k^2}{\varepsilon} \quad (22)$$

Those symbols basically refer to the RNG k-ε turbulence model of the present CFD model, and the exact values associated with the model parameters $C_\mu, C_{1_\varepsilon}, C_{2_\varepsilon}, \sigma_k, \sigma_\varepsilon$ are 0845, 1. 42, 1. 68, 1. 0 & 1. 3, respectively.

Transport Equation for the Realizable k-ε model:

$$\frac{\partial}{\partial t}(\rho k) + \frac{\partial}{\partial x_i}(\rho k u_j) = \frac{\partial}{\partial x_j}\left[\left(\mu + \frac{\mu_t}{\sigma_k}\right)\frac{\partial k}{\partial x_i}\right] + G_k + G_b - \rho\varepsilon - Y_M + S_k \quad (23)$$

$$\frac{\partial}{\partial t}(\rho\varepsilon) + \frac{\partial}{\partial x_j}(\rho\varepsilon u_j) = \frac{\partial}{\partial x_j}\left[\left(\mu + \frac{\mu_t}{\sigma_\varepsilon}\right)\frac{\partial \varepsilon}{\partial x_i}\right] + \rho C_1 S\varepsilon - \rho C_2 \frac{\varepsilon^2}{k + \sqrt{\nu\varepsilon}} + C_{1\varepsilon}\frac{\varepsilon}{k}C_{3\varepsilon}G_b + S_\varepsilon \quad (24)$$

Where;

$$C_1 = max\left[0.43, \frac{\eta}{\eta+5}\right], \quad \eta = S\frac{k}{\varepsilon}, \quad S = \sqrt{2S_{ij}S_{ij}}, \quad \mu_t = C_\mu \frac{\rho k^2}{\varepsilon}$$

The difference between the realizable, standard and RNG k-ε models is that C_μ is not constant any longer; rather it is calculated using

$$C_\mu = \frac{1}{A_o + A_s \frac{kU^*}{\varepsilon}} \quad (25)$$

$C_{1_\varepsilon}, C_2, \sigma_k, \sigma_\varepsilon$ are the model parameters of realizable k-ε turbulence model; these constants have following values: 1.44, 1.9, 1.0 & 1.2, respectively.

k: The Turbulent kinetic energy is degree of energy related to the turbulent velocity fluctuations in the given fluid flow. This measures or quantifies the nature of the turbulence in the given flow of the fluid.

ε: Proportion of the energy contained within the turbulence to the rate at which the energy from turbulence is dissipated. This is the rate at which energy of turbulence is dissipated as heat, because of viscosity.

t: time variable.

ρ: density of the fluid.

x_i: coordinate in the i-axis of a Cartesian reference system.

μ: dynamic viscosity of the fluid.

μ_t: Turbulent eddy dynamic viscosity literally refers to the ability of the turbulent eddy movement to result to higher dynamic viscosity. It is an effective model parameter which describes turbulence effects or more strictly the effective viscosity connected with them.

G_k: the technical term for the kinetic energy of the turbulence generally used in wind power production. It is the provision of the rate of production of turbulent kinetic energy stemming from the active extrapolation of turbulent stresses.

G_b: buoyancy effect term. It is the reflection of the effect of Buoyancy forces on the modelling of turbulence of the flow.

Y_M: dilatation oscillation effect term. This applies how the variation in forms of the elements of fluids affects the turbulence.

$S_k$and S_ε: these terms are logarithmic of 'k' and 'ε'. These terms provide further details of the variation in the rate of change in k and ε in the model of turbulence.

Transport Equation for the SST k-ω model:

$$\frac{\partial}{\partial t}(\rho k) + \frac{\partial}{\partial x_i}(\rho k u_i) = \frac{\partial}{\partial x_j}\left(\left(\mu + \frac{\mu_t}{\sigma_k}\right)\frac{\partial k}{\partial x_j}\right) + \tilde{G}_k - Y_k + S_k \quad (26)$$

$$\frac{\partial}{\partial t}(\rho\omega) + \frac{\partial}{\partial x_i}(\rho\omega u_i) = \frac{\partial}{\partial x_j}\left(\left(\mu + \frac{\mu_t}{\sigma_\omega}\right)\frac{\partial \omega}{\partial x_j}\right) + G_\omega - Y_\omega + D_\omega + S_\omega \quad (27)$$

Where;

$$\mu_t = \frac{\rho k}{\omega}\frac{1}{max\left[\frac{1}{\alpha^*}, \frac{SF_2}{\alpha_1 \omega}\right]}, \qquad \tilde{G}_k = \min(G_k, 10\beta^*\rho k\omega), \qquad Y_k = \beta^*\rho k\omega,$$

$$D_\omega = 2(1 - F_1)\frac{\rho\sigma\omega_2}{\omega}\frac{\partial k}{\partial x_j}\frac{\partial \omega}{\partial x_j}$$

36

$\tilde{G}_k$: stands for production of turbulence kinetic energy by mean velocity gradients

G_ω:represents the generation of ω

S_k & S_ω: are user defined source term

D_ω: represents the cross-diffusion term

F_1 is a blending function

3.4 Geometry

Figure 3.4 illustrates the overall geometry of the numerical simulation, which was constructed using Ansys Design Modular to match the dimensions of the experimental flume. The position of the sluice gate was adjusted to 0.87 m in the direction of flow.

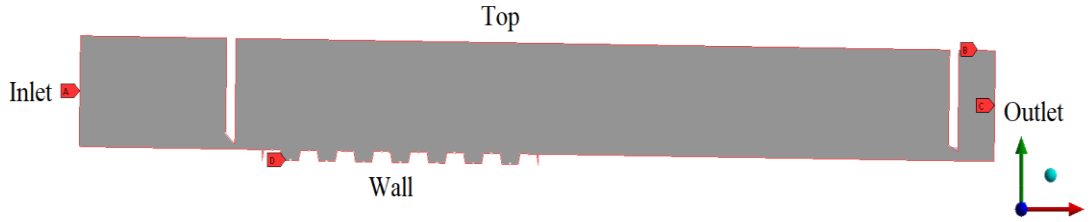

(a)

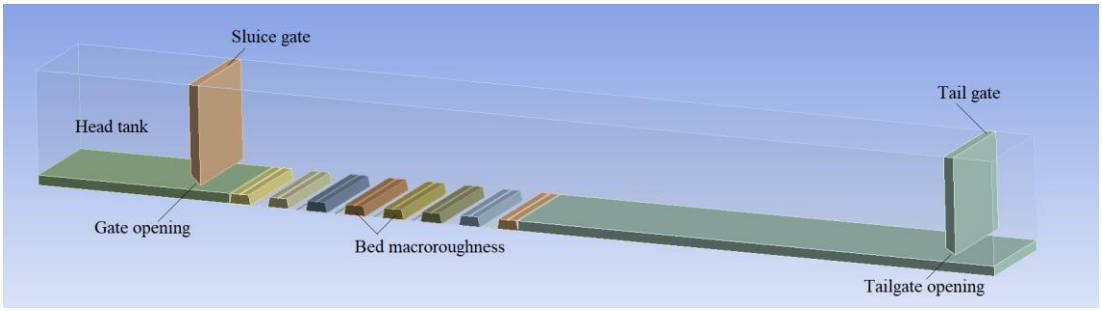

(b)

Figure 3.4 Model geometry of simulation setup showing relevant parameters associated with the flume (a) 2-dimensional; (b) 3-dimensional

3.5 Meshing

The Ansys Fluent software requires a finite volume mesh to be present in the computational domain for accurate calculations Canonsburg [24]. Two crucial aspects must be taken into account when creating the mesh in the computational domain. It is important to ensure that the mesh is sufficiently refined to accurately capture the rapid spatial variations of velocity or other significant flow characteristics, such as temperature. These pertains especially to parts close to a wall or a solid formation in the flow path especially when in turbulent flow regime where the possibility of significant changes in the flow across a short distance is rather high. Hydraulic jump simulation is the main focus of enquiry in this study. Due to the instability of hydraulic jump, it obviously requires a more number cells or fine mesh to obtain a high accuracy and reliability of the simulation results. One disadvantage of having a higher number of cells in a simulation is that the more cells there are the longer it will take to compute and the greater the amount charged. Additionally, it is important to acknowledge that dealing with a higher number of cells can make the post processing of the results more challenging.

Figure 3.5 demonstrates the mesh surrounding the geometry. A mesh analysis was conducted in a meshing setup, where the different faces were assigned suitable names. Additionally, inflation layers were incorporated at the flume's bed to enhance the flow behaviour.

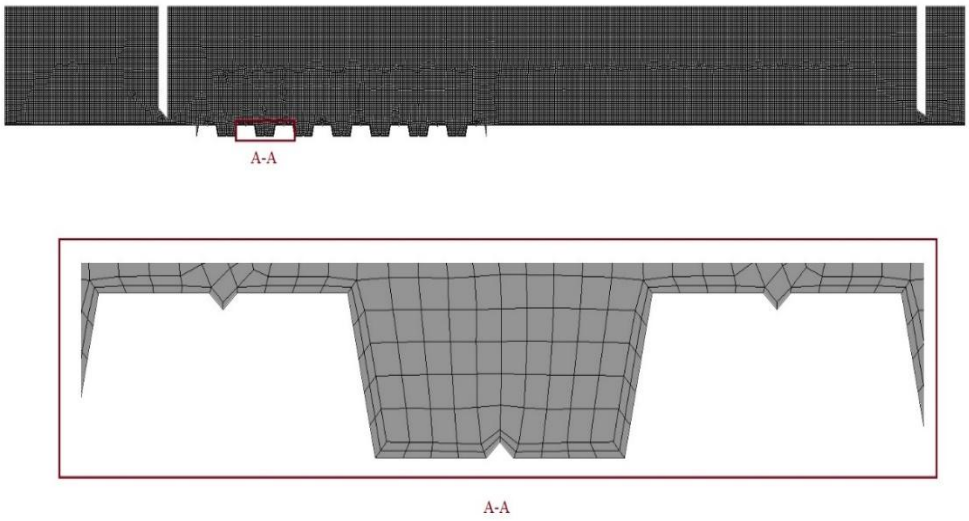

Figure 3.5 Mesh structure allocated to model geometry

3.5.1 Mesh sensitivity analysis

Mesh sensitivity analysis is a statistical technique used to evaluate the impact of parameter or input changes on a model's output. In order to achieve accurate results while keeping computational costs at a minimum, it is necessary to perform sensitivity analysis during the numerical simulation. This analysis helps determine the ideal combination of mesh and turbulence for the simulation. This study conducted a sensitivity analysis on grid independency and turbulence models. This study examined the sequent depth ratio (y_2/y_1) as a key parameter for conducting a sensitivity analysis on the grid and turbulence model. The approach used in this study was similar to that of previous research conducted by Bayon-Barrachina and Lopez-Jimenez (2015) [55] and Dasineh et al. (2021) [89]. For the sensitivity analysis six different grid sizes ranging from coarse to fine were considered. Figure 3.*6* illustrates the fluctuation of the relative error in predicting the sequent depth ratio across various turbulence models and mesh element sizes. The various models demonstrate minimal variation in their predictions of sequent depth ratio. The RNG k-ε model produced the best results with the least amount of error, followed by the realizable k-ε, SST k-ω, and standard k-ε models. Figure 3.*6* demonstrates that as the mesh element size decreases, the relative error in predicting the sequent depth ratio also decreases. After reaching a mesh element size of 9 mm, the error remains constant, indicating that further reduction in size is not necessary to avoid excessive computational cost. The reported maximum error at a size of 9 mm with RNG k- ε was less than 2%.

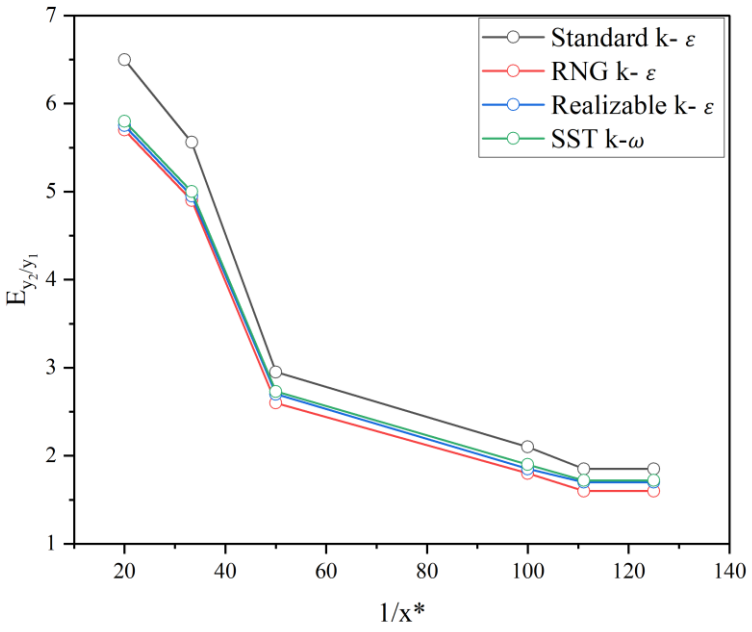

Figure 3.6 Mesh and turbulence model sensitivity analysis on y2/y1 prediction

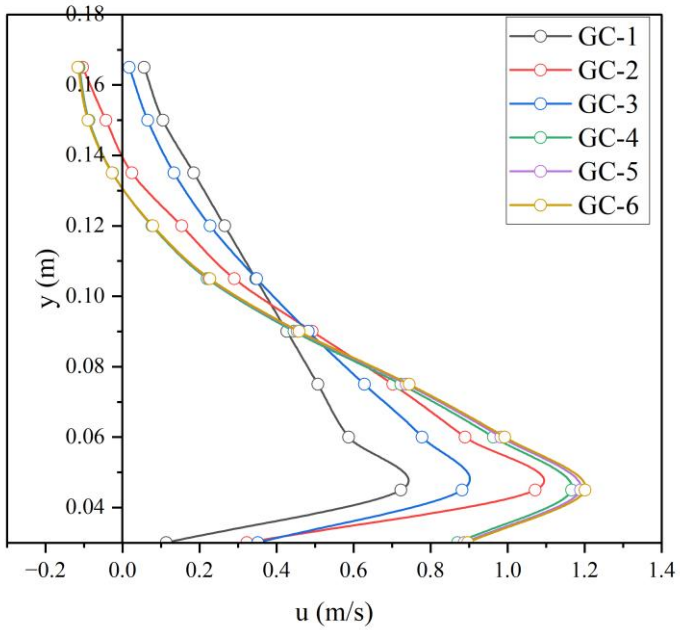

Figure 3.7 Sensitivity analysis of mesh size for horizontal component of velocity profile

In addition, Figure 3.7 illustrates the results of a mesh sensitivity analysis on the longitudinal velocity profile of a free hydraulic jump on a smooth bed. The analysis was conducted using the RNG k- ε turbulence model, following the procedure outlined by Celik et al. (2008) [96]. From Figure 3.7 it is evident that the fluctuation in the longitudinal velocity profile is minimal for GC-5 & GC-6. Therefore, there is no need for further reduction in mesh size to save computational costs. Therefore, the present study considered the 9 mm mesh size and RNG k- ε turbulence model to analyse the hydraulic jump over smooth and macrorough beds using cost-effective numerical methods.

3.6 Boundary conditions

Specifically for hydraulic jump replication and especially when trying to obtain highly accurate results, the boundary conditions should be selected properly. Typically, boundary conditions address inlet, outlet, wall and atmosphere surfaces.

3.6.1 Inlet and outlet

The pressure inlet has been selected to create a sudden increase near the flume, while gauge pressure has been chosen for the top surface and outflow of the flume. The initial settings at the inlet and outflow are adjusted to replicate the conditions found in experimental scenarios. However, Chapter 4 discussed the various boundary conditions to conduct the numerical simulations of hydraulic jump.

3.6.2 Near wall treatment

Wall functions are based on empirical correlations that utilise information from adjacent cells to estimate flow variables along the wall. These functions help to reduce processing time by bypassing the need to calculate the near-wall region. Bayon-Barrachina and Lopez-Jimenez (2015) [55] highlighted the issues of flow along the wall for accurate findings and suggested to avoid over-refinement of the mesh, as this could compromise the accuracy of the results. Canonsburg (2013) [24] explained the crucial aspect of wall functions involves the non-dimensional distance between the wall and the first node away from the wall (The turbulent boundary layer is composed of three sections: the laminar sub-layer ($y^+ < 5$), the transition layer ($5 < y^+ < 30$), and the turbulence layer ($y^+ > 30$). Ansys Fluent offers a range of options for near wall treatment in the k-ε turbulence models, including normal wall function, non-equilibrium wall function, and improved wall treatment. Due to its ability to provide reasonably accurate predictions for most high Reynolds-number (Re), wall-bounded flows and its ability to reduce computational effort by eliminating the need to resolve the near-wall region, the standard wall function was utilised in this study. With the standard wall function, one can easily customise the shear stress and decide whether or not to include roughness on the wall. Throughout the simulations, the wall is considered to be a no-slip wall. It is assumed to have a wall roughness constant of 0.5 and a flow velocity of zero at the wall. The y^+ values for all the grid systems range from 46 to 113, indicating the necessity of using the wall function technique. The inlet Reynold number ranged from 31,654 to 52,861.

3.7 Discretization scheme

When it comes to numerical simulation, discretization of data has a significant influence on the parameters that ultimately shape the results. Based on a study by Bayon-Barrachina and Lopez-Jimenez (2015) [55], it was found that upwind schemes in the RANS model exhibit decreased instability. Therefore, the present investigation opted for the use of upwind schemes. In numerical simulations, the Courant number (Cr) is a dimensionless measurement that indicates the relationship between the time step and the spacing between the computing grid points. It is important to assess the stability of the simulation, as a high Courant number can lead to numerical instability. In the present simulation of the hydraulic jump, the highest Cr used was 0.40, which falls within the safe range for this type of simulation. A widely used algorithm called SIMPLE (Semi-Implicit Method for Pressure-Linked Equations) was used to resolve fluid flow issues. The density and momentum equations were discretised using the first and second-order upwind techniques, respectively.

3.8 Stability & convergence criteria

In this study, the residuals were set to 10^{-6} to analyse the convergence criteria. Due to the abrupt nature of the hydraulic jump, it can be quite challenging to ensure the stability of the numerical model. In this study, a method of trial and error was employed to stabilise the jump by analysing the discharge equilibrium curve for the inflow and outflow. It becomes evident that the jump's stable conditions were apparent after 11 seconds of time steps.

3.9 Validation of numerical model

Numerical simulation validation is the process of confirming that computer simulation findings accurately reflect the processes being examined in reality. To determine the simulation's accuracy and dependability, experimental data are compared to the results of the simulation. Quantifying the disparities between simulation results and experimental data and locating potential areas for simulation improvement can help to determine the simulation's accuracy and reliability. For validating any numerical model with physical model it must be insure that the numerical model is more or less similar. (Chanson and Gualtieri, 2008) [37] studied the scale effect while analysing the hydraulic jump in two different channel dimensions, they found that some scale, effect the void fraction and bubble count rate, to overcome such issues the present numerical study considered the dimensions of flume and roughness elements identical to physical setup.

3.9.1 Longitudinal velocity variation

Figure 3.*8* illustrate the general longitudinal velocity profile of developed hydraulic jump in a smooth rectangular channel as discussed by Rajaratnam (1967) [12]. An inverse relationship between velocity magnitude and the upstream Froude number (Fr_1) was reported by Wang and Chanson (2016) [58].

Rajaratnam (1967) [12] discussed that the maximum velocity observed at a vertical distance of y* from the bed level, and at a vertical distance of b′, velocity drops to approximately half of the maximum velocity. This is a typical velocity fluctuation in a fully developed roller zone; just above point b′, reverse flow happens due to velocity stagnation.

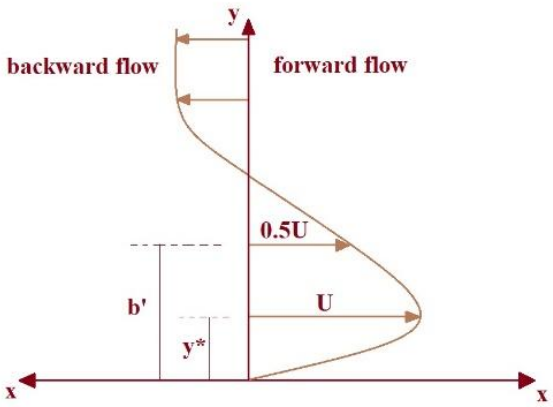

Figure 3.8 Typical longitudinal velocity profile for a hydraulic jump

The standard pictorial representation of the numerically obtained free & submerged hydraulic jump's longitudinal velocity profile on smooth and macrorough beds are shown in Figure 3.9 & Figure 3.10 respectively.

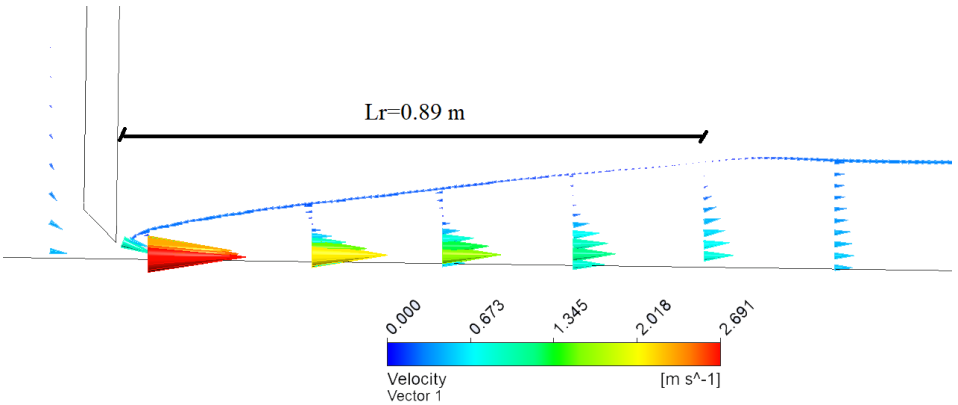

(a)

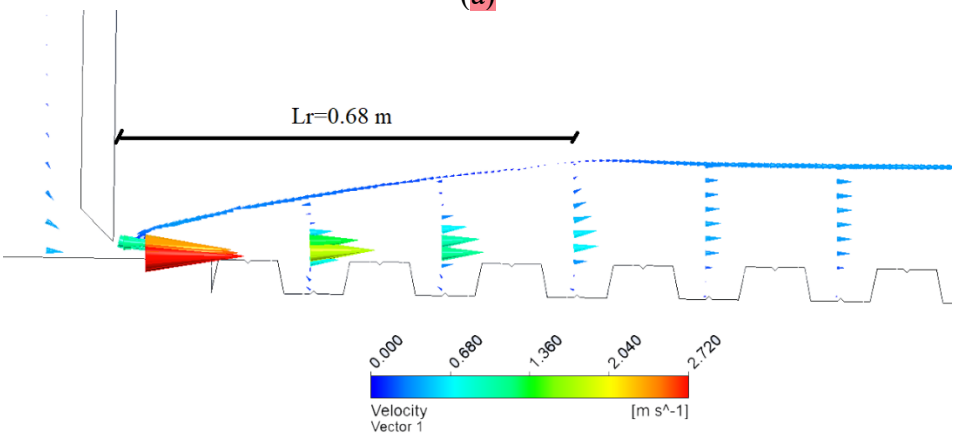

(b)

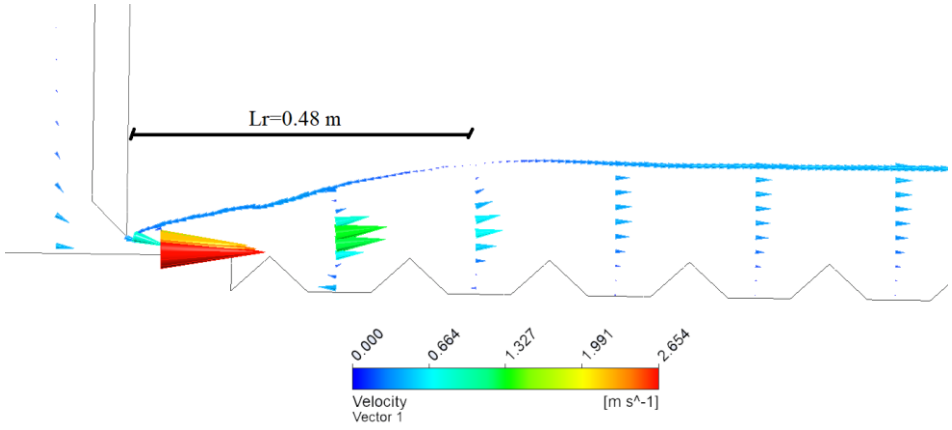

(c)

Figure 3.9 Pictorial representation of velocity profile in free hydraulic jump (a) smooth bed (b) trapezoidal macroroughness (c) triangular macroroughness (Fr_1=5.45)

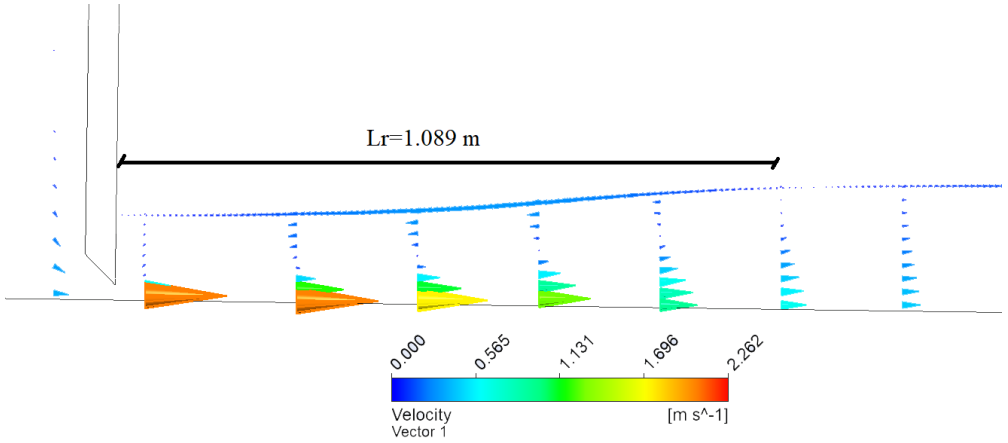

(a)

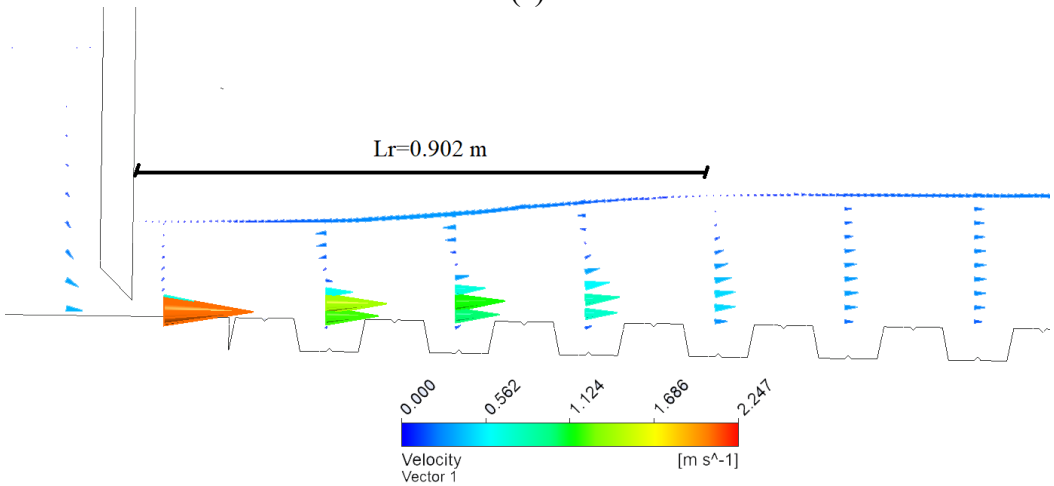

(b)

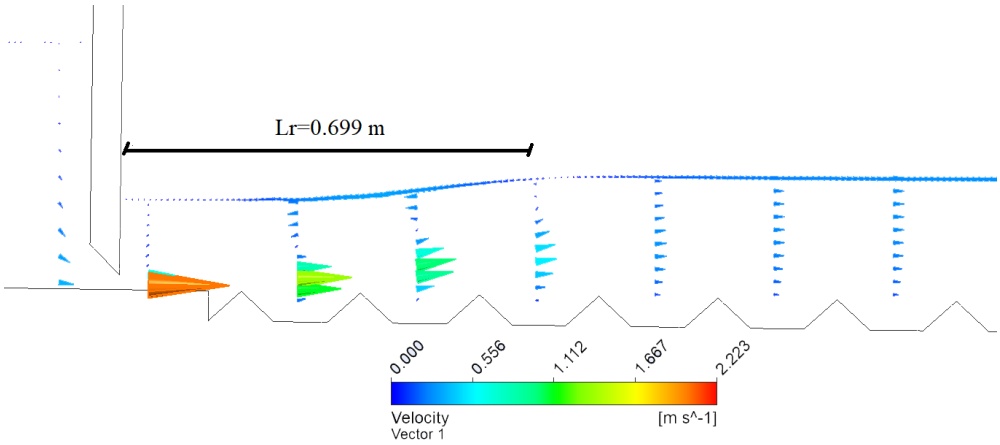

(c)

Figure 3.10 Pictorial representation of velocity profile in submerged hydraulic jump (a) smooth bed (b) trapezoidal macroroughness (c) triangular macroroughness (Fr_1=6.12)

By examining the results of Figure 3.9 & Figure 3.10, it can be deduced that the mean flow velocity falls at the topmost region of the gate opening because this is where it is highest. Following the development of the jump, the jump velocity in the roller zone reverses with a stagnation point in a backward direction. Such a description is valid for both macrorough and smooth beds. Velocity distribution obtained for present study well confirms the past velocity distribution of Rajaratnam (1967) [12], Ead and Rajaratnam (2002) [34] and Ghaderi et al. (2021) [18].

Figure 3.11 represents the dimensionless velocity distribution of submerged hydraulic jump on smooth and macroroughness arrangements for Fr_1=6.12. Here, the vertical axis represents the ratio of y*/b', where y* is the distance from the bed and b' is the length scale at which velocity is half of maximum velocity. The horizontal axis represents the ratio of u'/U, where u is the time-averaged longitudinal velocity at any section and U is the maximum longitudinal velocity at that section.

The dimensionless velocity distribution graph is typically plotted for the point where the velocity is only half the maximum velocity, which is at a distance of b′ from the jump toe. This is due to the downstream region's generally flat velocity distribution, which does not exhibit much variance. Additional computations are made to normalize the velocity values depending on the mean velocity and the height of the jump in order to provide the dimensionless velocity distribution. For validation purposes, previous studies of Ghaderi et al. (2021) [18] are used as the references and presented in comparison with the present findings in Figure 3.11. It is discovered that the trend of dimensionless velocity profiles is more or less similar to the previous research and that the maximum horizontal forward velocity occurred at a shallower flow depth than the depth obtained by Rajaratnam (1967) [12], and Jesudhas et al. (2018) [69].

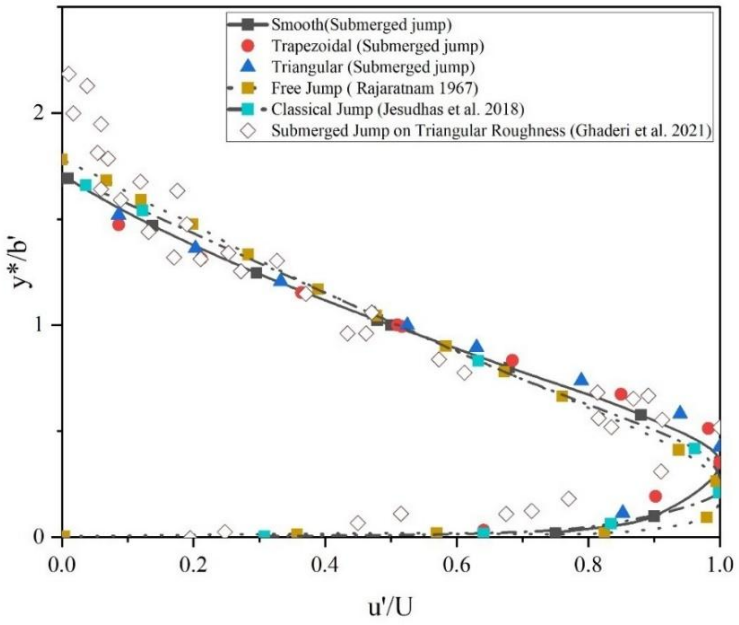

Figure 3.11 Combined dimensionless flow velocity distribution of submerged hydraulic jump for smooth and macroroughness arrangements at Fr_1=6.1

3.9.2 Dimensionless parameters

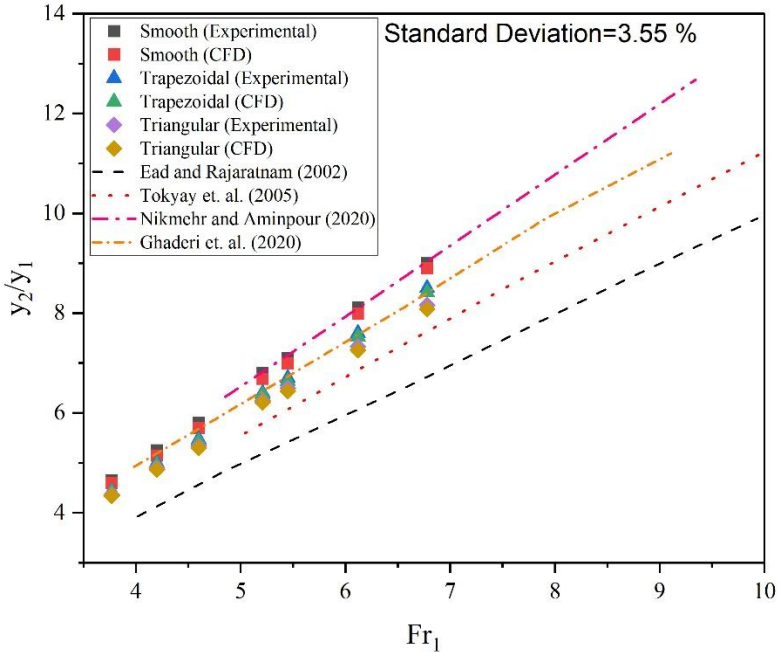

(a)

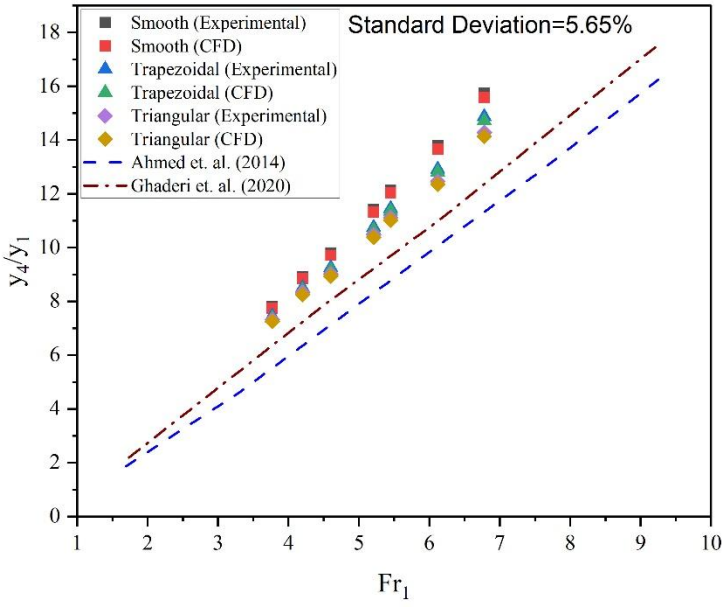

(b)

Figure 3.12 Comparison of a numerical model with experimental model for basic parameters of hydraulic jump (a) y_2/y_1 (b) y_4/y_1

In Figure 3.12, which compares numerical and experimental findings on fundamental jump parameters including the sequent depth ratio (y_2/y_1) and tail-water depth ratio (y_4/y_1), there is good agreement between the two models, with a standard deviation of less than 6%. This degree of agreement demonstrates that CFD modelling may faithfully simulate complex fluid dynamics issues like hydraulic jumps.

$$y_2/y_1 = 1.4569\ F_{r1} - 0.8975 \qquad R^2 = 0.99 \text{ (smooth bed)} \qquad (28)$$

$$y_2/y_1 = 1.3042\ F_{r1} - 0.547 \qquad R^2 = 0.99 \text{ (macrorough bed)} \qquad (29)$$

$$y_4/y_1 = 2.6059\ F_{r1} - 2.1254 \qquad R^2 = 0.99 \text{ (smooth bed)} \qquad (30)$$

$$y_4/y_1 = 2.4229\ Fr_1 - 1.8121 \qquad R^2 = 0.99 \text{ (macrorough bed)} \qquad (31)$$

Further, the comparative evaluation of the Present Study (CFD) against multiple established works Ghaderi et al. (2020), Nikmehr & Aminpour (2020), Ead and Rajaratnam (2002), and Tokyay et al. (2005) confirms the robustness of the CFD approach in capturing the fundamental hydraulic behaviour of free hydraulic jumps. Despite minor discrepancies in the magnitude of the sequent depth ratio (y_2/y_1),

primarily attributable to differences in experimental setups, modelling assumptions, and turbulence closure strategies, all studies consistently demonstrate an increasing trend of y_2/y_1 with rising Froude numbers. This agreement reinforces the physical accuracy of the CFD model in reflecting supercritical flow transitions. Notably, the CFD predictions generally fall between the experimental results of Ead and Rajaratnam and the higher values reported by Tokyay et al. (2005), suggesting that the numerical model successfully balances between under and over prediction. These insights not only validate the present CFD methodology but also underscore the importance of model calibration and sensitivity to roughness configurations and turbulence treatments for achieving improved predictive fidelity in future investigations.

The comparative analysis of the submerged hydraulic jump characteristics highlights meaningful trends and deviations between the present CFD study and previous experimental investigations. The consistently higher sequent depth ratio (y_4/y_1) predicted in comparison to Ahmed et al. (2014), with a systematic deviation ranging between 1.7 and 2.8 and a relatively low standard error of 0.140, suggests a moderate yet reliable overestimation by the CFD model. This indicates a potential influence of model assumptions or boundary conditions on the simulated flow structure. Conversely, the comparison with Ghaderi et al. (2020) yields a standard error of 0.111, reflecting a relatively close agreement and reinforcing the predictive capability and reliability of the present CFD framework under varying Froude number regimes. Overall, while minor pointwise differences exist, the CFD model demonstrates a strong potential for accurately simulating submerged hydraulic jumps, particularly when validated against recent experimental findings.

CHAPTER 4

RESULT & DISCUSSION

4.1 General

This chapter is concerned with the various boundary conditions which may be chosen in dissimilar flume conditions in order to analyse the hydraulic jump phenomenon numerically and to understand the influence of dissimilar shape of artificial macroroughness on hydraulic jump characteristics.

4.2 Effect of various flume configurations on characteristics of classical hydraulic jump

In past studies researchers used different inlet and outlet boundary conditions to perform numerical simulation. On observing the past numerical studies to investigate the hydraulic jump phenomenon it was noticed that the hydraulic jump phenomenon can be studied numerically by creating different types of flumes with appropriate boundary conditions. Earlier work of Bayon-Barrachina and Lopez-Jimenez (2015) [55] considered two types of flumes to investigate the hydraulic jump phenomenon in a smooth rectangular channel and found negligible effect on jump characteristics however the computational cost was reduced significantly.

This study considered two different approaches to prevail the initial jump conditions. In first approach the effect of upstream water head is considered and in second approach same is neglected. In this regard, four different geometries considering different arrangement in downstream were created for first and second approach separately. Therefore, this section analysed eight feasible flumes.

First approach: In Model I, flume created similar to the laboratory flume where inlet sluice gate and outlet tailgate is equipped. In Model II & III, flume created where inlet sluice gate is provided but in downstream, weir in form of obstruction is provided instead of tailgate. In Model IV, flume is created with inlet sluice gate but without any obstruction in downstream. Figure 4.1 illustrate the different models of flume considered for first approach.

Boundary condition used in first approach:

(a) Inlet: $u = u_1, \frac{\partial p}{\partial x} = 0, \alpha = f(y), \mathrm{k} = k_{inlet}, \varepsilon = \varepsilon_{inlet}$

(b) Outlet for Model I, II & III: $\frac{\partial p}{\partial x_i} = 0, p = 0, \frac{\partial \alpha}{\partial x_i} = 0, \frac{\partial k}{\partial x_i} = 0, \frac{\partial \varepsilon}{\partial x_i} = 0$

(c) Outlet for Model IV: $u = f(y), p = f(y), \alpha = f(y), \frac{\partial k}{\partial x_i} = 0, \frac{\partial \varepsilon}{\partial x_i} = 0$

(d) Atmosphere: $\frac{\partial u}{\partial x_i} = 0, p = 0, \frac{\partial \alpha}{\partial x_i} = 0, \frac{\partial k}{\partial x_i} = 0, \frac{\partial \varepsilon}{\partial x_i} = 0$

(e) Wall & Floor: $u = 0, \frac{\partial p}{\partial x_i} = 0, \frac{\partial \alpha}{\partial x_i} = 0, k = f(y), \varepsilon = f(y)$

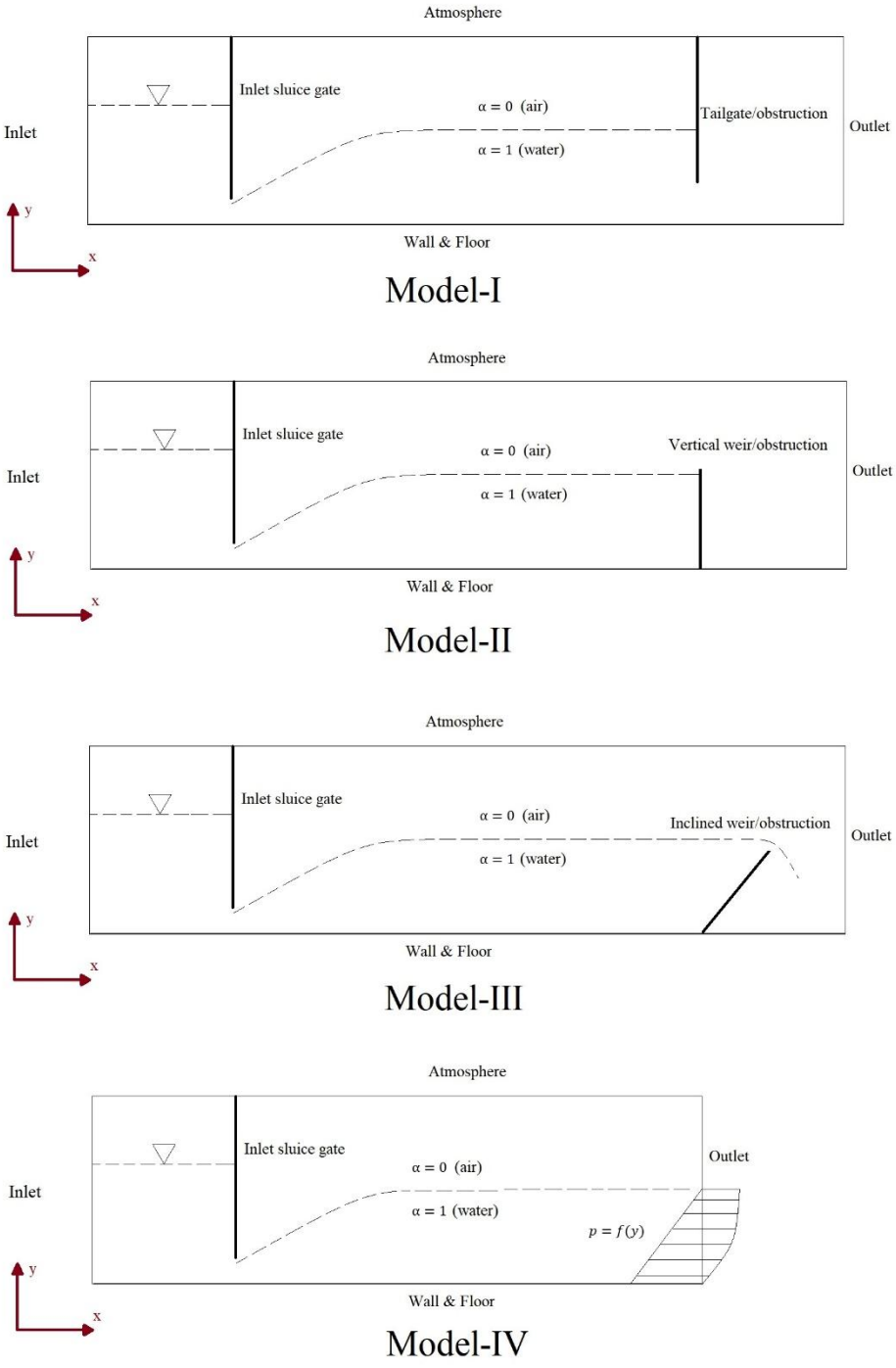

Figure 4.1 Sketch of different types of flumes used in first approach

Second approach: In Model V, flume created without inlet sluice gate but equipped with tailgate as an obstruction to form the jump. In Model VI & VII, flume created without inlet sluice gate but equipped with weir as an obstruction instead of tailgate. In Model VIII, flume created without inlet sluice gate and without any obstruction in downstream. Figure 4.*2* illustrate the different models of flume considered for second approach.

Boundary condition used in second approach:

(a) Inlet: $u = f(y), p = f(y), \alpha = f(y), \mathrm{k} = k_{inlet}, \varepsilon = \varepsilon_{inlet}$

(b) Outlet for Model V, VI & VII: $\frac{\partial p}{\partial x_i} = 0, p = 0, \frac{\partial \alpha}{\partial x_i} = 0, \frac{\partial k}{\partial x_i} = 0, \frac{\partial \varepsilon}{\partial x_i} = 0$

(c) Outlet for Model VIII: $u = f(y), p = f(y), \alpha = f(y), \frac{\partial k}{\partial x_i} = 0, \frac{\partial \varepsilon}{\partial x_i} = 0$

(d) Atmosphere: $\frac{\partial u}{\partial x_i} = 0, p = 0, \frac{\partial \alpha}{\partial x_i} = 0, \frac{\partial k}{\partial x_i} = 0, \frac{\partial \varepsilon}{\partial x_i} = 0$

(e) Wall & Floor: $u = 0, \frac{\partial p}{\partial x_i} = 0, \frac{\partial \alpha}{\partial x_i} = 0, k = f(y), \varepsilon = f(y)$

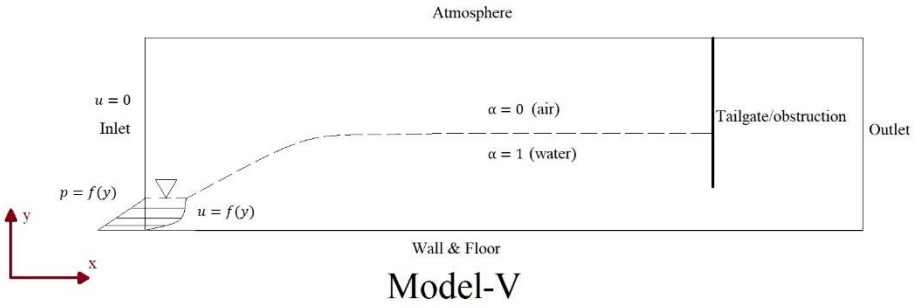

Model-V

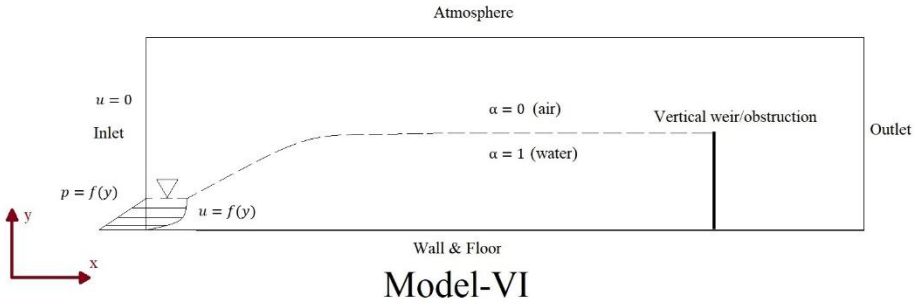

Model-VI

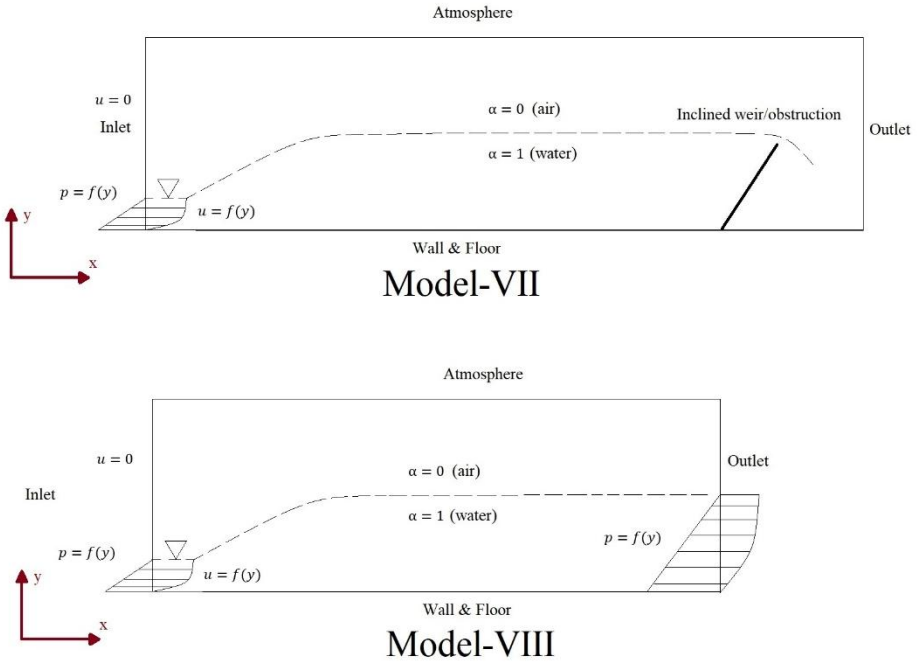

Figure 4.2 Sketch of different types of flumes used in second approach

4.2.1 CFD generated flow profile including longitudinal velocity profile of hydraulic jump

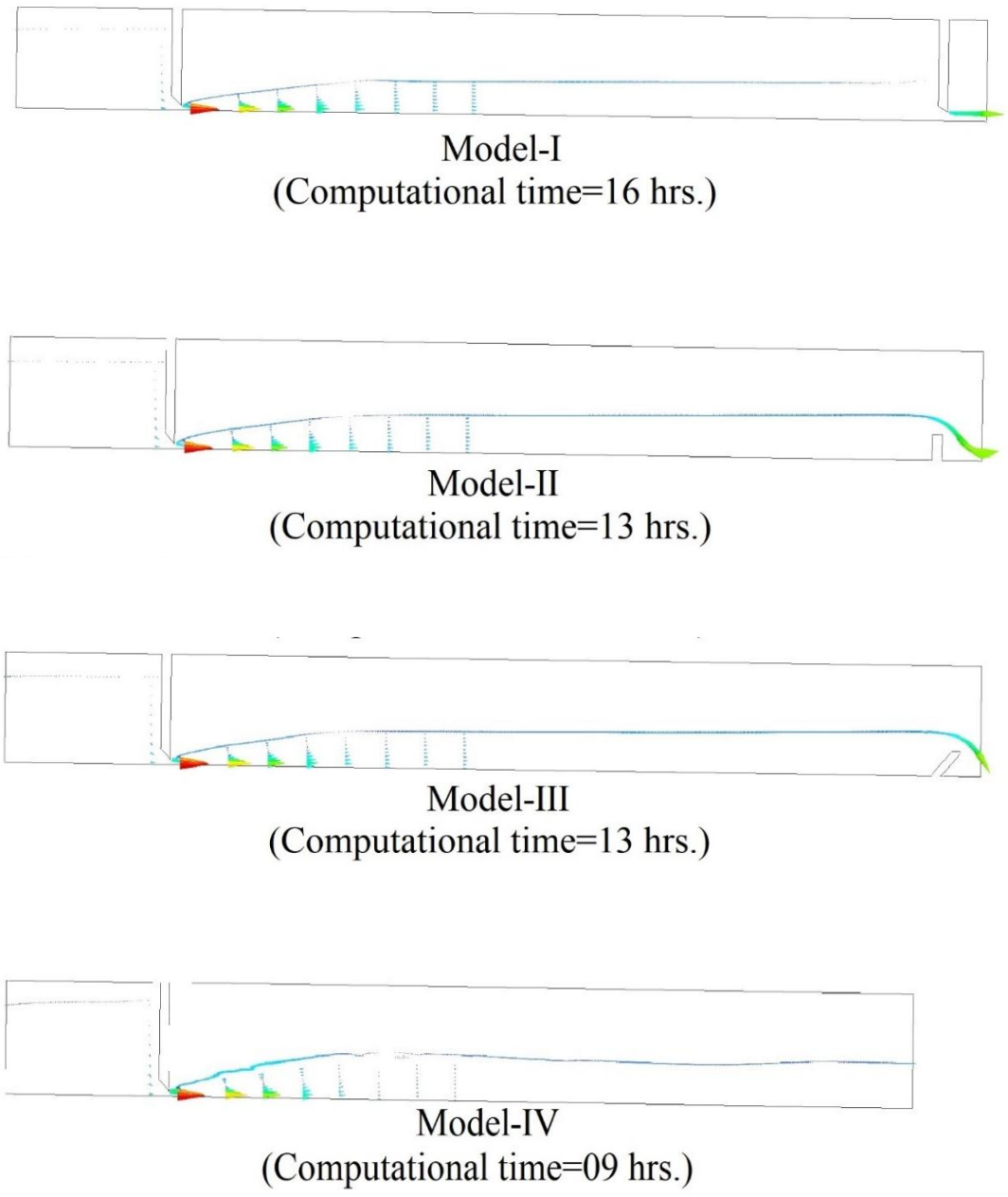

Figure 4.3 Numerically simulated flow profile & longitudinal velocity profile at different sections of flume for first approach

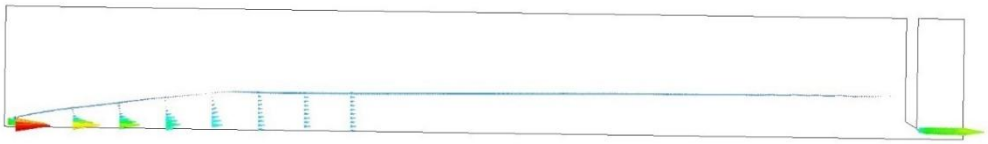

Model-V
(Computational time=13 hrs.)

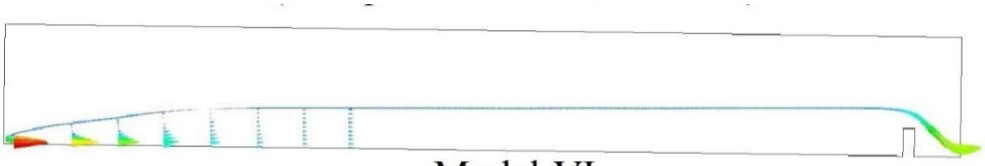

Model-VI
(Computational time=10.5 hrs.)

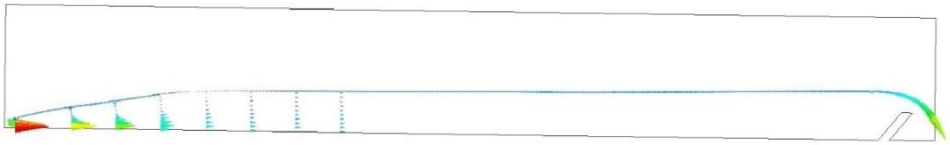

Model-VII
(Computational time=10.5 hrs.)

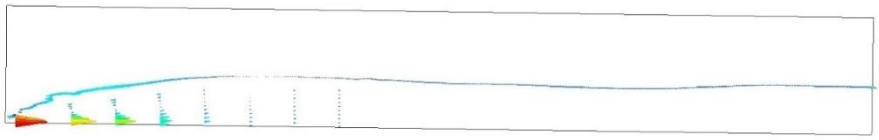

Model-VIII
(Computational time=07 hrs.)

Figure 4.4 Numerically simulated flow profile & longitudinal velocity profile at different sections of flume for second approach

Figure 4.3 & Figure 4.4 illustrate the flow profiles & longitudinal velocity profiles at different section within hydraulic jump for each model and represents the examples of hydraulic jump simulated using possible approaches. It can be clearly identified that the flow profiles are almost similar in nature and no major variations are reported. Hence, when comparing them closely between each other there remains no substantial impact on the accuracy of the model outcomes. There are no undesirable effects including wave formation despite the fact that the new approach means moving the boundary conditions much closer to the phenomenon of interest. The velocity profiles are almost similar for most of the models but small variation is seen in last model of the both cases. However, these small variation in model disappears on averaging the velocities. However, the computational time in all four models is not same which may be a major outcome of providing different boundary conditions to the outlet. Domain reduction helps to reach computational times up to 50% shorter in some cases which also correlates to the statements made by Bayon-Barrachina and Lopez-Jimenez (2015) [55].

4.3 Comparative analysis of eight (08) different types of strip macroroughness configurations

The incorporation of various artificial strip macroroughness shapes such as triangular, rectangular, trapezoidal, and semicircular within stilling basins is a deliberate hydraulic engineering strategy that may enhance energy dissipation, stabilize hydraulic jumps, and help control turbulence. Each shape may uniquely disturb the flow field, potentially influencing roller length, sequent depth, jump position, and air entrainment characteristics. For instance, triangular and trapezoidal shapes could promote rapid jump initiation and upward flow deflection, thereby increasing turbulence and energy loss. Rectangular elements may provide strong obstruction and pronounced wake formation, while semicircular shapes might encourage smoother recirculation and reduce local flow separation making them potentially effective in minimizing sediment deposition and local scour.

The selection of roughness shape may also depend on practical factors such as ease of construction, cavitation resistance, and long-term durability. Rectangular and semicircular shapes are often preferred due to their fabrication simplicity and maintenance advantages. Ultimately, the choice of macroroughness geometry should be tailored to site-specific flow conditions and design objectives, aiming to ensure maximum hydraulic efficiency, structural stability, and operational sustainability.

During this investigation, macrorough strips are positioned across the flow so that they would be most effective. This design is selected according to accepted hydraulic concepts, literature on the topic and stability criteria. Having perpendicular strips strategically placed inside the stilling basin helps break the water's momentum and makes it dissipate better.

Additionally, this arrangement supports the formation of a strong roller and increased air entrainment, improving oxygen transfer and aeration efficiency. It also aligns with practical and field-tested designs such as U.S. Bureau of Reclamation Type II basins use flow-normal energy dissipating features such as baffle blocks, sills, or roughness strips in this manner. The perpendicular orientation therefore provides comparative relevance and design continuity with field-tested systems.

While alternative orientations such as angled, parallel, or staggered arrangements may influence flow behaviour differently potentially causing asymmetric flow separation, uneven roller development, or reduced turbulence generation.

Figure 4.5 illustrate the eight (08) different types of strip macroroughness models *i.e.,* S_1, S_2, S_3, S_4, S_5, S_6, S_7, S_8 for the analysis of the free and submerged hydraulic jump characteristics. Here, eight different possible structures in form of strips are choosen and spread to the downstream bed of the hydraulic structure. In previous studies strip macroroughness was found benificial to improve the jump characteristics. However, past studied investigated only few possible strip macroroughness shapes.

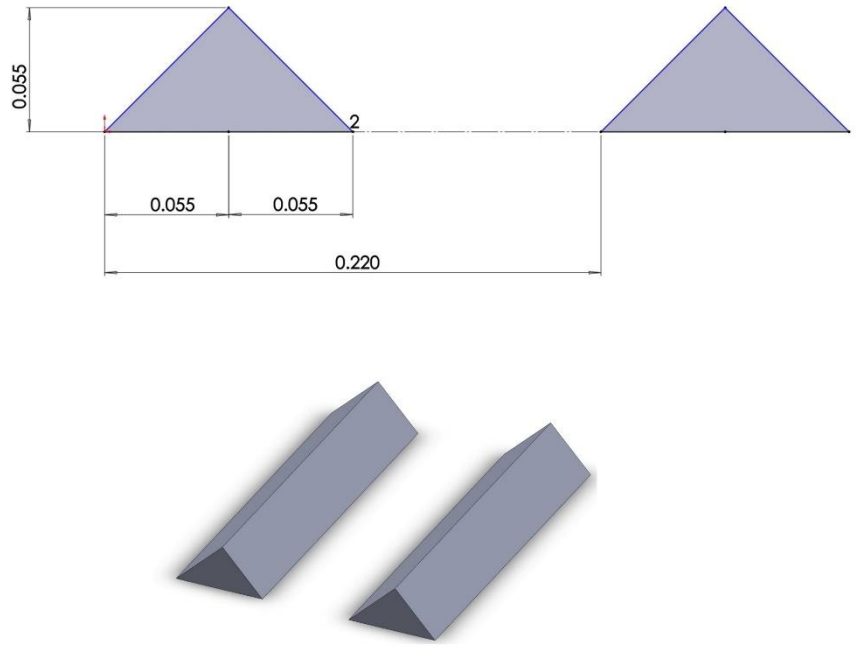

(a) Model S_1

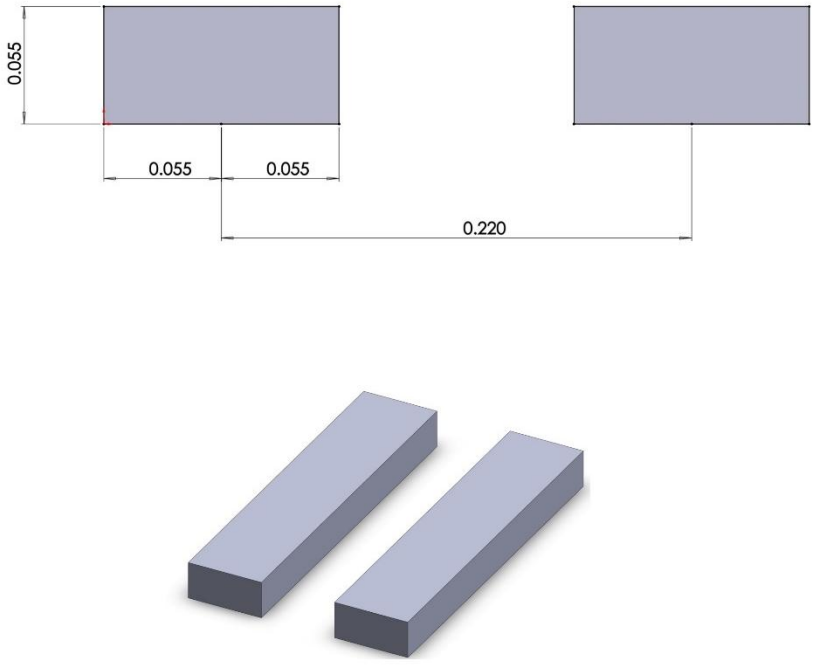

(b) Model S_2

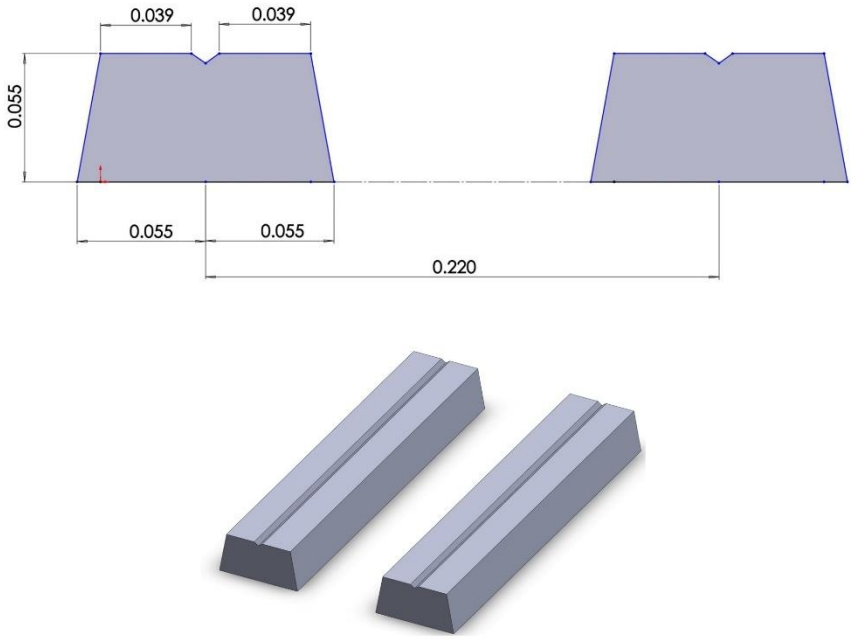

(c) Model S_3

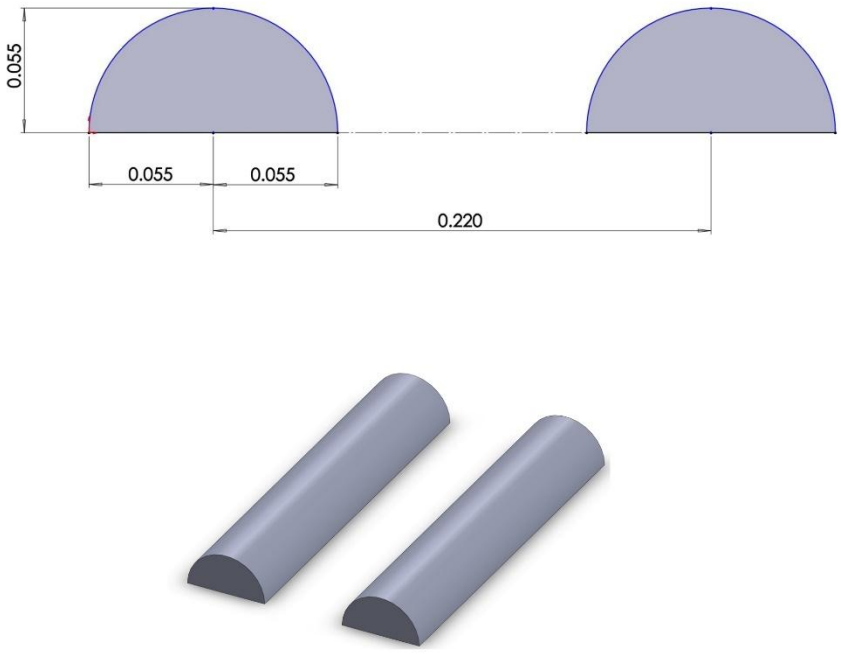

(d) Model S_4

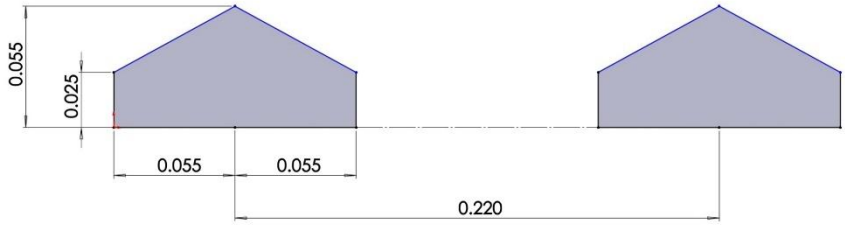

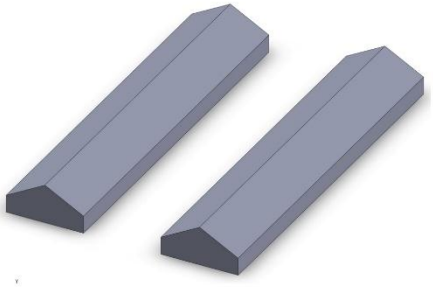

(e) Model S_5

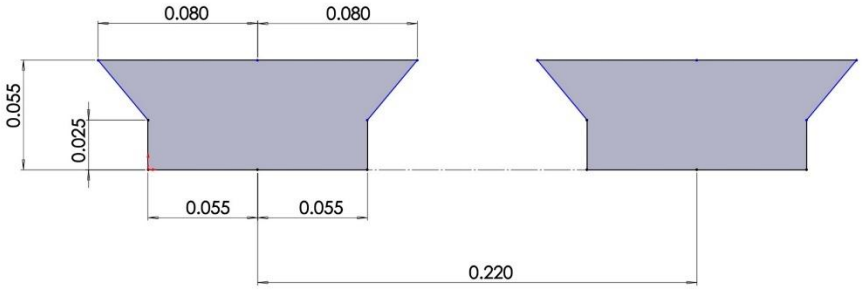

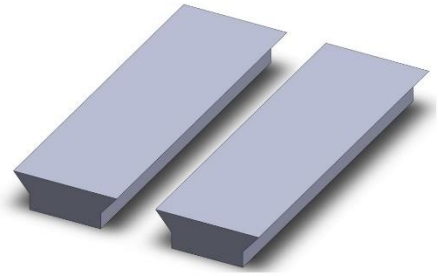

(f) Model S_6

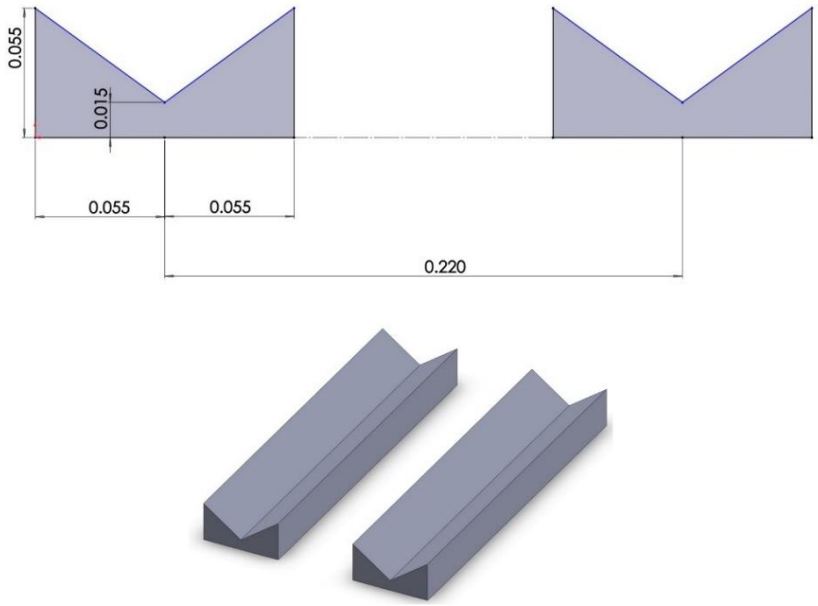

(g) Model S_6

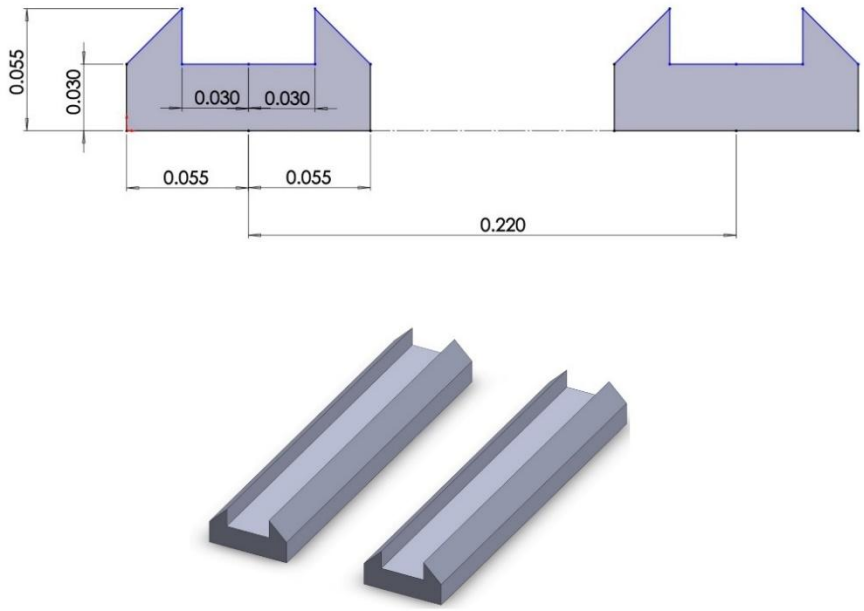

(h) Model S_8
(*Note:Above dimensions are in meter*)

Figure 4.5 Model sketch of adopted different strip macroroughness shapes

4.3.1 Flow profiles & Velocity profile

This section shows the flow profiles and longitudian velocity profiles of free and submerged hydraulic jump over various strip macroroughness *i.e.*, S_1, S_2, S_3, S_4, S_5, S_6, S_7, S_8 downstream of the hydraulic structure. This section also include the values of length of roller for each case.

4.3.1.1 Flow profile and velocity variation in case of free hydraulic jump

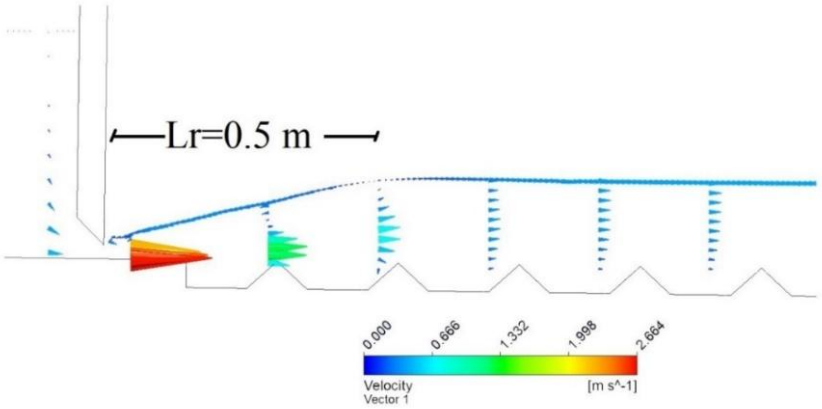

(a)

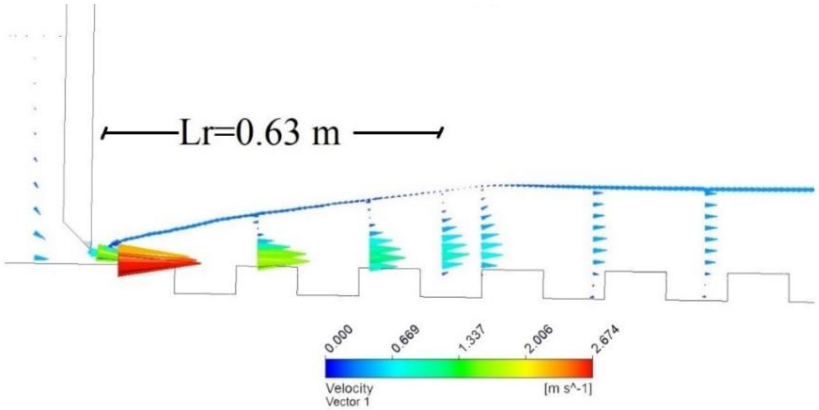

(b)

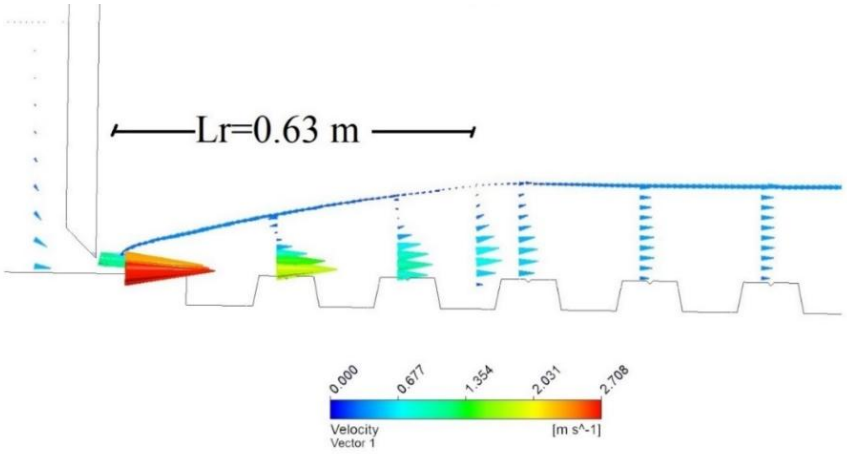
Lr=0.63 m
0.000
0.677
1.354
2.031
2.708
Velocity
Vector 1
[m s^-1]

(c)

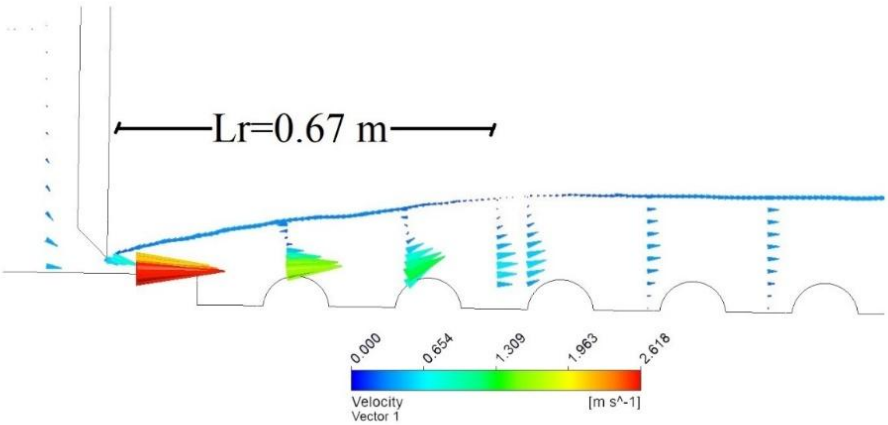
Lr=0.67 m
0.000
0.654
1.309
1.963
2.618
Velocity
Vector 1
[m s^-1]

(d)

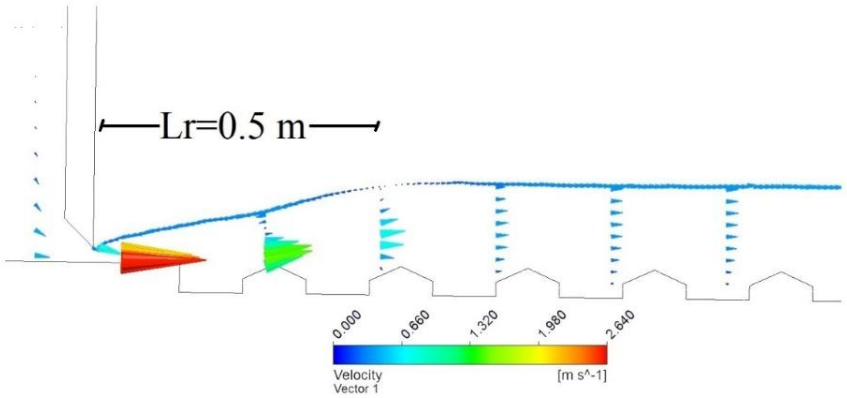
Lr=0.5 m
0.000
0.660
1.320
1.980
2.640
Velocity
Vector 1
[m s^-1]

(e)

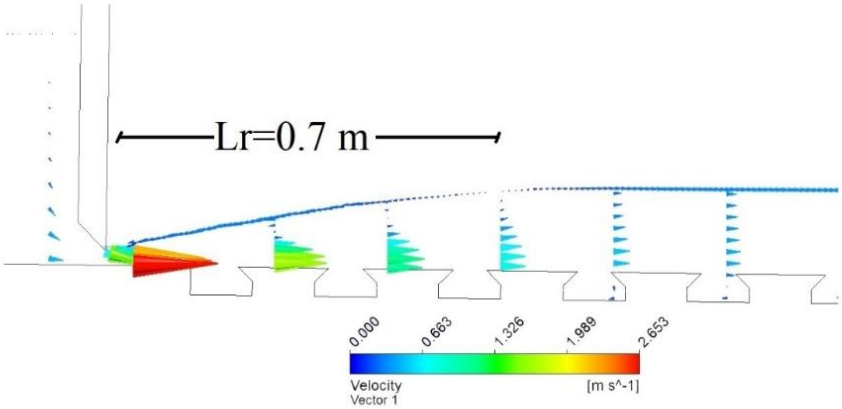

(f)

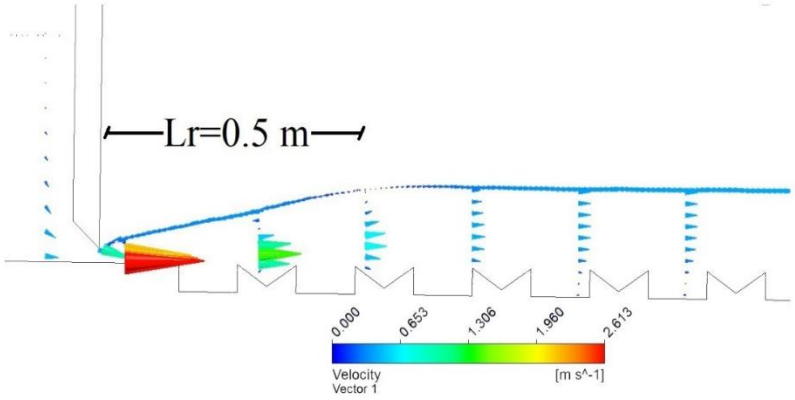

(g)

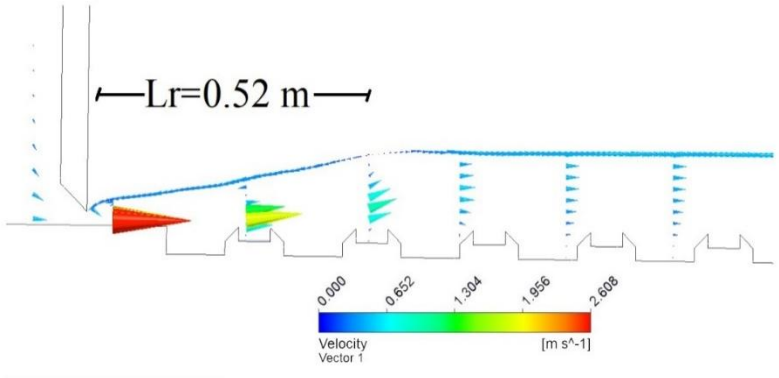

(h)

Figure 4.6 (a-h) Numerically generated flow profiles showing longitudinal velocities at different sections for each model for free hydraulic jump.

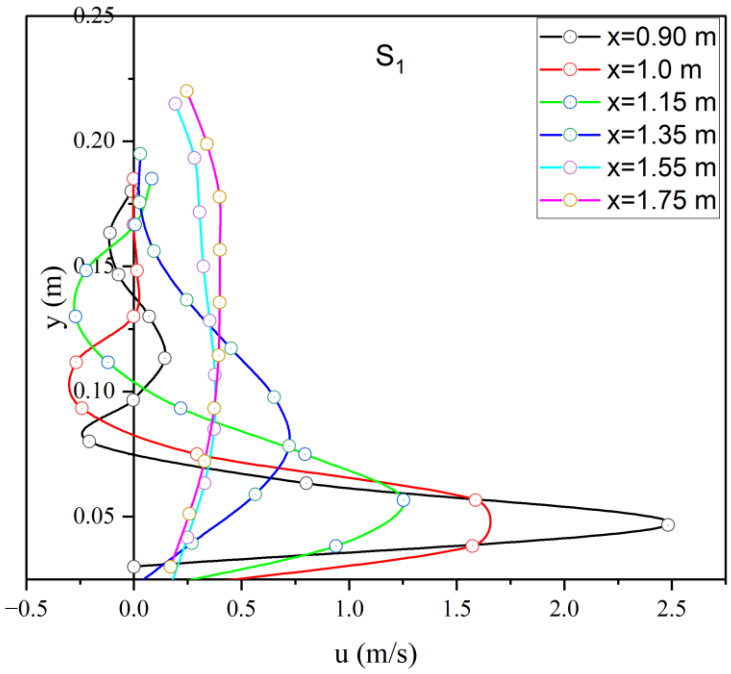
S1
x=0.90 m
x=1.0 m
x=1.15 m
x=1.35 m
x=1.55 m
x=1.75 m
y (m)
u (m/s)
0.25
0.20
0.15
0.10
0.05
−0.5
0.0
0.5
1.0
1.5
2.0
2.5

(a)

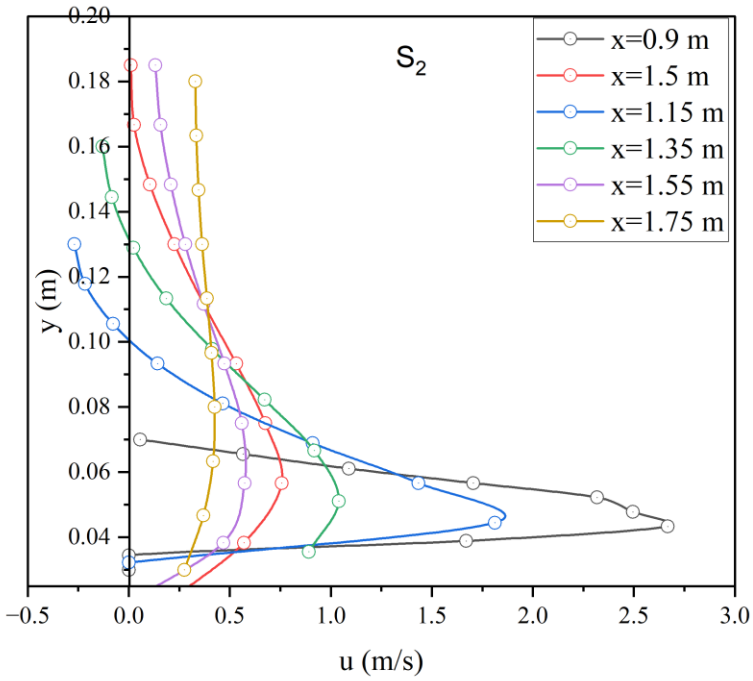
S2
x=0.9 m
x=1.5 m
x=1.15 m
x=1.35 m
x=1.55 m
x=1.75 m
y (m)
u (m/s)
0.20
0.18
0.16
0.14
0.12
0.10
0.08
0.06
0.04
−0.5
0.0
0.5
1.0
1.5
2.0
2.5
3.0

(b)

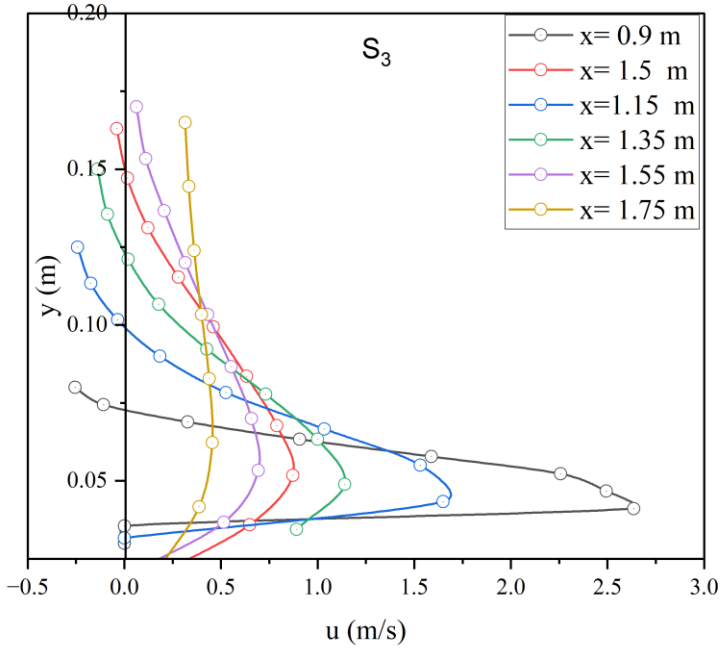
S3
x= 0.9 m
x= 1.5 m
x=1.15 m
x= 1.35 m
x= 1.55 m
x= 1.75 m
y (m)
u (m/s)
0.20
0.15
0.10
0.05
−0.5
0.0
0.5
1.0
1.5
2.0
2.5
3.0

(c)

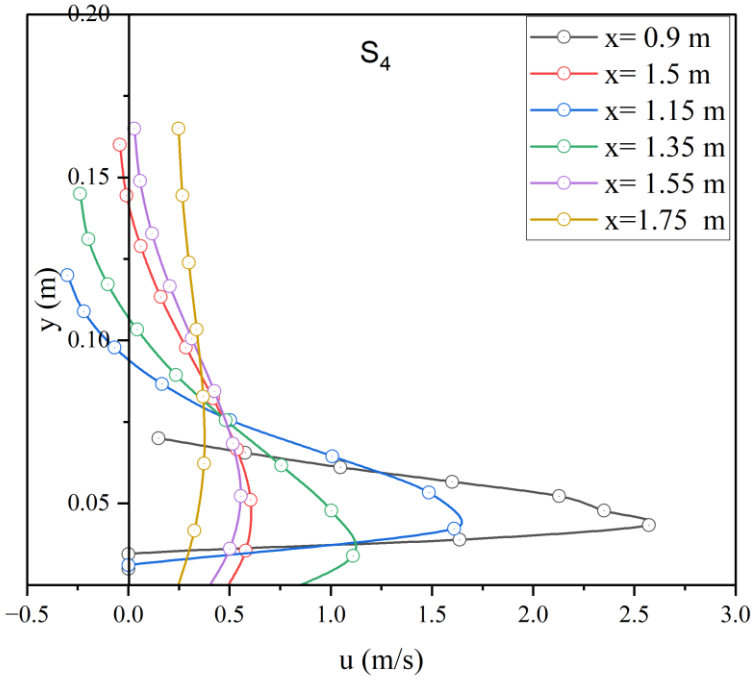
S4
x= 0.9 m
x= 1.5 m
x= 1.15 m
x= 1.35 m
x= 1.55 m
x=1.75 m
y (m)
u (m/s)
0.20
0.15
0.10
0.05
−0.5
0.0
0.5
1.0
1.5
2.0
2.5
3.0

(d)

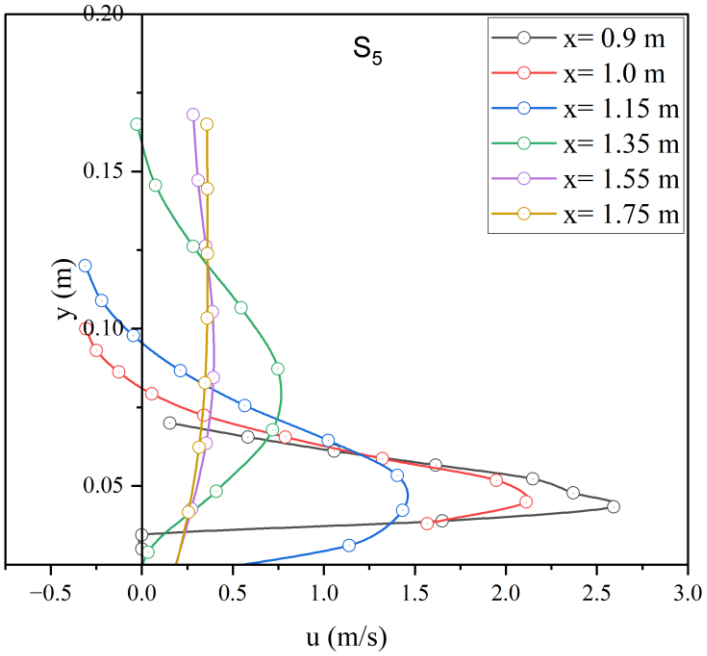
S5
x= 0.9 m
x= 1.0 m
x= 1.15 m
x= 1.35 m
x= 1.55 m
x= 1.75 m
y (m)
u (m/s)
0.20
0.15
0.10
0.05
−0.5
0.0
0.5
1.0
1.5
2.0
2.5
3.0

(e)

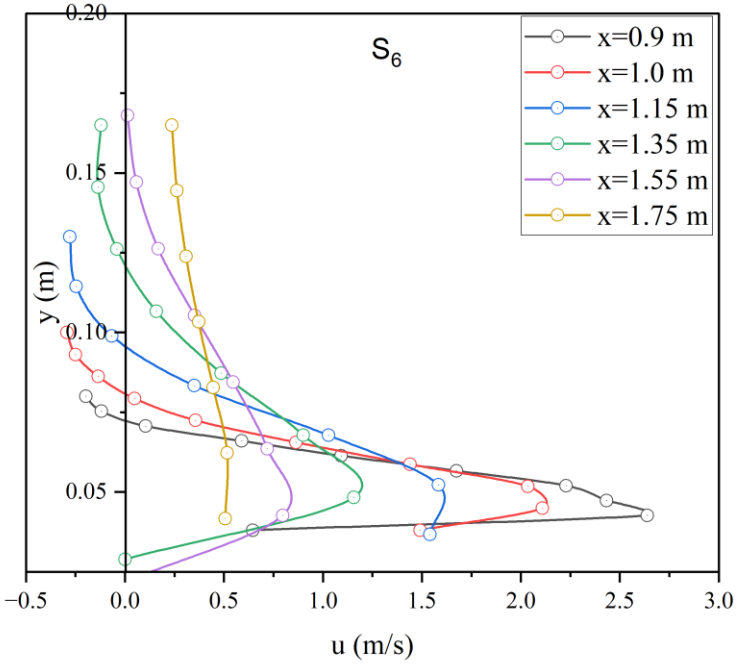
S6
x=0.9 m
x=1.0 m
x=1.15 m
x=1.35 m
x=1.55 m
x=1.75 m
y (m)
u (m/s)
0.20
0.15
0.10
0.05
−0.5
0.0
0.5
1.0
1.5
2.0
2.5
3.0

(f)

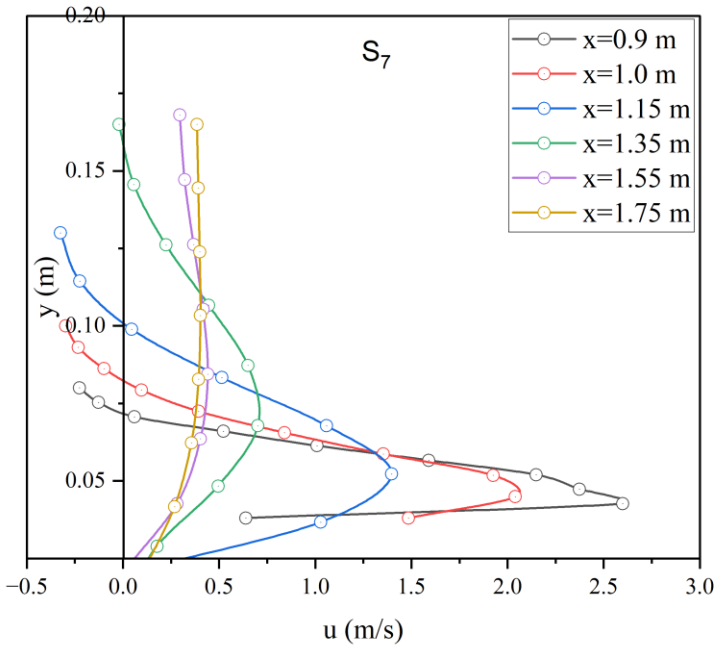

(g)

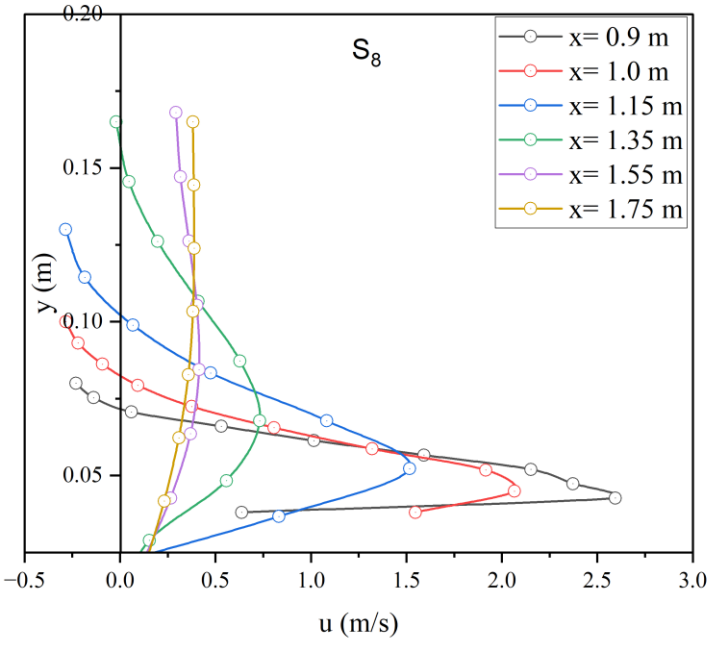

(h)

Figure 4.7 (a-h) Graphical representation of longitudinal velocity profiles of free hydraulic jump

4.3.1.2 Flow profile and velocity variation in case of submerged hydraulic jump

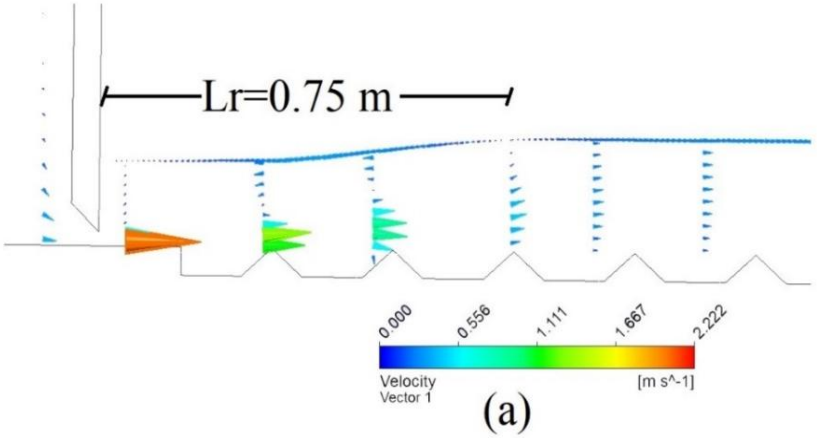

(a)

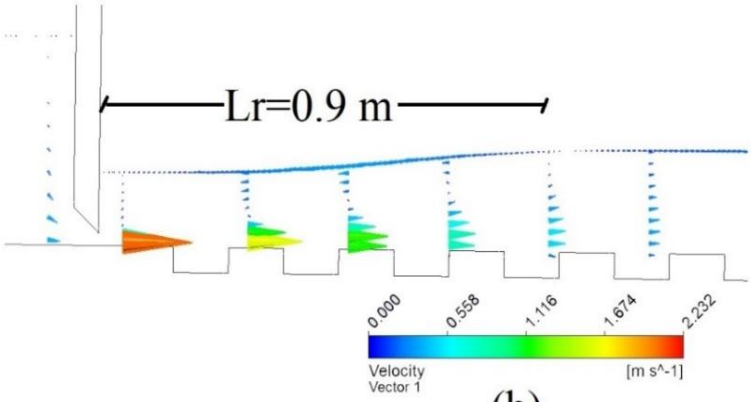

(b)

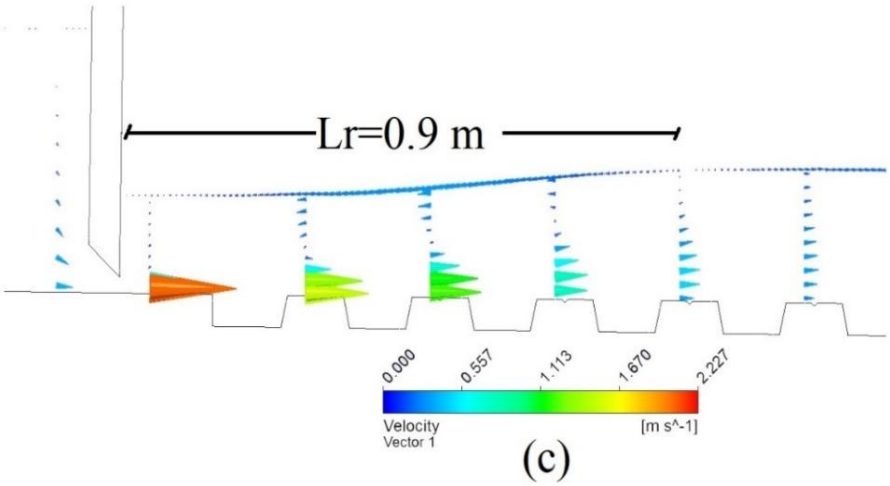

(c)

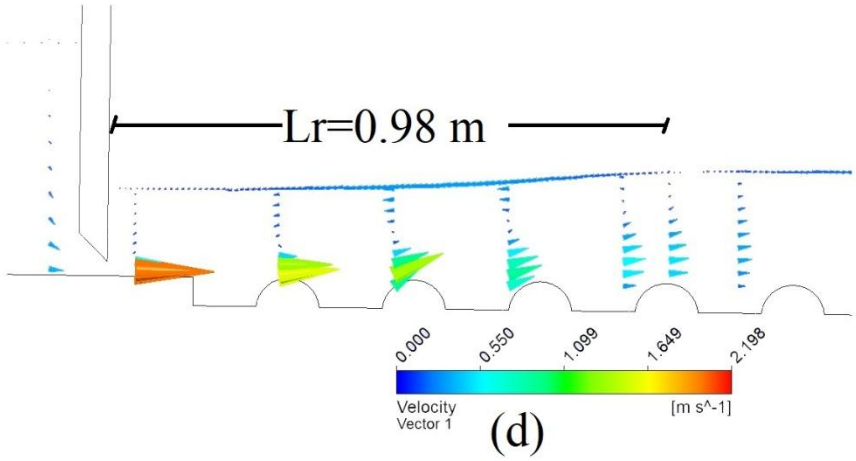
Lr=0.98 m
0.000
0.550
1.099
1.649
2.198
Velocity
Vector 1
[m s^-1]

(d)

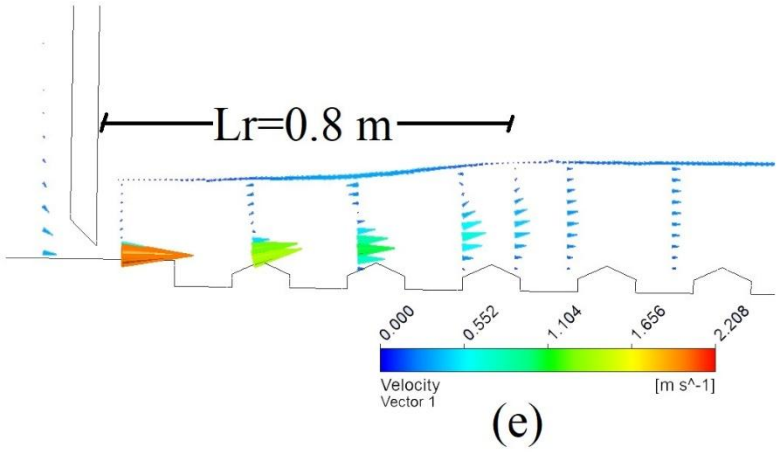
Lr=0.8 m
0.000
0.552
1.104
1.656
2.208
Velocity
Vector 1
[m s^-1]

(e)

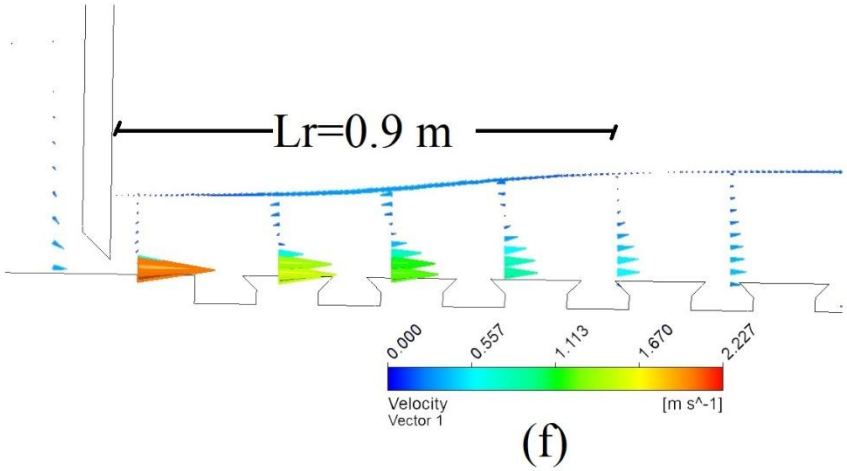
Lr=0.9 m
0.000
0.557
1.113
1.670
2.227
Velocity
Vector 1
[m s^-1]

(f)

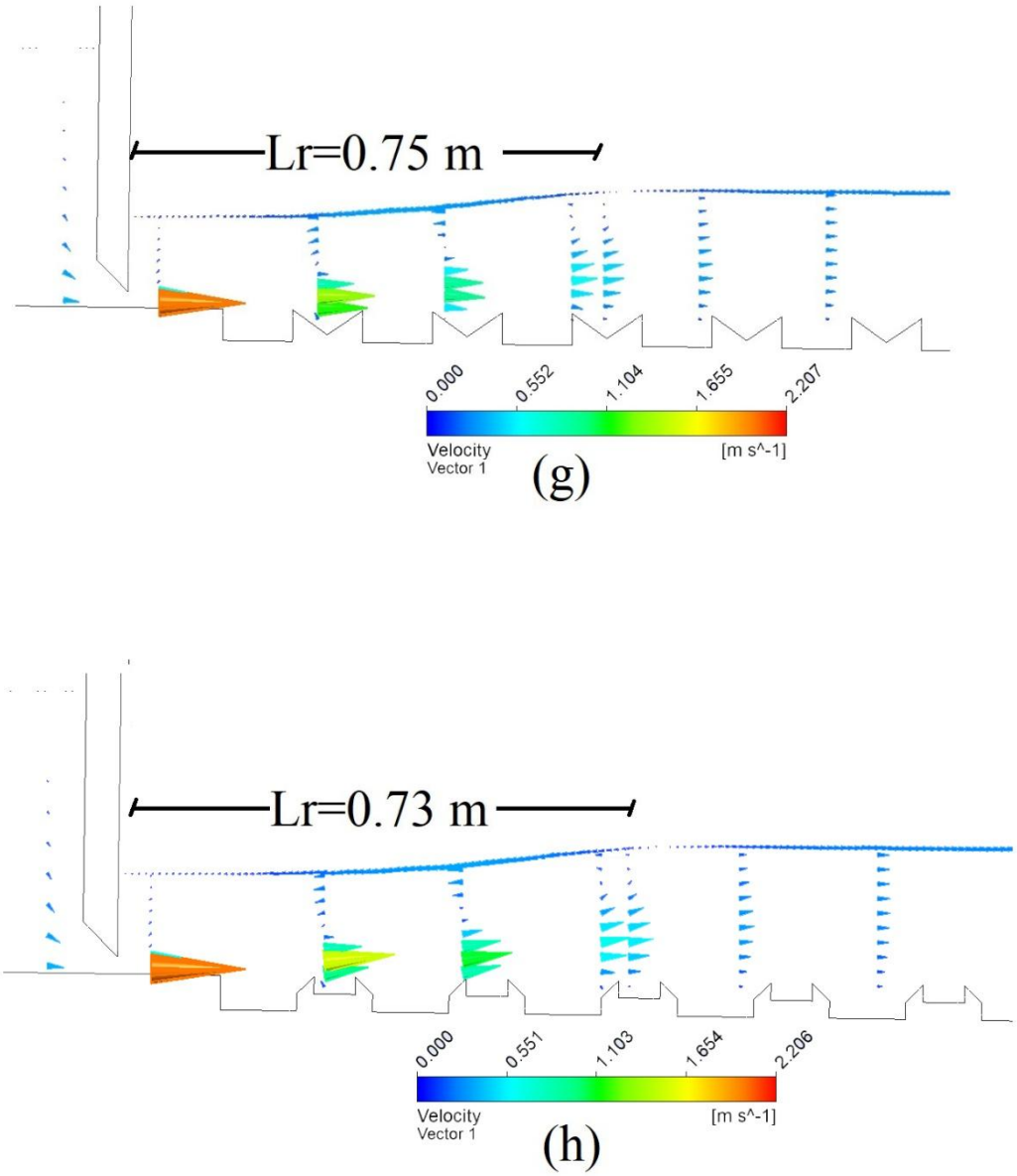

Figure 4.8 (a-h) Numerically generated flow profiles showing longitudinal velocities at different sections for each model for submerged hydraulic jump

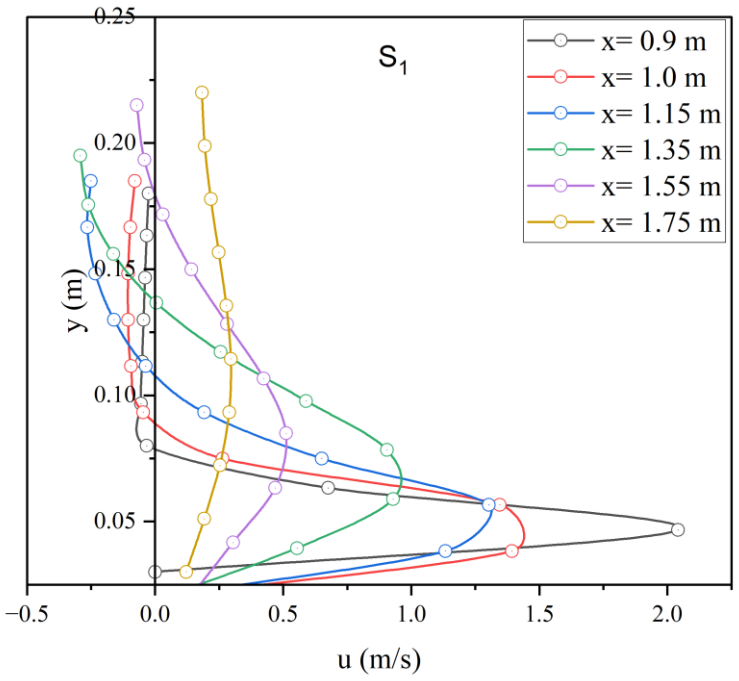
S1
x= 0.9 m
x= 1.0 m
x= 1.15 m
x= 1.35 m
x= 1.55 m
x= 1.75 m
y (m)
u (m/s)
0.25
0.20
0.15
0.10
0.05
−0.5
0.0
0.5
1.0
1.5
2.0

(a)

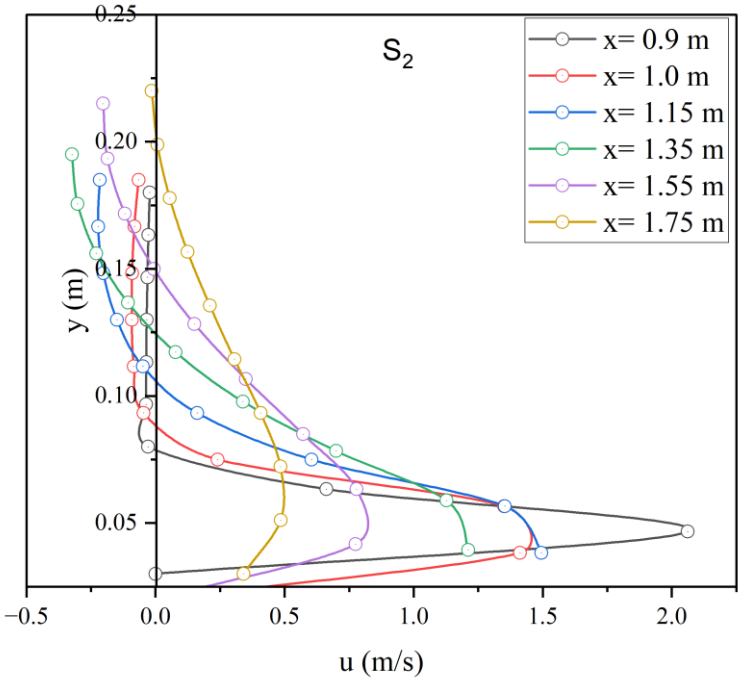
S2
x= 0.9 m
x= 1.0 m
x= 1.15 m
x= 1.35 m
x= 1.55 m
x= 1.75 m
y (m)
u (m/s)
0.25
0.20
0.15
0.10
0.05
−0.5
0.0
0.5
1.0
1.5
2.0

(b)

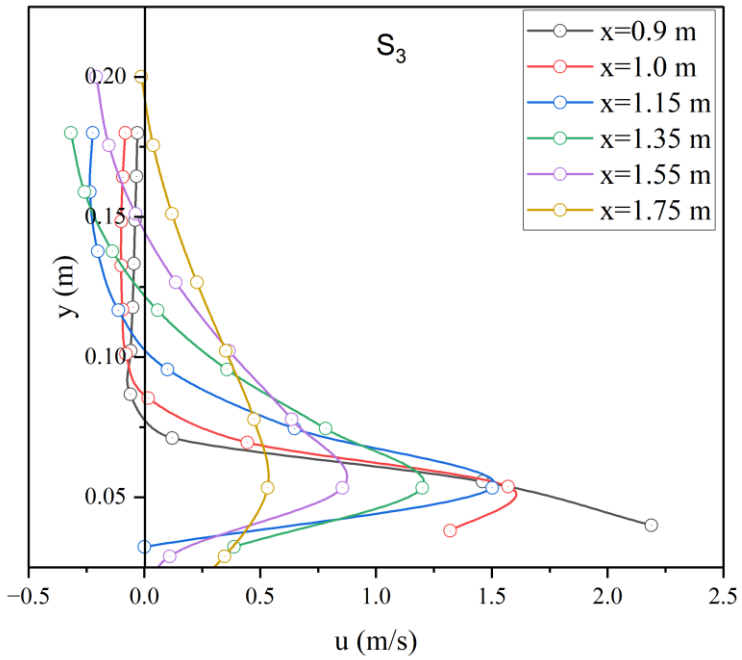
S3
x=0.9 m
x=1.0 m
x=1.15 m
x=1.35 m
x=1.55 m
x=1.75 m
y (m)
0.20
0.15
0.10
0.05
−0.5
0.0
0.5
1.0
1.5
2.0
2.5
u (m/s)

(c)

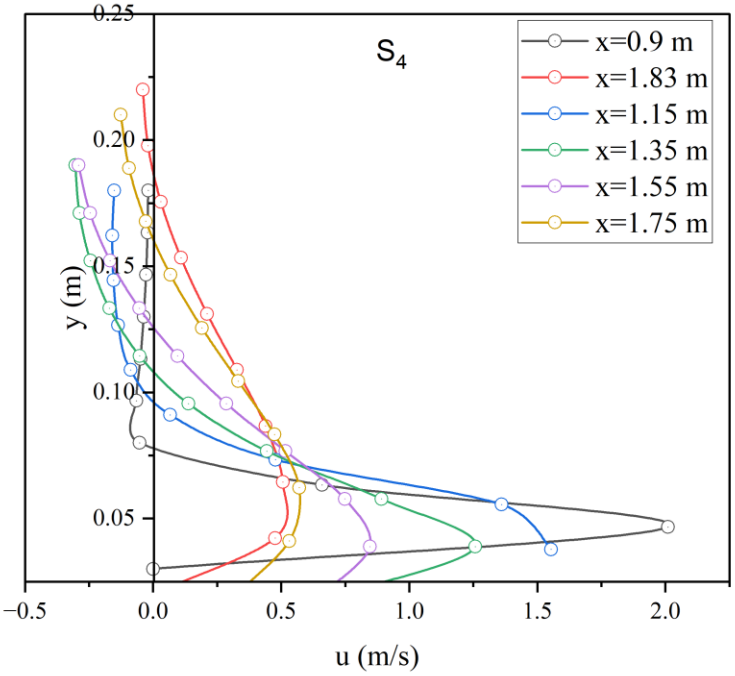
S4
x=0.9 m
x=1.83 m
x=1.15 m
x=1.35 m
x=1.55 m
x=1.75 m
y (m)
0.25
0.20
0.15
0.10
0.05
−0.5
0.0
0.5
1.0
1.5
2.0
u (m/s)

(d)

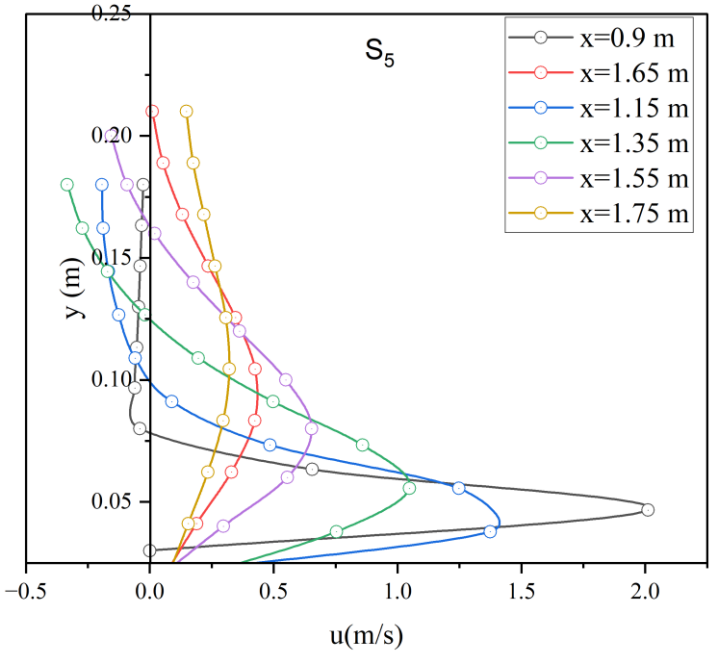
S5
x=0.9 m
x=1.65 m
x=1.15 m
x=1.35 m
x=1.55 m
x=1.75 m
y (m)
0.25
0.20
0.15
0.10
0.05
−0.5
0.0
0.5
1.0
1.5
2.0
u(m/s)

(e)

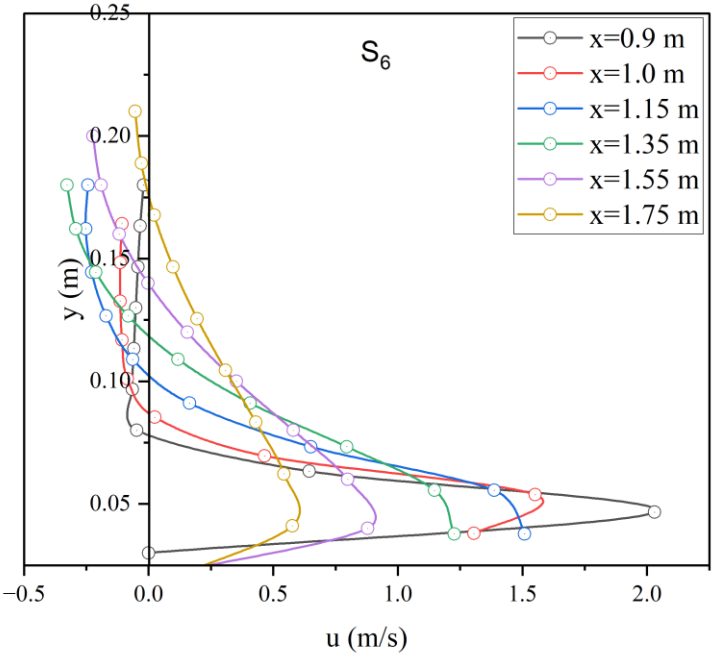
S6
x=0.9 m
x=1.0 m
x=1.15 m
x=1.35 m
x=1.55 m
x=1.75 m
y (m)
0.25
0.20
0.15
0.10
0.05
−0.5
0.0
0.5
1.0
1.5
2.0
u (m/s)

(f)

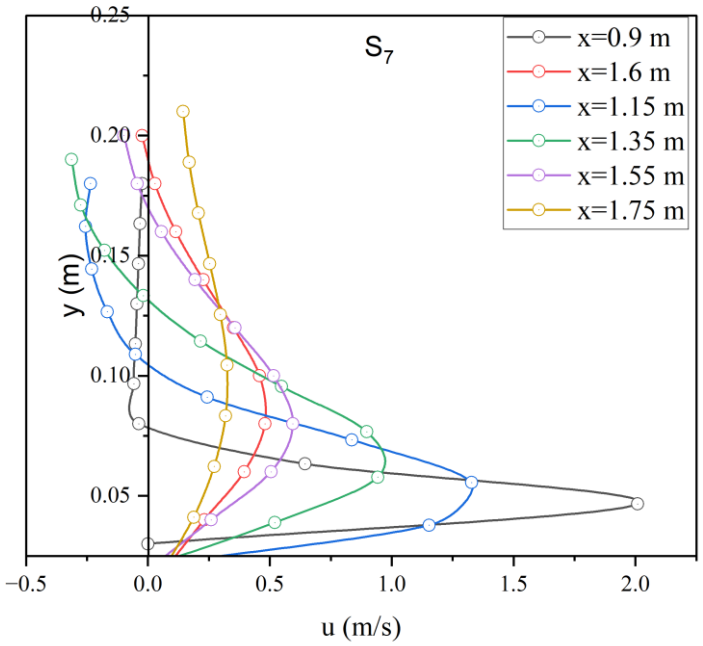

(g)

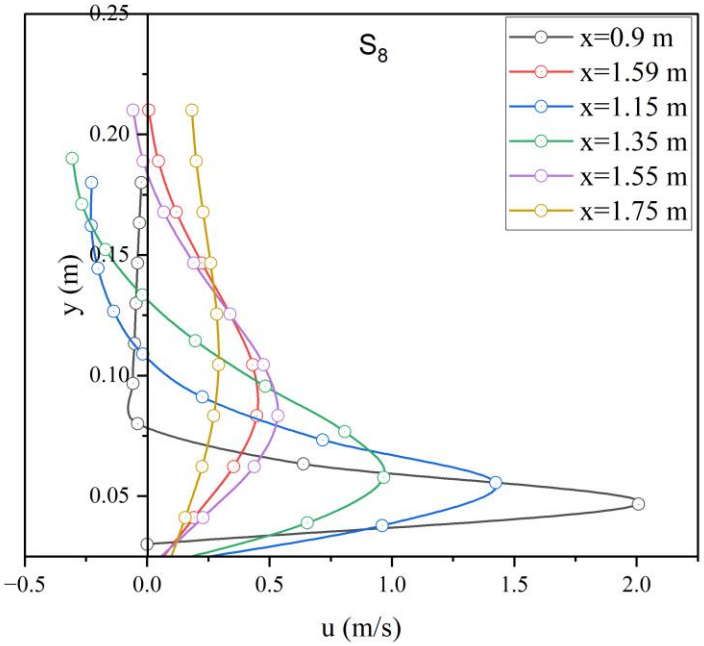

(h)

Figure 4.9 Graphical representation of longitudinal velocity profiles of submerged hydraulic jump

Figure 4.6 & Figure 4.8 illustrate the flow profiles and velocity distribution at different sections of flume. From the results of Figure 4.6 & Figure 4.8, as expected, the flow profiles and velocity distributions are almost similar in nature and in good agreement with the previous findings of Ghaderi et al. (2021) [18].

Due the contracted jet below the gate and flow, longitudinal velocities are less at the upper part of the gate opening, because the magnitude of longitudinal flow velocity is more at the vicinity of gate. A rise in reverse flow phenomena is observed in the vicinity of gates over the time and then begins to decline and represents the stagnation zone on the surface of the atmosphere. In the case of free and submerged hydraulic jump the observations were also used to infer that the recirculation area takes place near the sluice gate. Further it is observed that the negative magnitude of velocity is higher in mid of the recirculation zone than near the sluice gate. After propagations of fluid the magnitude of the velocity becomes positive and somehow higher positive magnitudes are observed at free levelled surface. The above statements are true for both smooth and macrorough beds. In macrorough beds it is identified that the velocity magnitude in vicinity of two consecutive macroroughness regions are quite less than average velocity.

Figure 4.7 & Figure 4.9 shows the graphical representation of longitudinal velocity distribution at six different sections in case of free and submerged hydraulic jump respectively. These sections are the same for each arrangement of roughness. The velocity was measured from the bottom of the bed and up to the free surface. The velocity profile follows the nature of past studies of hydraulic jump in which the velocity varies parabolically up to certain length in the direction of flow due to upcoming water jet and the due to circulation and huge turbulence the velocity decay starts and the graph follow a backward movement. Further a moment comes when the velocity becomes almost zero for a while and becomes negative in the roller regions.

4.3.2 Velocity vector variation

A velocity vector is a mathematical representation used in physics to describe the motion of an object or fluid particle. It is a vector quantity because it has both magnitude and direction. In fluid dynamics, velocity vectors are often used to depict the flow of a fluid at various points in space. The velocity vector is normally indicated in diagrams by a line with an arrow-head, where the length of the line gives a measure of the velocity and the direction of the arrow head gives a measure of the direction of motion.

In fluid dynamics, the concepts of velocity vectors play a significant role in determining the representation of flow fields in the form of vectors, assessment of the behaviour of fluids in given conditions. Velocity vectors are generally acquired from measurements through flow visualization or computational modelling. Below section represented the velocity vector to know the behaviour of individual fluid particle over macrorough beds in case of hydraulic jump.

4.3.2.1 Free hydraulic jump

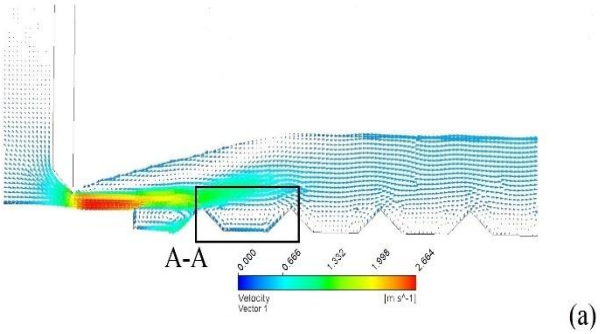

(a)

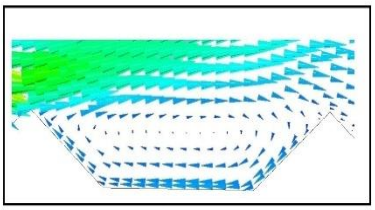

A-A

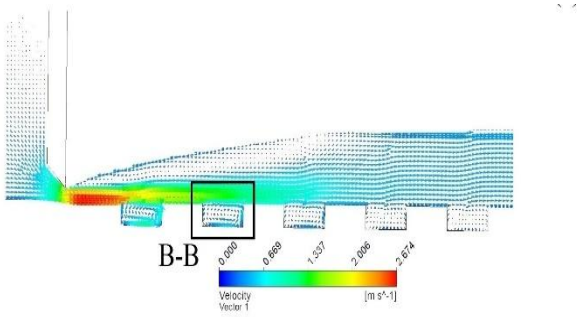

(b)

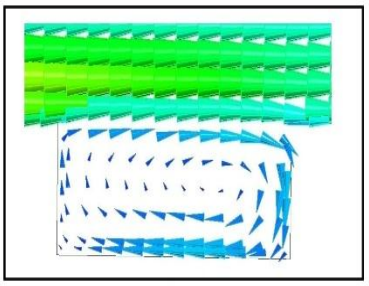

B-B

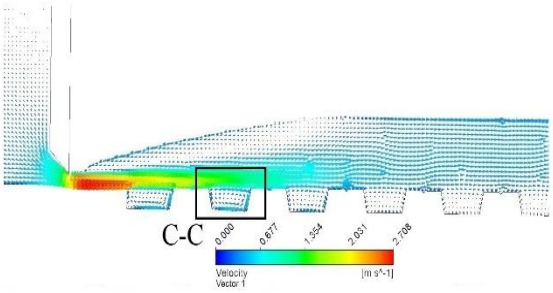

(c)

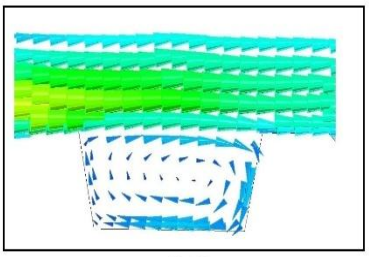

C-C

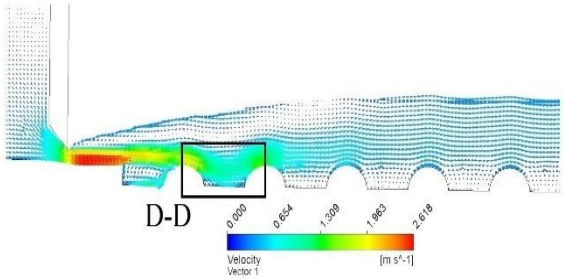
D-D
0.000
0.654
1.309
1.963
2.618
Velocity
Vector 1
[m s^-1]

(d)

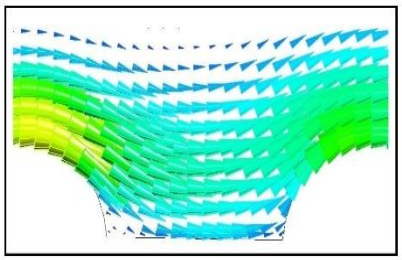

D-D

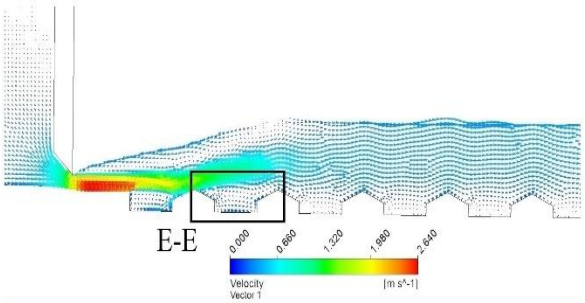
E-E
0.000
0.660
1.320
1.980
2.640
Velocity
Vector 1
[m s^-1]

(e)

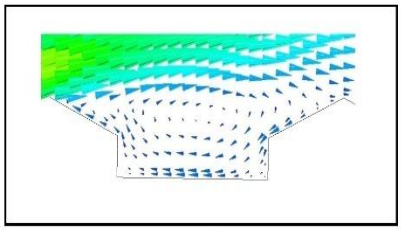

E-E

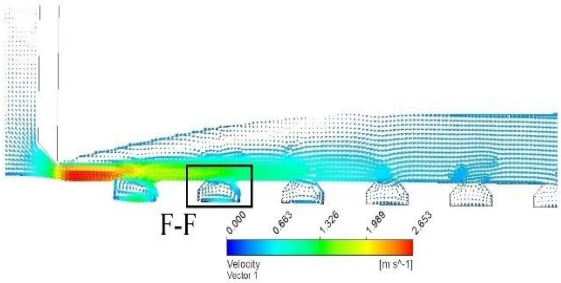
F-F
0.000
0.663
1.326
1.989
2.653
Velocity
Vector 1
[m s^-1]

(f)

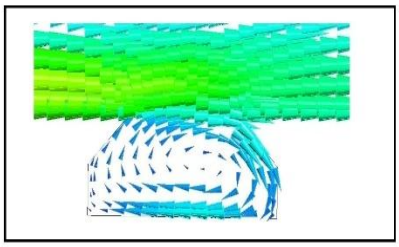

F-F

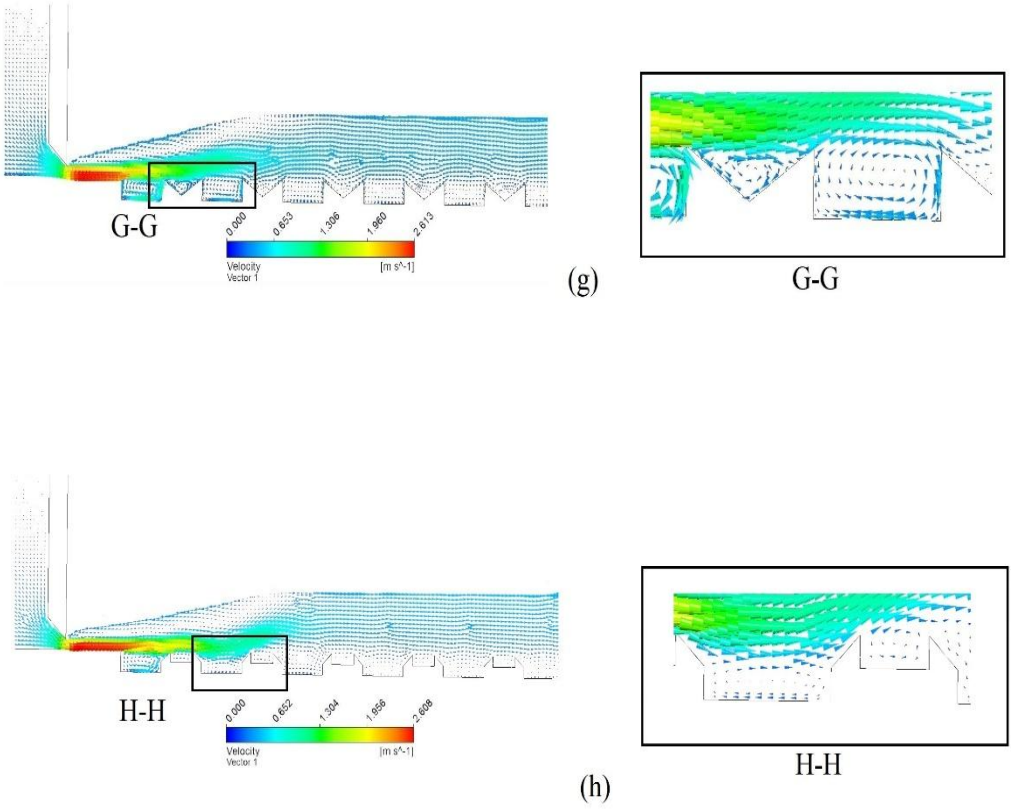

Figure 4.10 Numerically generated velocity vector for each case of free hydraulic jump

4.3.2.2 Submerged hydraulic jump

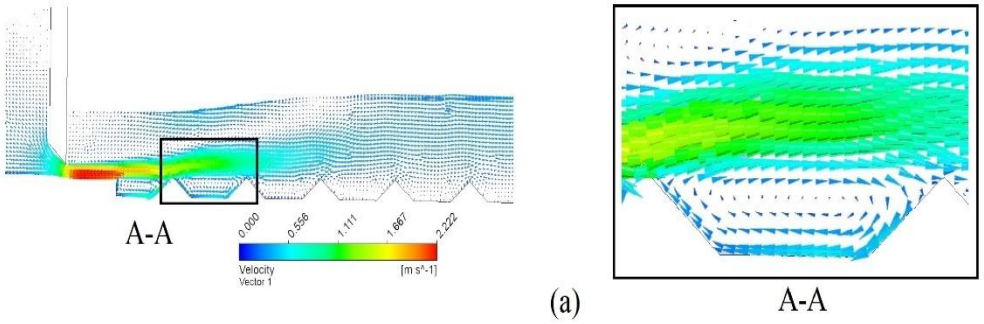

(a)

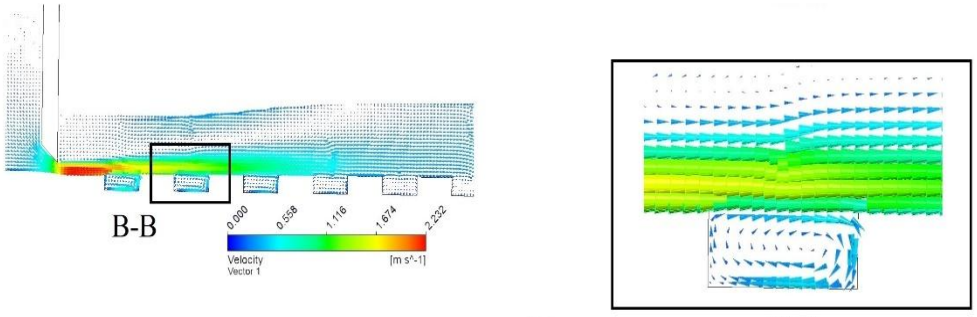

(b)

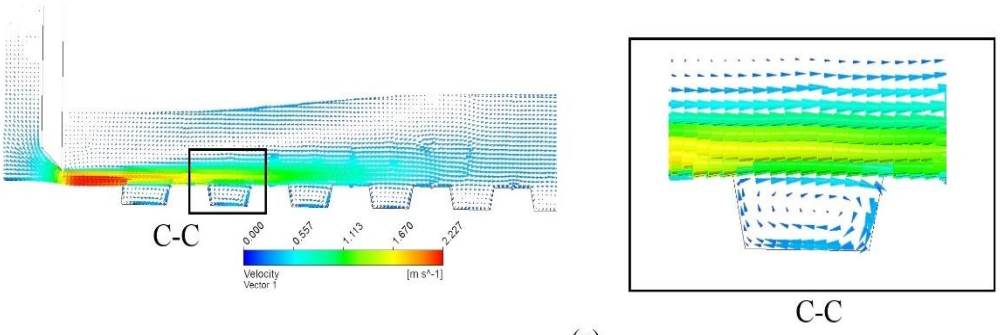

(c)

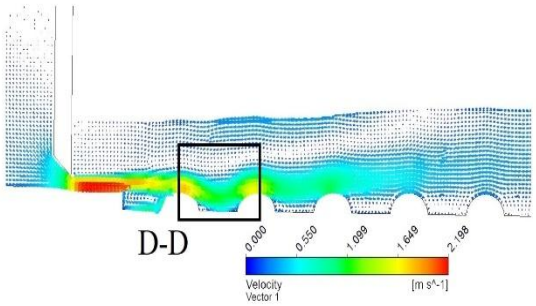
D-D
0.000
0.550
1.099
1.649
2.198
Velocity
Vector 1
[m s^-1]

(d)

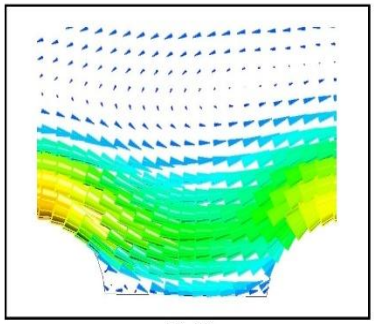
D-D

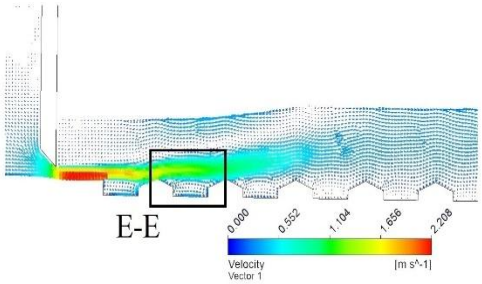
E-E
0.000
0.552
1.104
1.656
2.208
Velocity
Vector 1
[m s^-1]

(e)

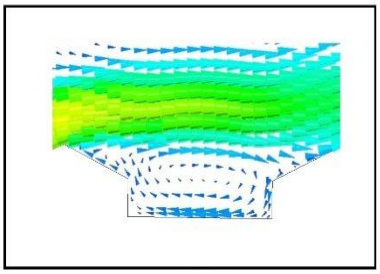
E-E

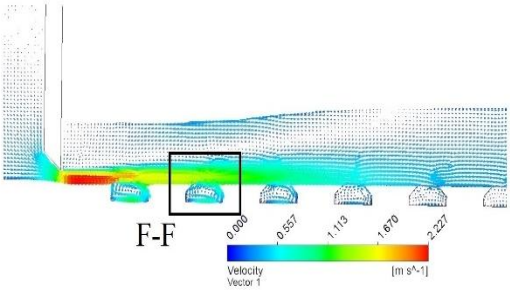
F-F
0.000
0.557
1.113
1.670
2.227
Velocity
Vector 1
[m s^-1]

(f)

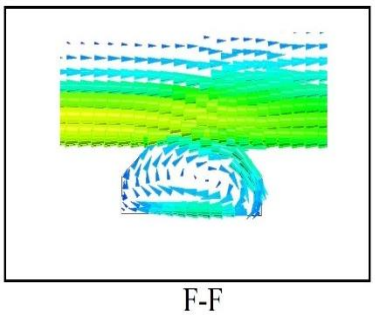
F-F

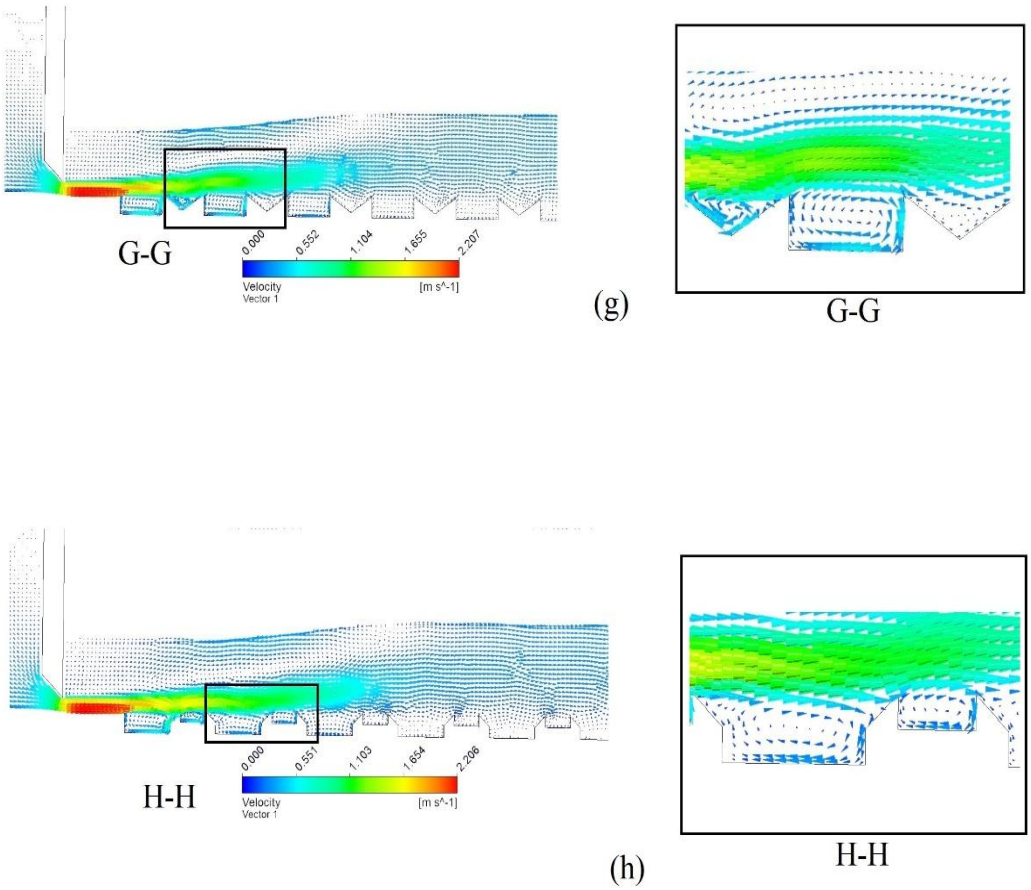

Figure 4.11 (a-h) Numerically generated velocity vector for each case of submerged hydraulic jump

Figure 4.10 & Figure 4.11 illustrate the numerically predicted velocity vectors under the sluice gates on macrorough beds for free and submerged hydraulic jump respectively. It is observed that the flow pattern in the sluice gate with macroroughness for all the models is almost similar. However, the clock wise circulation are noticed in between two consecutive macroroughness elements for most of the shapes and the fluctuation in clockwise circulation are also seen in some models and this may be due to the structural properties of the particular model. Thus, it can be inferred that the circulation of the fluid depends on the shape of the macroroughness.

The circulation of fluid between the two consecutive strip macroroughness reduces the velocity of fluid near the bed and reduces the length of jump. The space between two consecutive strip macroroughness may be termed as cavity region or dead zone as these spaces are occupied with water. The velocities in cavity region are

measured numerically and found that the velocities in these regions for most of the models are found approximately tenth part of the mean velocity. This type of justification is valid for both free and submerged hydraulic jump. Such remarks states that the cavity regions are more influencing parameters in case of fast-moving fluid flow for minimizing or dissipating the fluid velocities and to minimize the chance of erosion of downstream channel bed.

4.3.3 Turbulent Kinetic Energy (TKE)

TKE is one of those descriptions that pertain to energy in a turbulent fluid flow situation. Turbulence is another phenomenon in fluid dynamics which is accompanied by unsteady, random, erratic or Zone turbulent flow of fluids where three-dimensional flow velocity, pressure and density are in constant variation. These fluctuations occur on a wide range of spatial and temporal scales. Turbulent kinetic energy is important in various fields of science and engineering, including meteorology, oceanography, aerospace engineering, and civil engineering. Understanding and predicting turbulent flows and their associated kinetic energy are crucial for designing efficient and safe systems, such as aircraft, wind turbines, and pipelines, and for modelling atmospheric and oceanic circulation patterns.

In view of the mathematical definition, TKE is referred to as the mean kinetic energy per unit mass of the turbulent velocity fluctuations and can be written as below.

$$TKE = \frac{1}{2}(\overline{u'^2} + \overline{v'^2} + \overline{w'^2}) \tag{32}$$

Where, the fluctuating velocity components from the mean velocities in x, y and z- direction are u', v', w' respectively. $\overline{u'^2}, \overline{v'^2}, \overline{w'^2}$ are thought to be the time-averaged of the squared velocity fluctuations which measures the magnitude of turbulence in each direction.

Below sections describe the contours of turbulent kinetic energy over macrorough beds in case of hydraulic jumps.

4.3.3.1 Free hydraulic jump

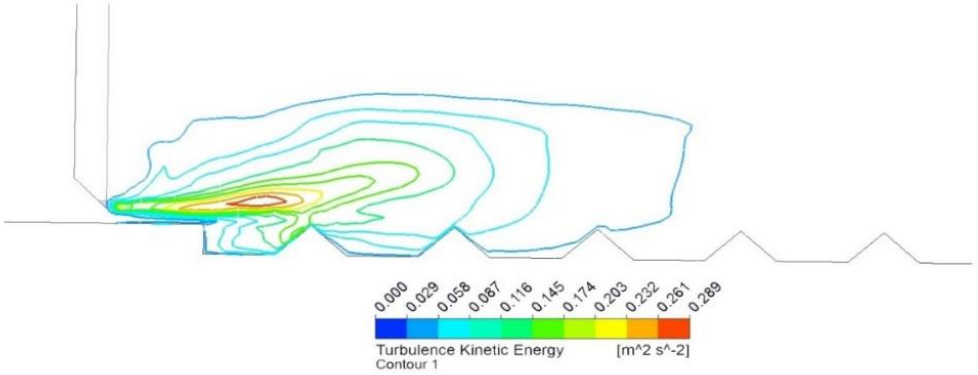

(a)

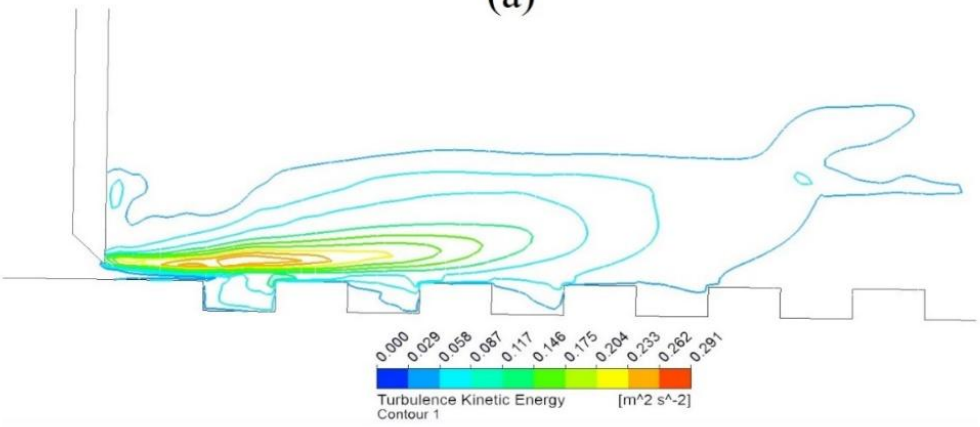

(b)

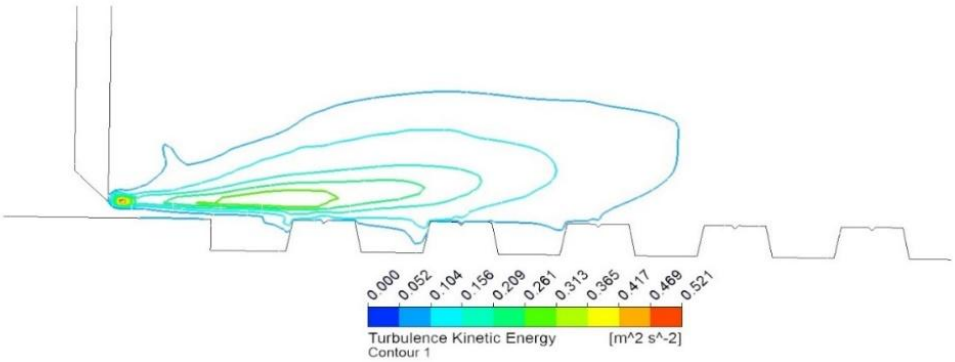

(c)

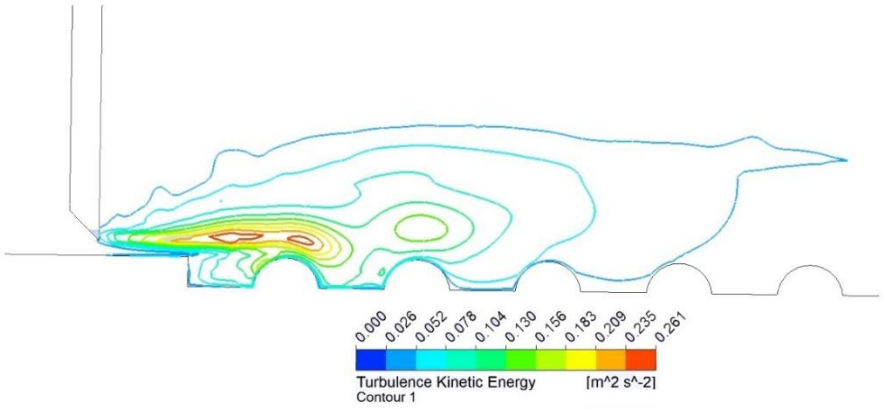
0.000
0.026
0.052
0.078
0.104
0.130
0.156
0.183
0.209
0.235
0.261
Turbulence Kinetic Energy [m^2 s^-2]
Contour 1

(d)

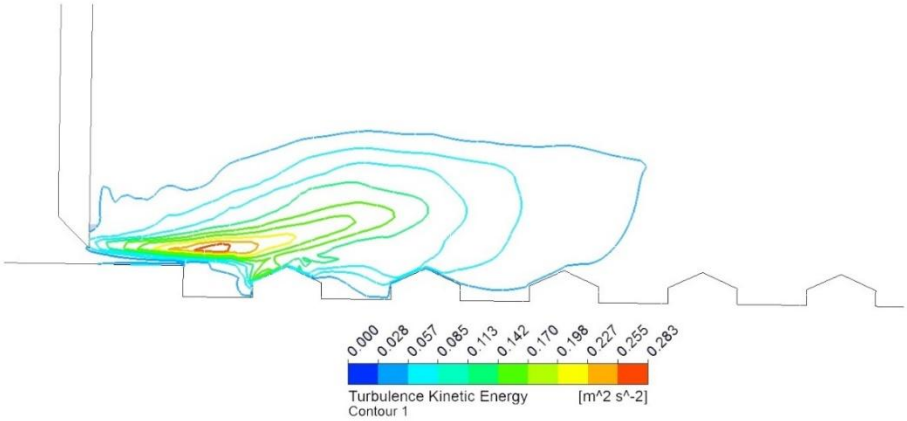
0.000
0.028
0.057
0.085
0.113
0.142
0.170
0.198
0.227
0.255
0.283
Turbulence Kinetic Energy [m^2 s^-2]
Contour 1

(e)

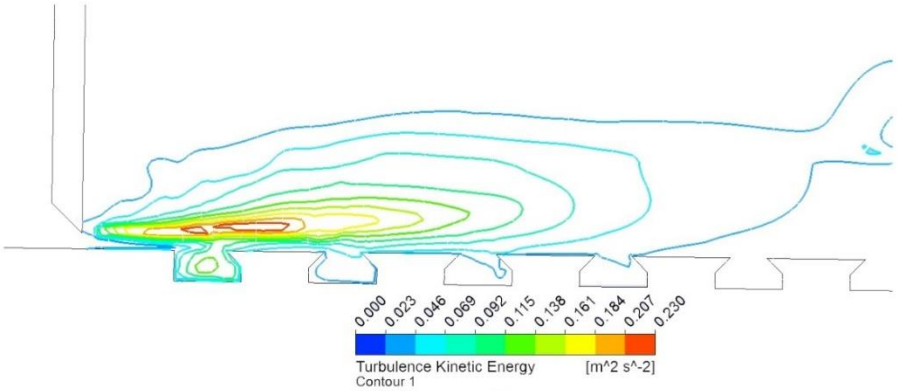
0.000
0.023
0.046
0.069
0.092
0.115
0.138
0.161
0.184
0.207
0.230
Turbulence Kinetic Energy [m^2 s^-2]
Contour 1

(f)

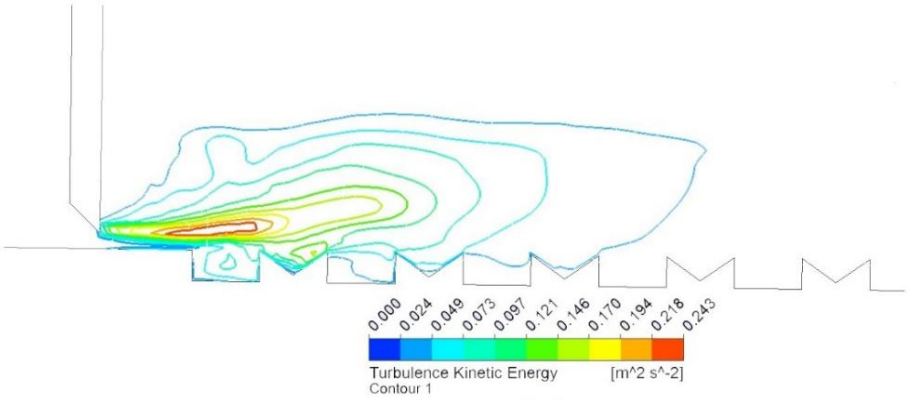

(g)

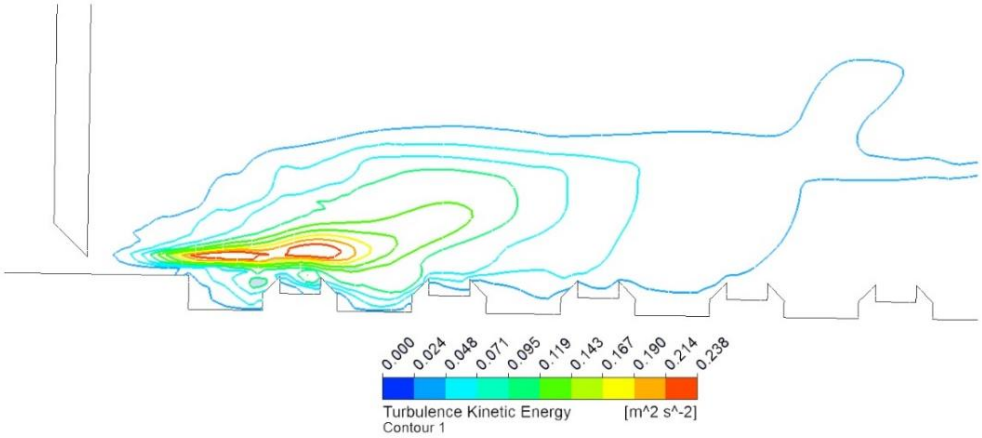

(h)

Figure 4.12 (a-h) Numerically generated turbulent kinetic energy contours for each case of free hydraulic jump

4.3.3.2 Submerged hydraulic jump

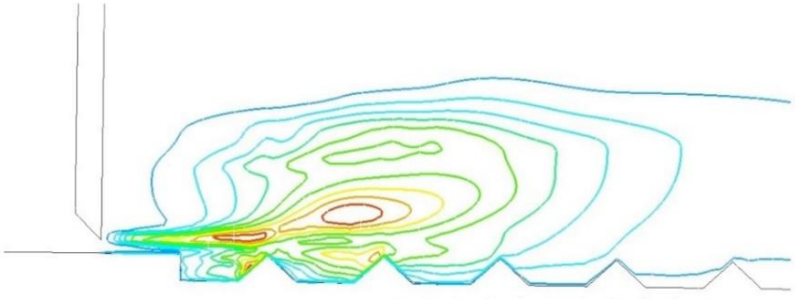

(a)

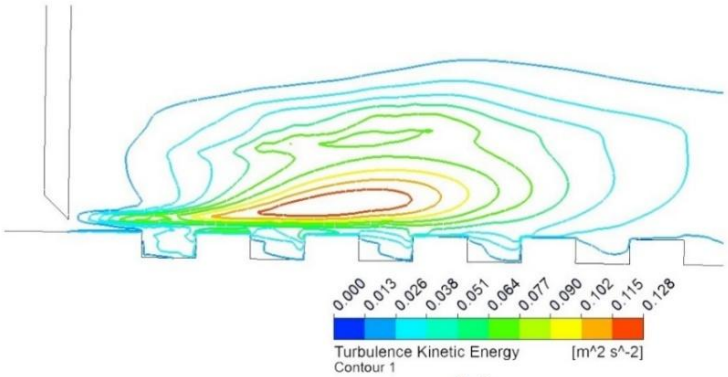

(b)

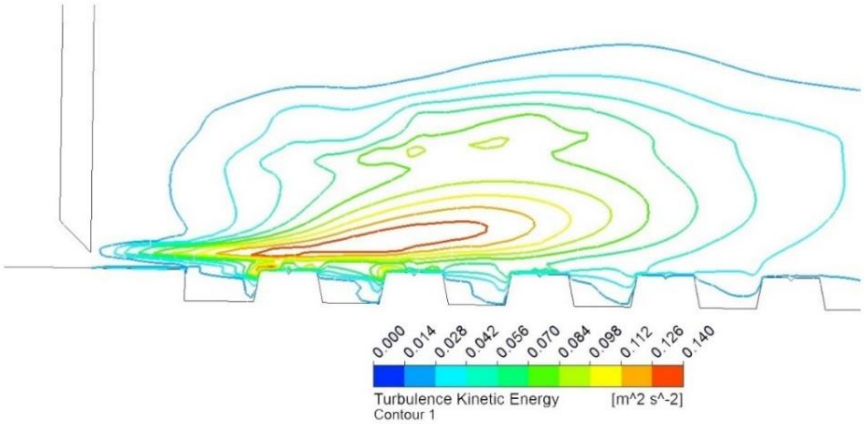

(c)

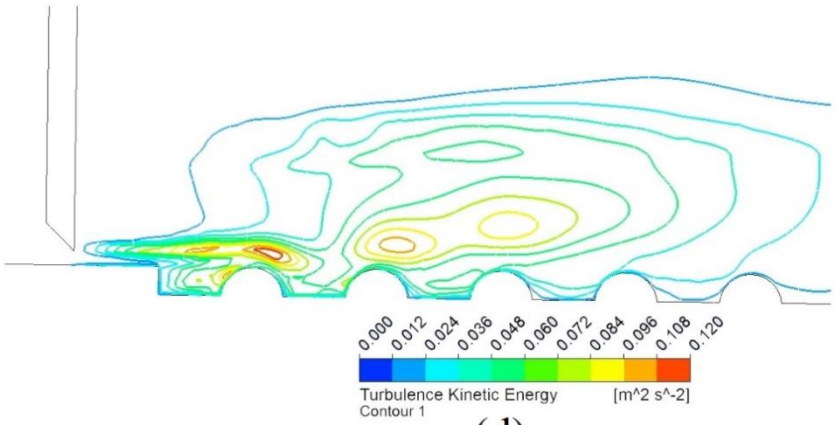
0.000 0.012 0.024 0.036 0.048 0.060 0.072 0.084 0.096 0.108 0.120
Turbulence Kinetic Energy [m^2 s^-2]
Contour 1

(d)

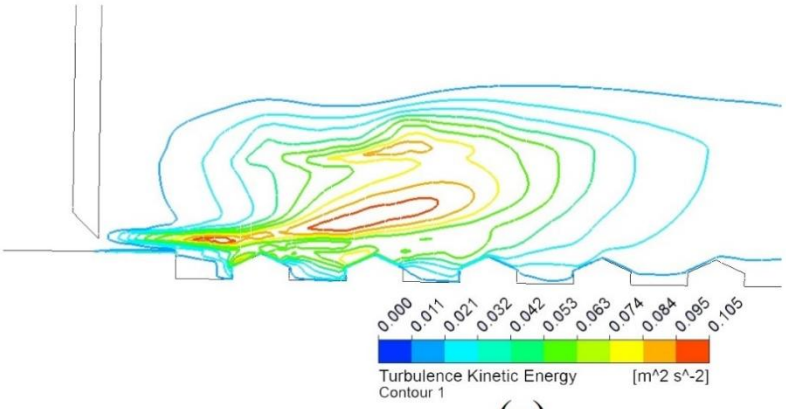
0.000 0.011 0.021 0.032 0.042 0.053 0.063 0.074 0.084 0.095 0.105
Turbulence Kinetic Energy [m^2 s^-2]
Contour 1

(e)

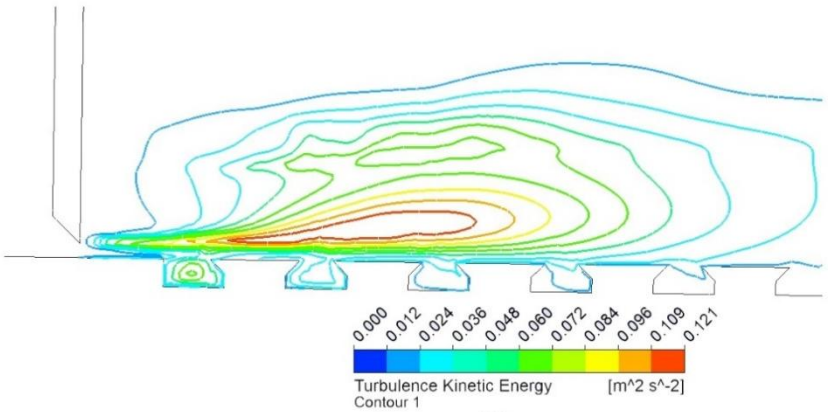
0.000 0.012 0.024 0.036 0.048 0.060 0.072 0.084 0.096 0.109 0.121
Turbulence Kinetic Energy [m^2 s^-2]
Contour 1

(f)

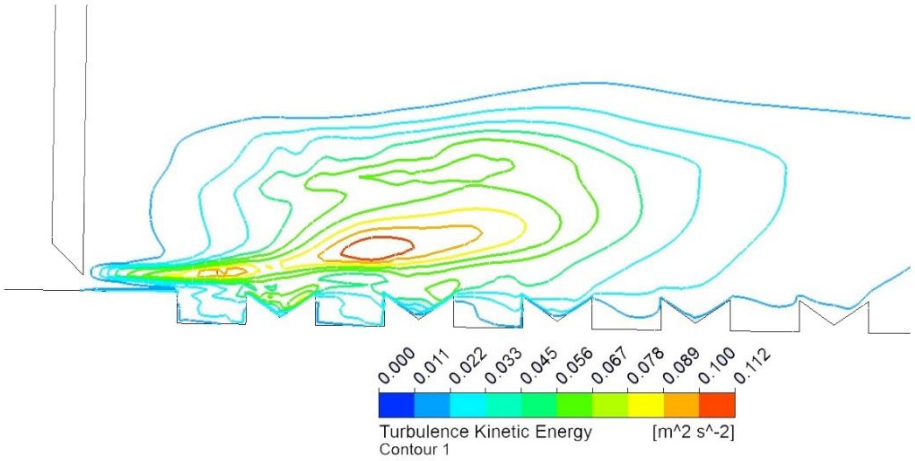

(g)

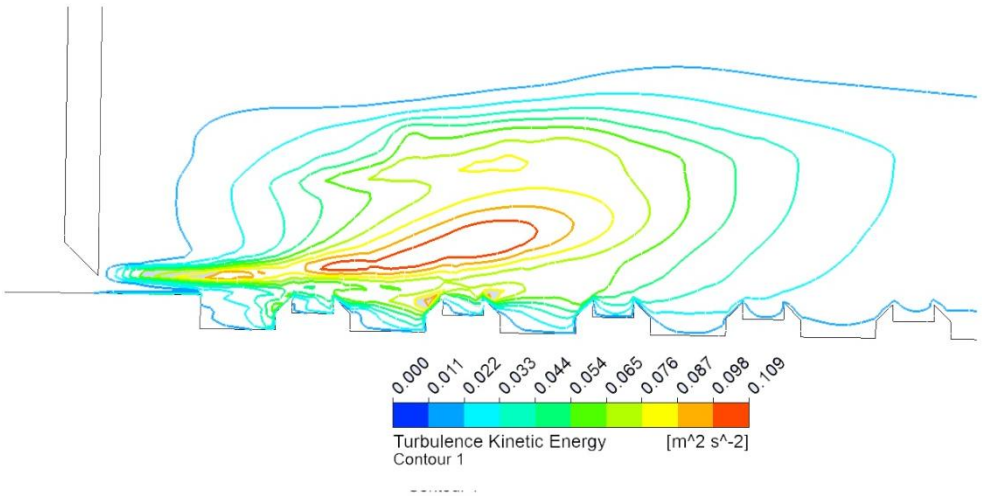

(h)

Figure 4.13 (a-h) Numerically generated turbulent kinetic energy contours for each case of submerged hydraulic jump

Figure 4.12 & Figure 4.13 illustrate the turbulent kinetic energy (TKE) counters for macrorough beds in case of free and submerged hydraulic jump respectively. The turbulence region over macrorough beds within the jump is shown by contours and it can be seen that by providing macroroughness near the bed turbulence kinetic energy reduces by considerable amount. The turbulence region begins near a sluice gate with higher intensity and reduces with the provisions of macroroughness and this is due to clockwise circulation motion of water in between two consecutive strip macroroughness i.e., cavity region.

4.3.4 Dimensionless Parameters

Dimensionless parameters provide valuable insights into the behaviour of hydraulic jumps and help in the design and analysis of hydraulic structures.

4.3.4.1 Sequent depth ratio (y_2/y_1)

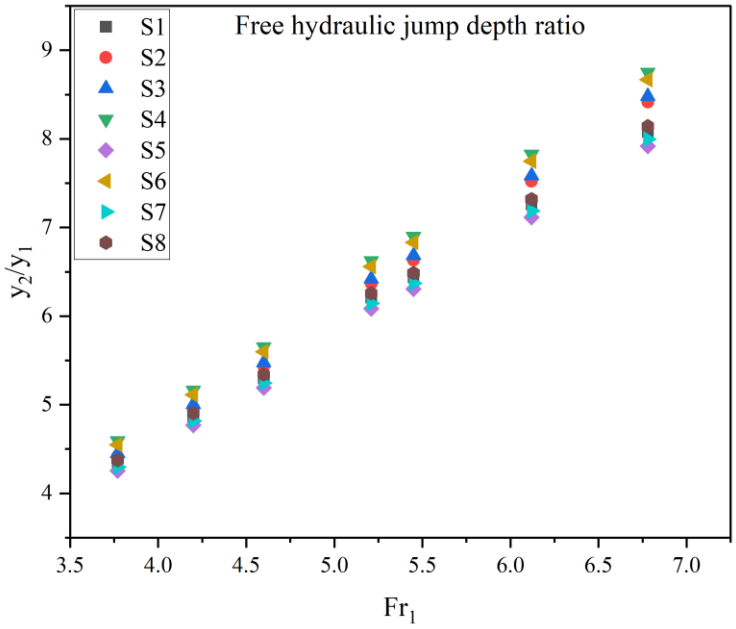

Figure 4.14 Sequent depth ratio vs initial Froud number in case of free hydraulic jump

Comparison of numerically generated results of sequent depth ratio for all eight models is graphically presented in Figure 4.14. From above graph it can be inferred that the model S_1, S_5, S_7 & S_8 yields almost similar results. However, S_1 *i.e.,* triangular model is more effective in enhancing the sequent depth ratio than other one. Quantitatively, it is reported that the sequent depth ratio for S_1 model is 3.13% shorter than S_2 model, 3.95 % shorter than S_3 model, 7.25 % shorter than S_4 model and 6.22 % shorter than S_6 model.

4.3.4.2 Tail water depth ratio (y_4/y_1)

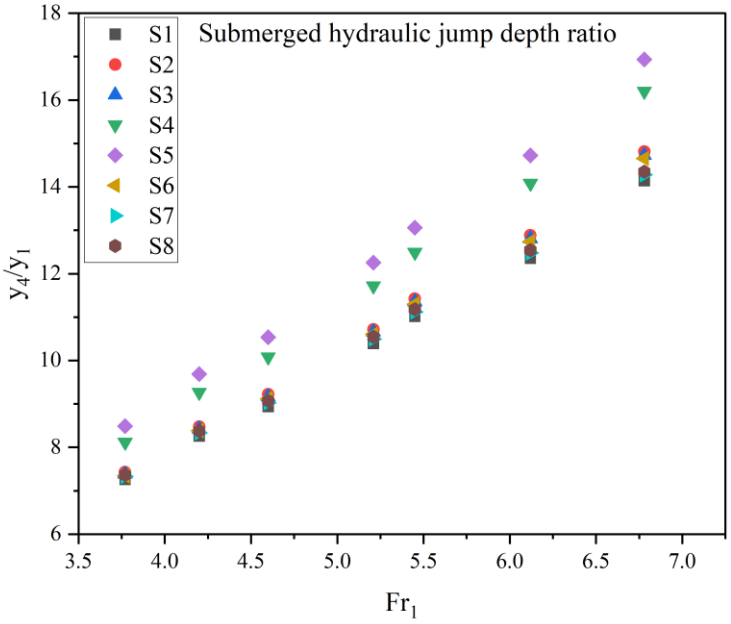

Figure 4.15 Tail water depth ratio versus initial Froude number in case of submerged hydraulic jump

Comparison of numerically generated results of tail-water depth ratio for all eight models are graphically presented in Figure 4.15. From above graph it can be inferred that the model S_1, S_7 & S_8 yields almost similar results. However, S_1 *i.e.,* triangular model is more effective in enhancing the tail-water depth ratio than other one. Quantitatively, it is reported that the tailwater depth ratio for S_1 model is 3.76% shorter than S_2 model, 3.14% shorter than S_3 model, 13.45% shorter than S_4 model, 12.21% shorter than S_5 model and 18.61% shorter than S_6 model.

4.3.4.3 Roller length of jump ratio (Lr/y_1)

Figure 4.16 & Figure 4.17 shows the plot between roller length of jump ratio and initial Froud number in case of free & submerged hydraulic jumps respectively. From Figure 4.16 it can be inferred that the model S_1, S_7 & S_8 has similar results and are more effective in enhancing the roller length of jump ratio than other one. Quantitatively, it is found that the roller length of jump ratio for S_1, S_7 & S_8 model is 5.72% shorter than S_2 or S_3 models and 17.28% shorter than S4 or S6 models.

From Figure 4.17 it can be reported that the model S_1, S_7 & S_8 yields almost similar results. Quantitatively, it is found that the roller length of jump ratio for S_1, S_7 & S_8 model is 5.72 % shorter than S_2 or S_3 or S_6 models and 4.37% shorter than S_4 or S_5 models.

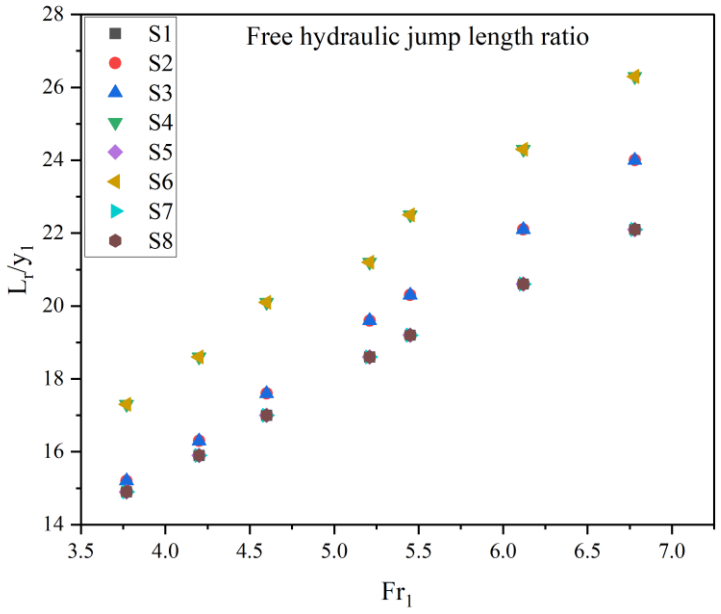

Figure 4.16 length of jump ratio versus initial Froude number in case of free hydraulic jump

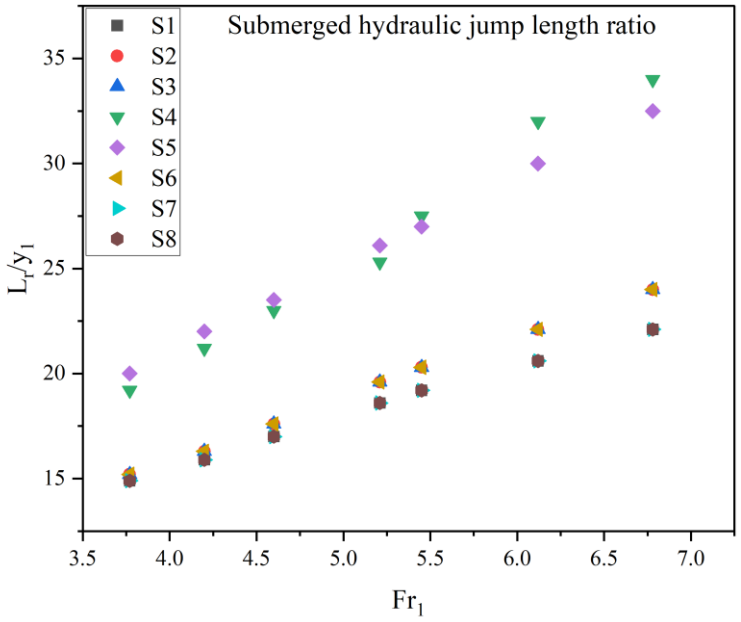

Figure 4.17 length of jump ratio versus initial Froude number in case of submerged hydraulic jump

4.3.4.5 Loss of energy through hydraulic jumps

Energy loss through hydraulic jumps is decided by the difference in specific energy between the pre jump flow states and the post jump flow states. This can be defined more particularly as the relationship between specific energy upstream and specific energy downstream across the jump and expressed in equation for free jump and submerged jump mathematically as follows respectively.

$$E_i = y_i + \frac{u_i^2}{2g} \tag{33}$$

$$E_L = \frac{E_1 - E_2}{E_1} \tag{34}$$

$$E_L = \frac{E_3 - E_4}{E_3} \tag{35}$$

Here, the longitudinal sections within the jump were indicated by the subscript "i" (*i.e.,* i= 0, 1, 2, 3, 4). E_L represents relative energy loss through free & submerged hydraulic jump whereas, E_1, E_2 is the specific energy calculated at the upstream and downstream ends of the free hydraulic jump, respectively. Similarly, E_3 and E_4 is the specific energy calculated at the upstream and downstream ends of the submerged hydraulic jump respectively.

Figure 4.18 & Figure 4.19 illustrate the relative energy loss through free & submerged hydraulic jumps. From the results of Figure 4.18 & Figure 4.19 it can be seen that S_1 *i.e.,* triangular model is dissipating more energy than other models.

From Figure 4.18 it can be reported that the relative energy loss in case of free hydraulic jump for S_1 model is 4.87 % higher than S_2 or S_3 model, 6.78% higher than S_4 model, 5.72% higher than S_5 model, 11.04% higher than S_6 model, 3.2% higher than S_7 model & 3.3% higher than S_8 model.

From Figure 4.19 it can be reported that the relative energy loss in case of submerged hydraulic jump for S_1 or S_7 model is 5.43% higher than S_2 or S_3 model, 10.97% higher than S_4 model, 8.41% higher than S_5 model, 6.31% higher than S_6 model & 1.2% higher than S_8 model.

Earlier research of Ghaderi et al. (2020) [76] shows that a free jump dissipates more energy as compared to the submerged hydraulic jump over macroroughness enhances more energy loss as compared to smooth bed. Findings of the presents study are in well agreement of findings of Ghaderi et al. (2020) [76] & Ghaderi et al. (2021) [18].

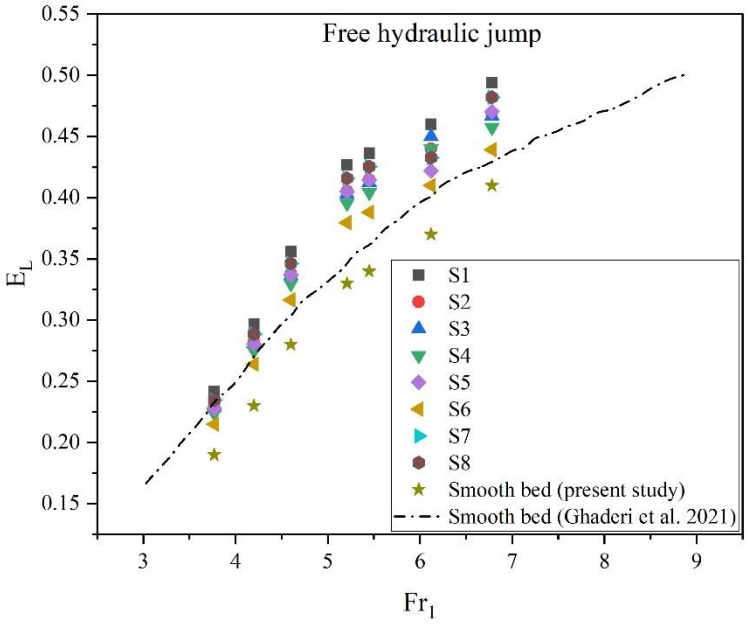

Figure 4.18 Relative energy loss versus initial Froude number in case of free hydraulic jump

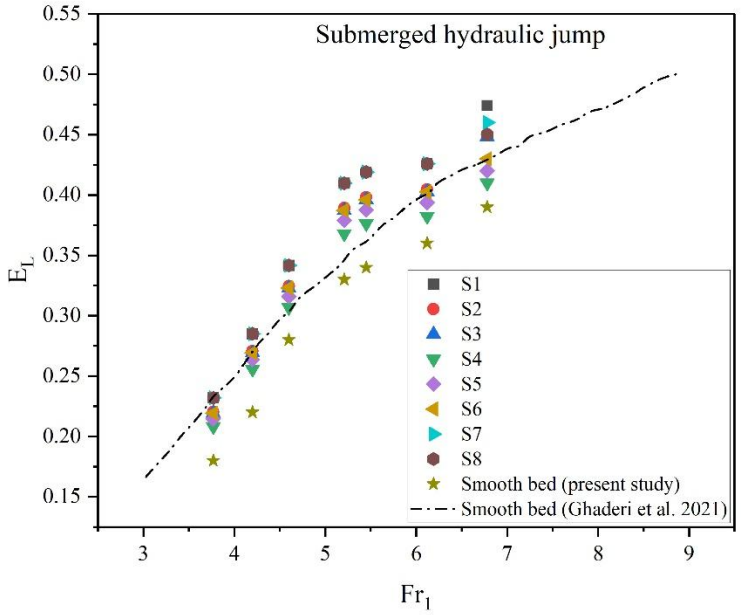

95

Figure 4.19 Relative energy loss in case of submerged hydraulic jump versus initial Froude number

4.3.5 H/B i.e., height to base width ratio of macroroughness

This section deals the effect of H/B *i.e* height to base ratio of macroroughness on free and submerged hydraulic jump. The possible arrangements are also investigated and graphically presented in below sections.

4.3.5.1 Flow profiles and velocity variation in case of free hydraulic jump

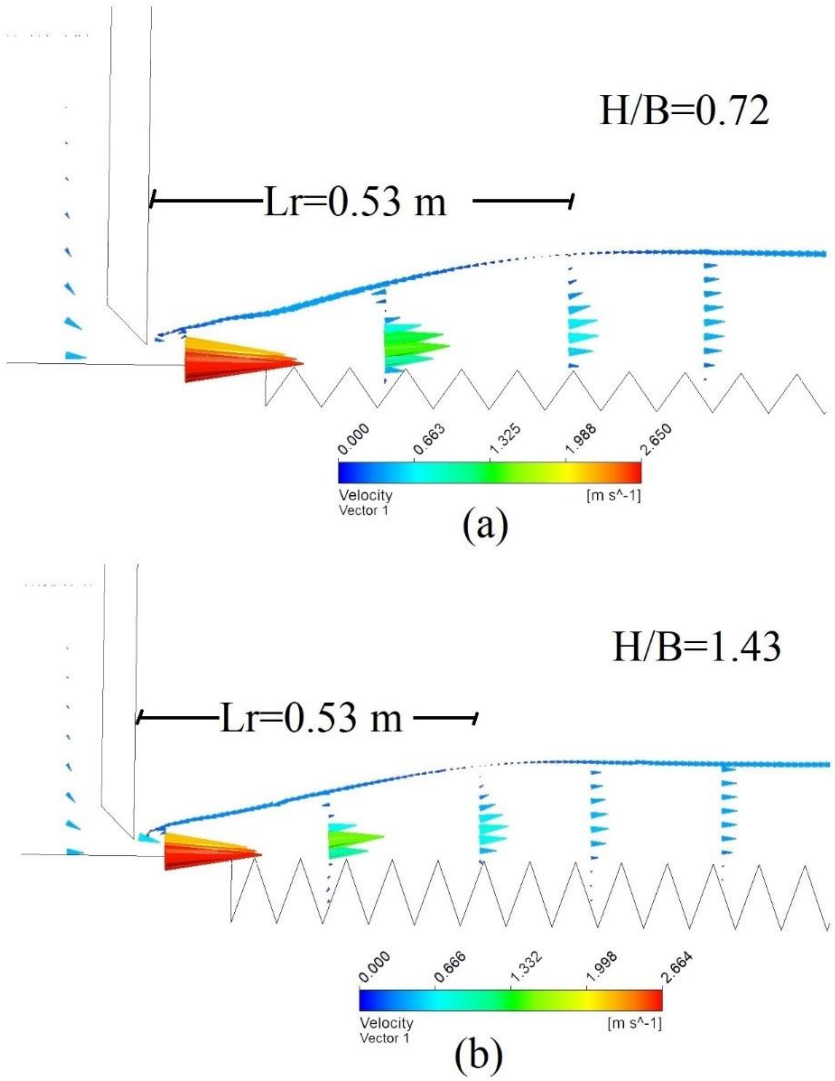

Figure 4.20 (a-b) Numerically generated flow profile of free hydraulic jump for H/B i.e., height to base width ratio of macroroughness

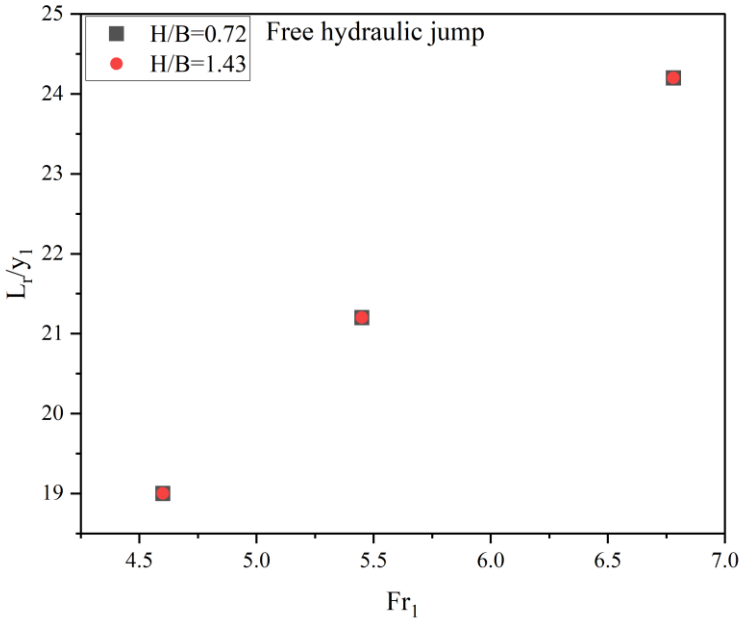

Figure 4.21 Graphical representation of length of jump ratio versus initial Froude number of free hydraulic jump for H/B i.e., height to base width ratio of macroroughness

4.3.5.2 Flow profiles and velocity variation in case of submerged hydraulic jump

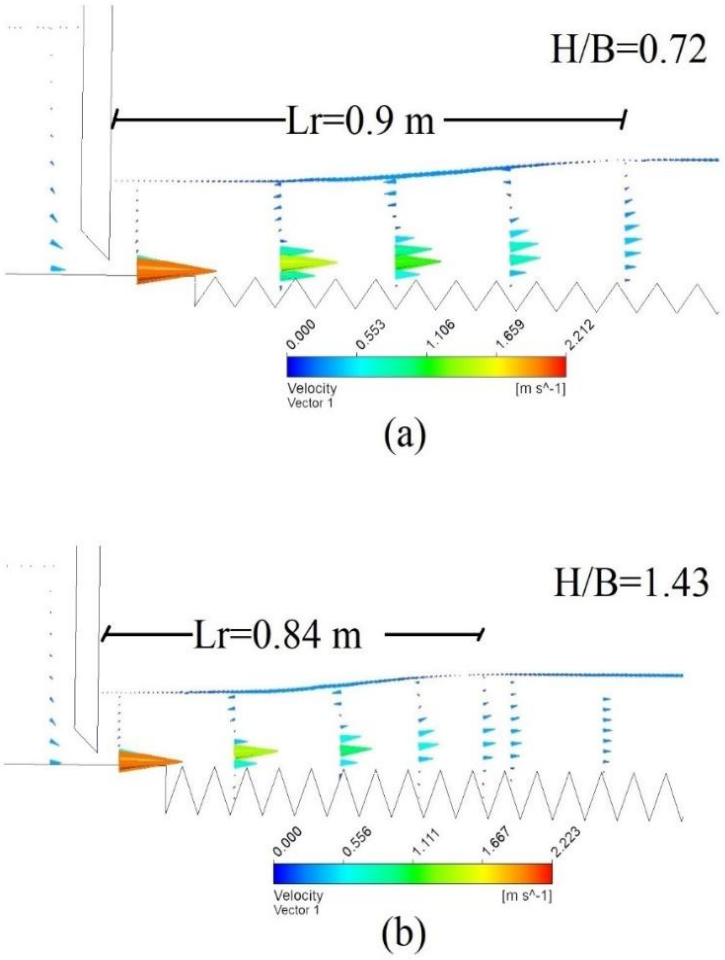

Figure 4.22 (a-b) Numerically generated flow profile with longitudinal velocity variation of submerged hydraulic jump for H/B i.e., height to base width ratio of macroroughness

Figure 4.20 & Figure 4.22 illustrate the pictorial representation of flow profile with longitudinal velocity profiles at different sections of the flume over various H/B ratio of macroroughness's for free and submerged hydraulic jump respectively. Figure 4.20 (a) & Figure 4.22 (a) shows the results of H/B ratio for 0.72 whereas Figure 4.20 (b) & Figure 4.22 (b) shows the result of H/B ratio for 1.43.

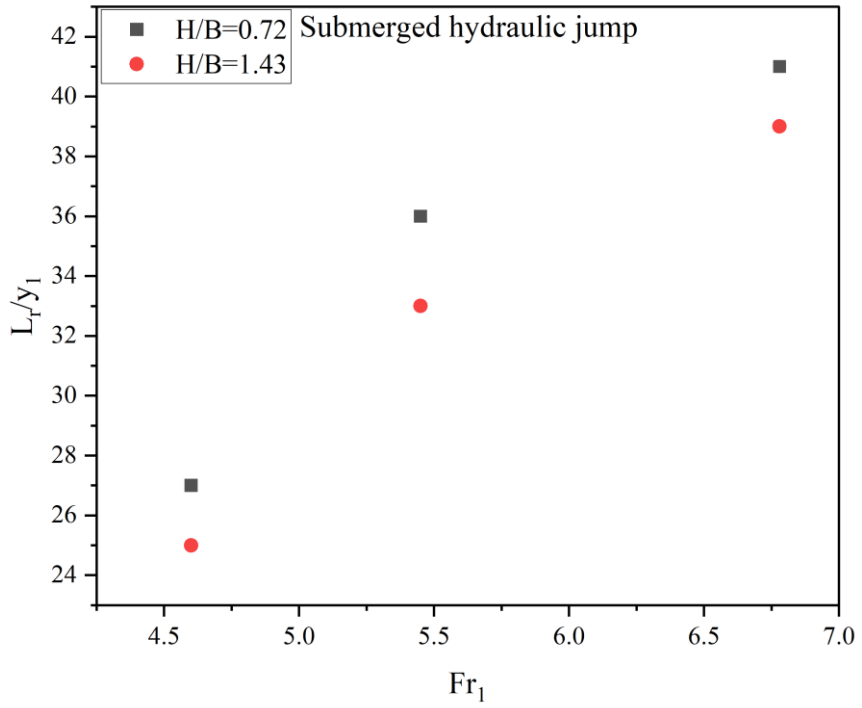

Figure 4.23 Graphical representation of length of jump ratio versus initial Froude number of submerged hydraulic jump for different possible arrangements of H/B i.e., height to base width ratio of macroroughness

To investigate the effect of height to base width ratio on jump characteristics two variations as discussed earlier are considered and the outcomes in the form of roller length of jump ratio is plotted against initial Froude number in Figure 4.21. From Figure 4.21 it can be inferred that on varying the H/B ratio the outcomes are almost same and no significant changes are reported in case of free hydraulic jump. However, from Figure 4.23 the roller length of jump ratio decreases with varying the H/B ratio in case of submerged hydraulic jump. This statement is valid for wide range of Froude numbers. Quantitatively, the roller length of jump for H/B =1.43 is reported 6.5% shorter than H/B=0.72.

4.3.6 Possible arrangements with H/B ratio

This section explain the effects of various macroroughness on jump characteristics.

4.3.6.1 Flow profiles and velocity variation in case of free hydraulic jump

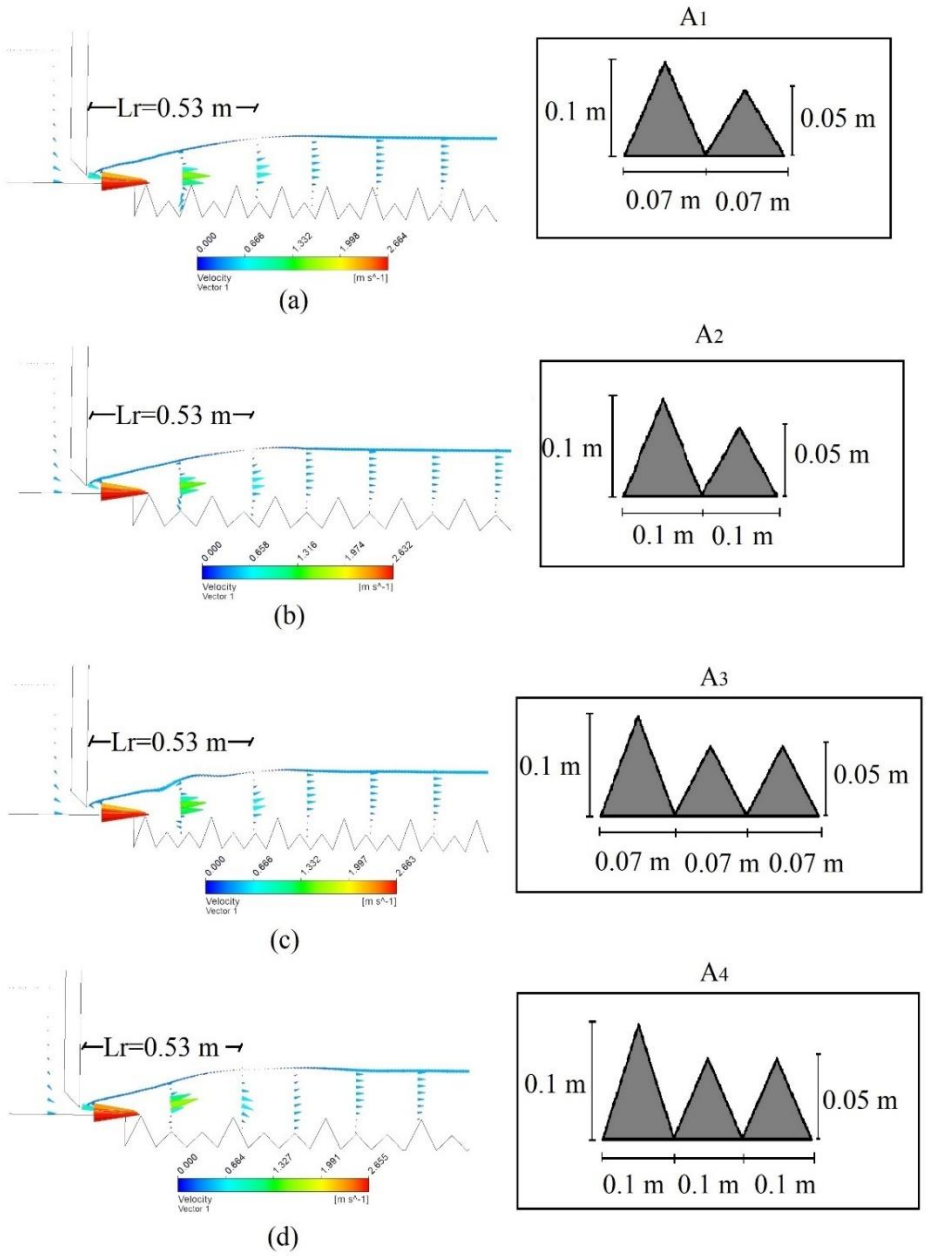

Figure 4.24 (a-d) Numerically generated flow profile with longitudinal velocity variation of free hydraulic jump for different possible arrangements of H/B i.e., height to base width ratio of macroroughness

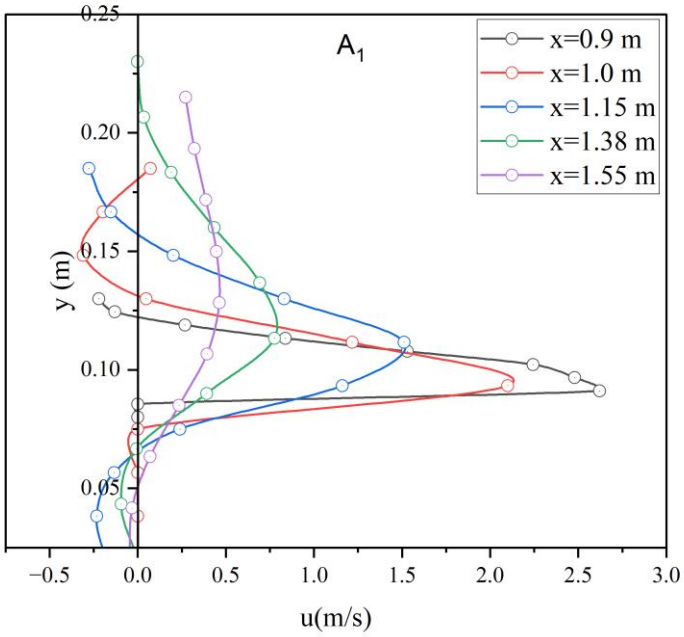
A1
x=0.9 m
x=1.0 m
x=1.15 m
x=1.38 m
x=1.55 m
y (m)
u(m/s)
0.25
0.20
0.15
0.10
0.05
−0.5
0.0
0.5
1.0
1.5
2.0
2.5
3.0

(a)

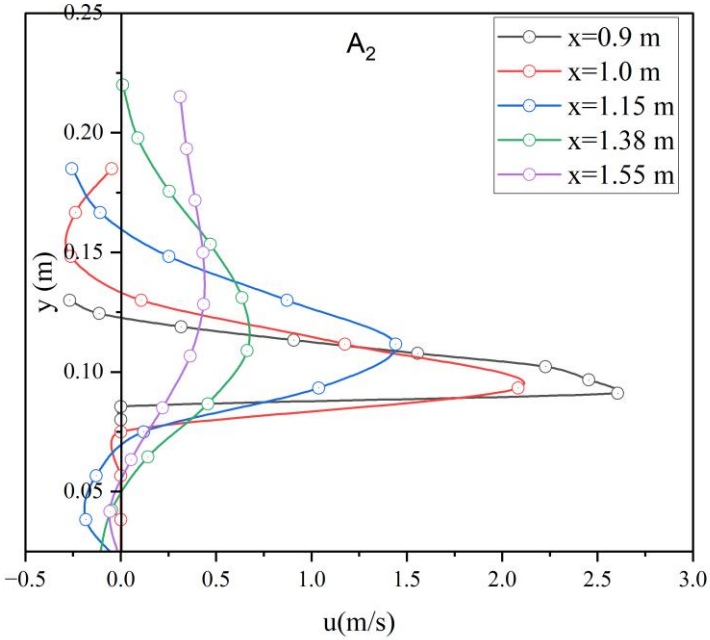
A2
x=0.9 m
x=1.0 m
x=1.15 m
x=1.38 m
x=1.55 m
y (m)
u(m/s)
0.25
0.20
0.15
0.10
0.05
−0.5
0.0
0.5
1.0
1.5
2.0
2.5
3.0

(b)

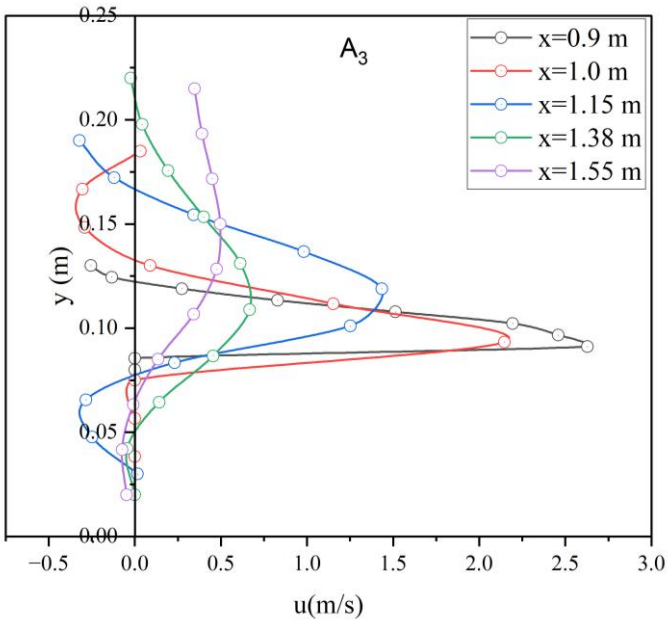

(c)

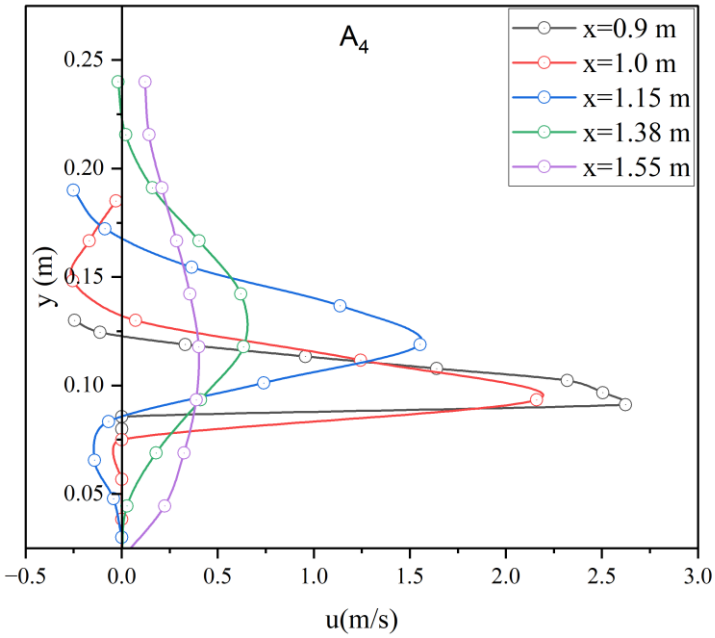

(d)

Figure 4.25 (a-d) Graphical representation of longitudinal velocity variation of free hydraulic jump for different possible arrangements of H/B i.e., height to base width ratio of macroroughness

4.3.6.2 Flow profiles and velocity variation in case of submerged hydraulic jump

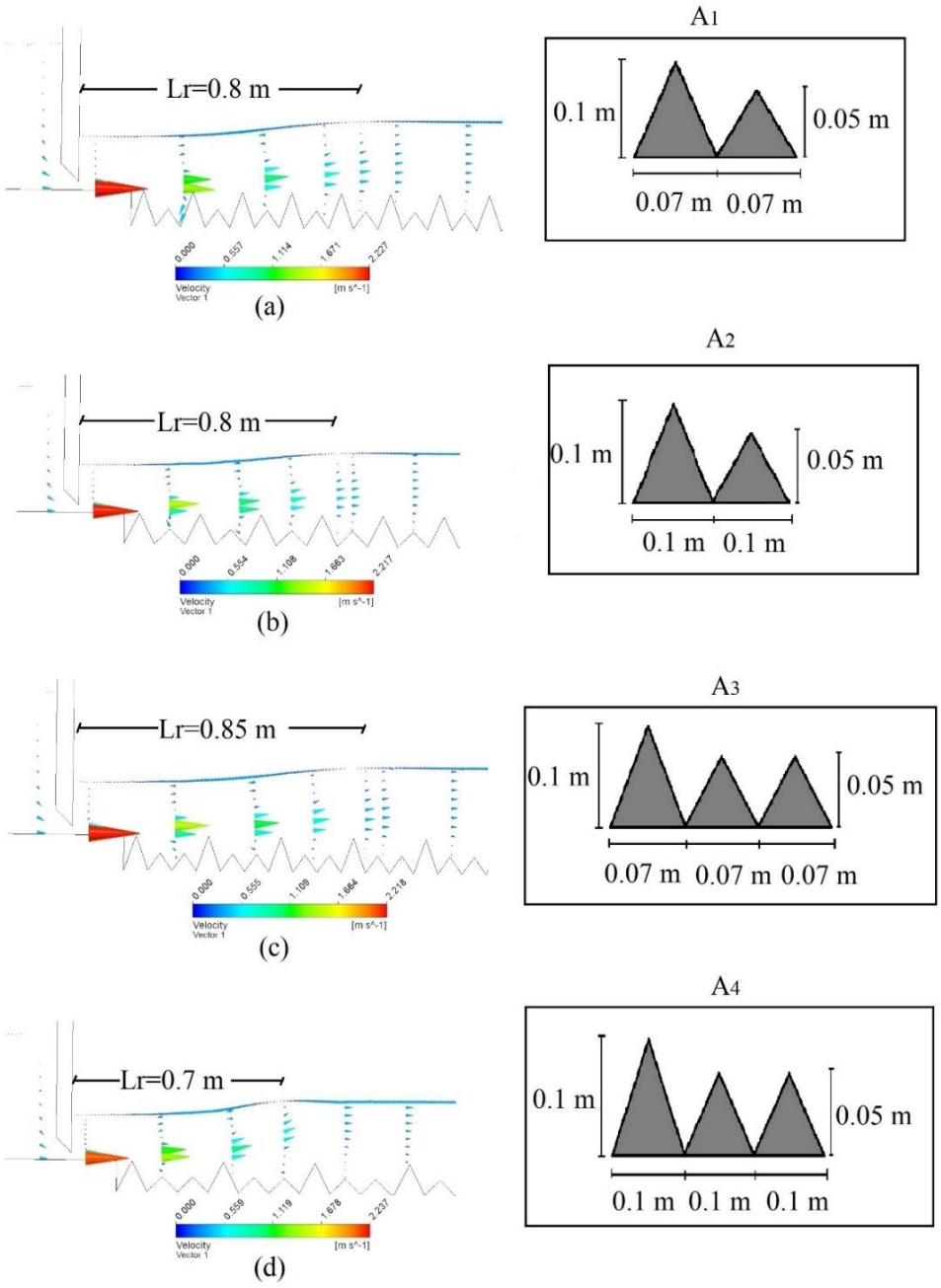

Figure 4.26 (a-d) Numerically generated flow profile with longitudinal velocity variation of submerged hydraulic jump for different possible arrangements of H/B i.e., height to base width ratio of macroroughness

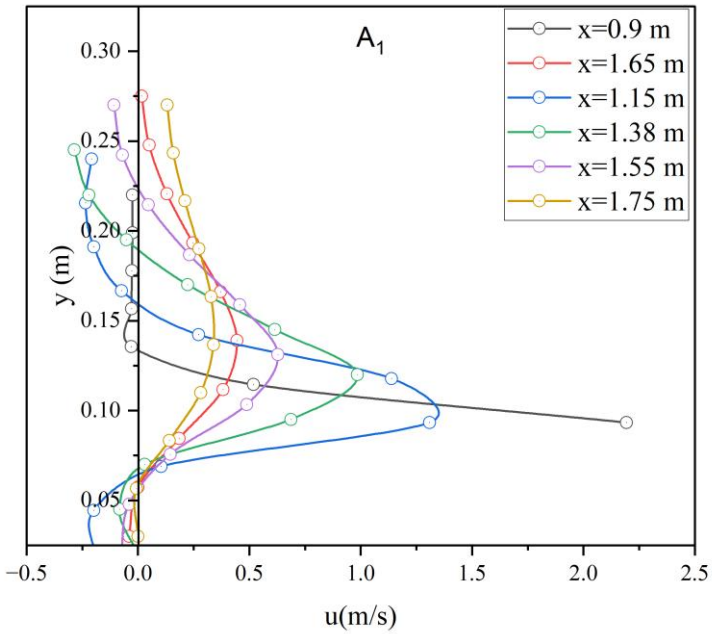
A1
x=0.9 m
x=1.65 m
x=1.15 m
x=1.38 m
x=1.55 m
x=1.75 m
y (m)
0.30
0.25
0.20
0.15
0.10
0.05
−0.5
0.0
0.5
1.0
1.5
2.0
2.5
u(m/s)

(a)

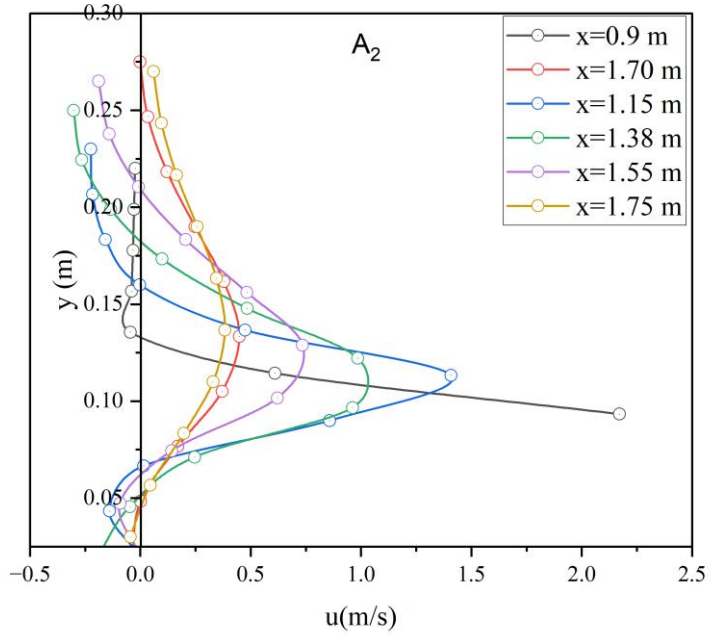
A2
x=0.9 m
x=1.70 m
x=1.15 m
x=1.38 m
x=1.55 m
x=1.75 m
y (m)
0.30
0.25
0.20
0.15
0.10
0.05
−0.5
0.0
0.5
1.0
1.5
2.0
2.5
u(m/s)

(b)

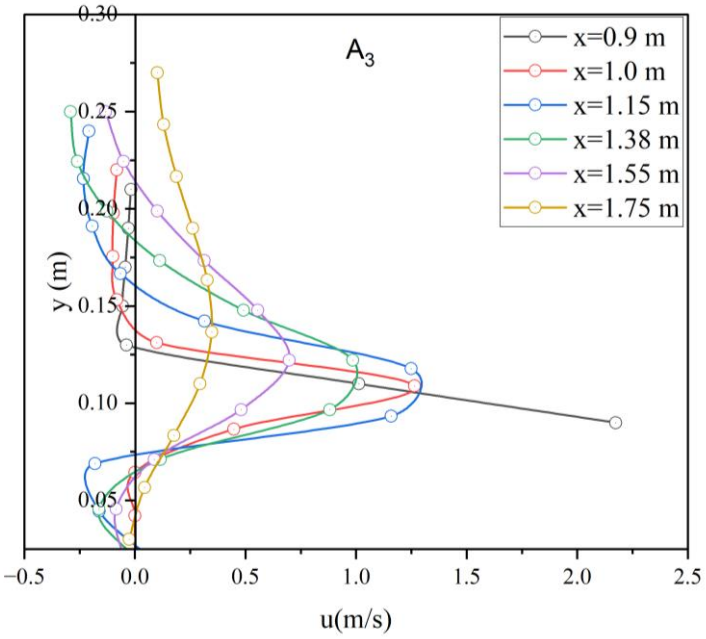

(c)

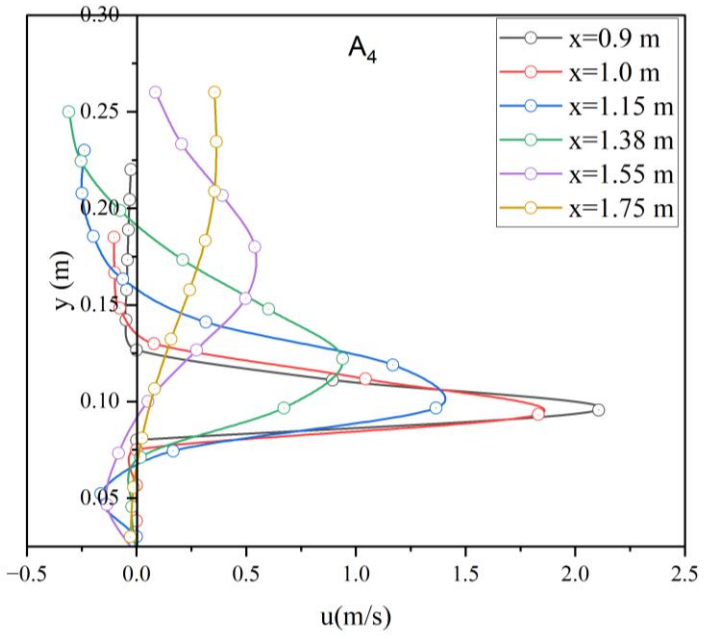

(d)

Figure 4.27 (a-d) Graphical representation of longitudinal velocity variation of submerged hydraulic jump for different possible arrangements of H/B i.e., height to base width ratio of macroroughness

Figure 4.24 & Figure 4.26 illustrate the flow profiles with longitudinal velocities at various sections of the flume including roller length of jump for various arrangement made with the combination of H/B ratio. Here, four combinations *i.e.,* A_1, A_2, A_3, A_4 are prepared using two values of H/B ratio as discussed in earlier sections for free and submerged hydraulic jumps. From Figure 4.25 it is clear that by considering different arrangements the roller length of jump does not change and the flow profile including longitudinal velocities are almost same for all models in case of free hydraulic jump. However, from Figure 4.27 it is clear that on considering different arrangements the roller length of jump changes to some extent in case of submerged hydraulic jump.

4.3.7 H/I i.e., height to wavelength ratio of macroroughness

Height to wavelength ratio is a critical parameter that influences flow turbulence, energy dissipation in open channel flows.

4.3.7.1 Flow profiles and velocity variation in case of free hydraulic jump

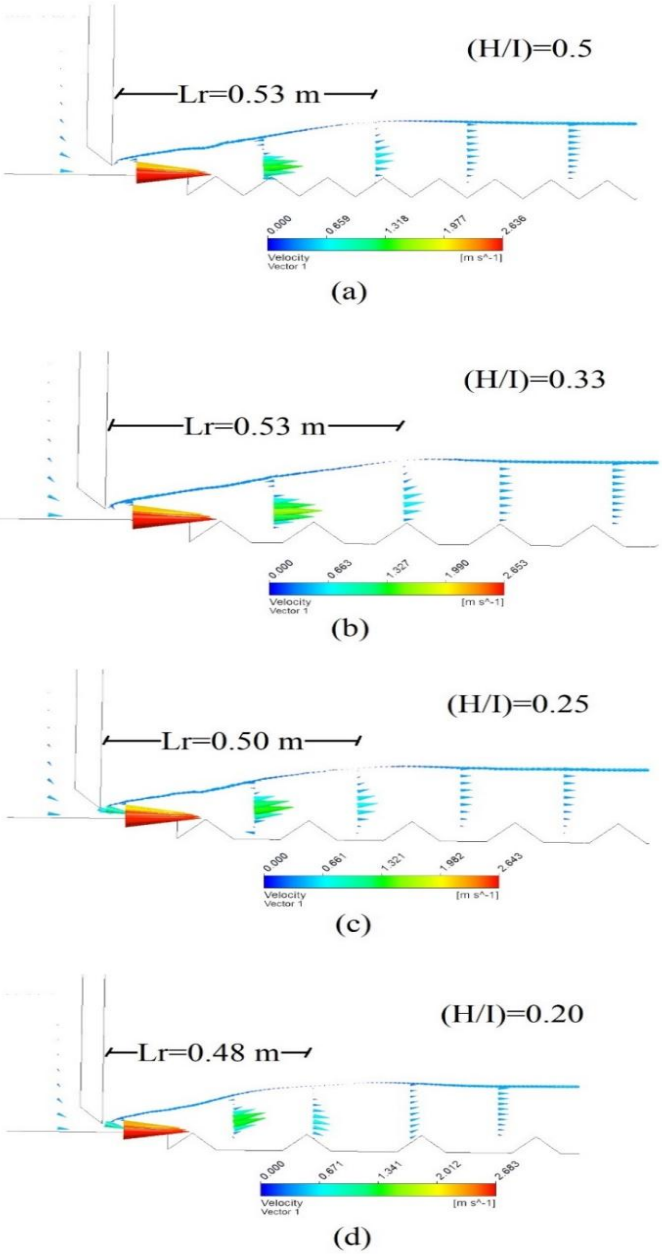

Figure 4.28 (a-d) Numerically generated flow profile with longitudinal velocity variation of free hydraulic jump for H/I i.e., height to wavelength ratio of macroroughness

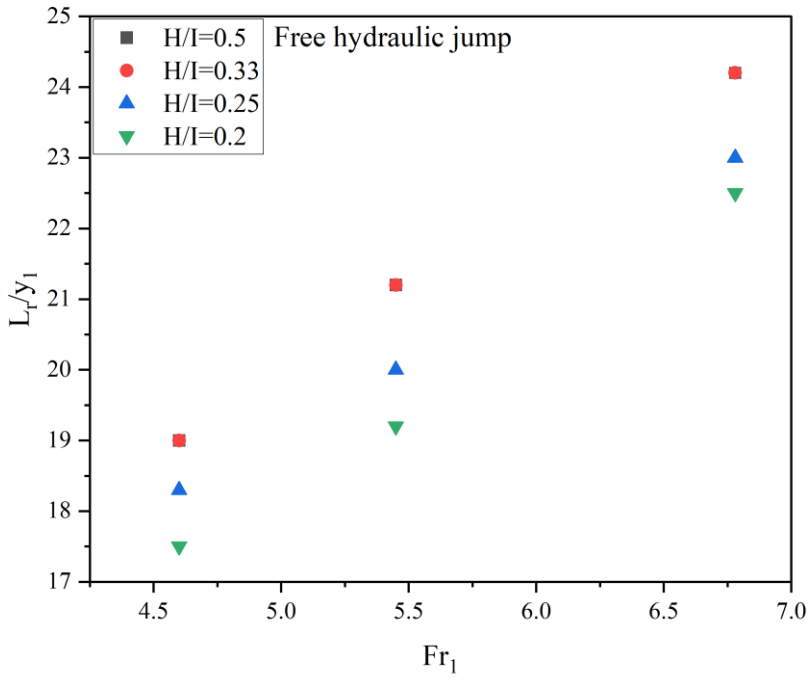

Figure 4.29 Graphical representation of length of jump ratio versus initial Froude number of free hydraulic jump for H/I i.e., height to wavelength ratio of macroroughness

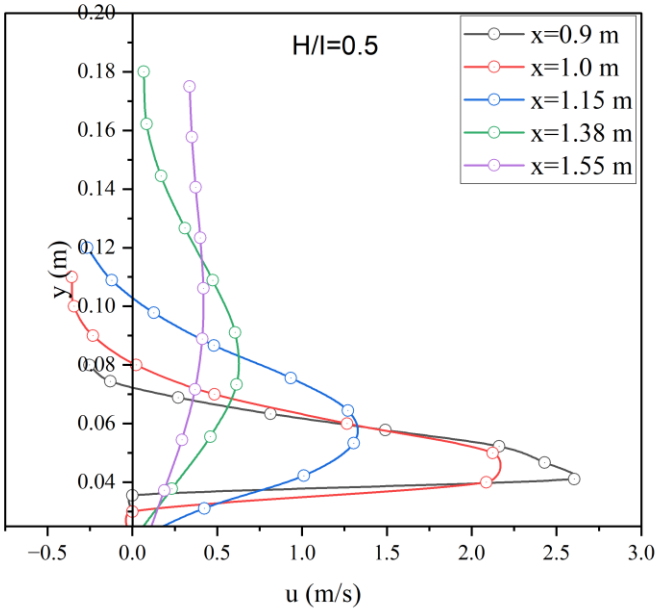
H/l=0.5
x=0.9 m
x=1.0 m
x=1.15 m
x=1.38 m
x=1.55 m
y (m)
u (m/s)
0.20
0.18
0.16
0.14
0.12
0.10
0.08
0.06
0.04
−0.5
0.0
0.5
1.0
1.5
2.0
2.5
3.0

(a)

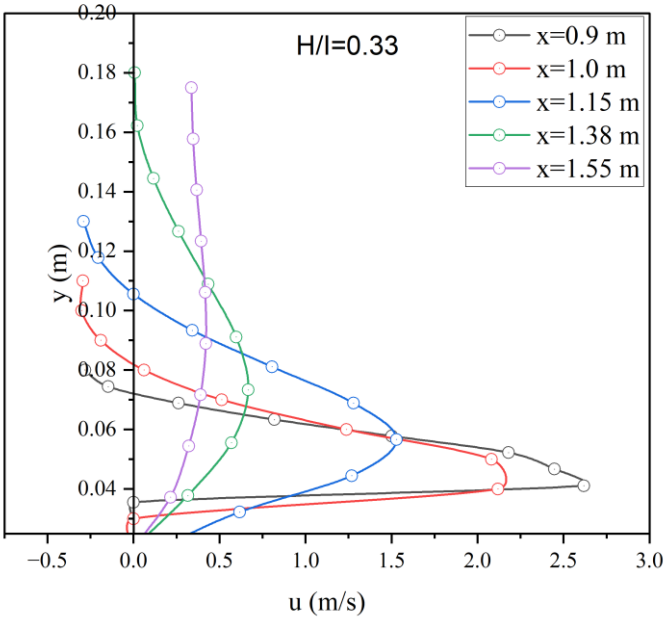
H/l=0.33
x=0.9 m
x=1.0 m
x=1.15 m
x=1.38 m
x=1.55 m
y (m)
u (m/s)
0.20
0.18
0.16
0.14
0.12
0.10
0.08
0.06
0.04
−0.5
0.0
0.5
1.0
1.5
2.0
2.5
3.0

(b)

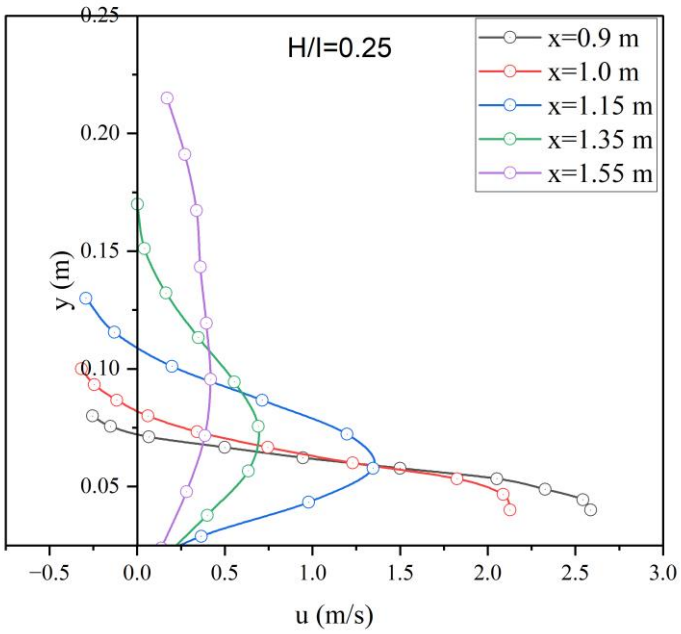

(c)

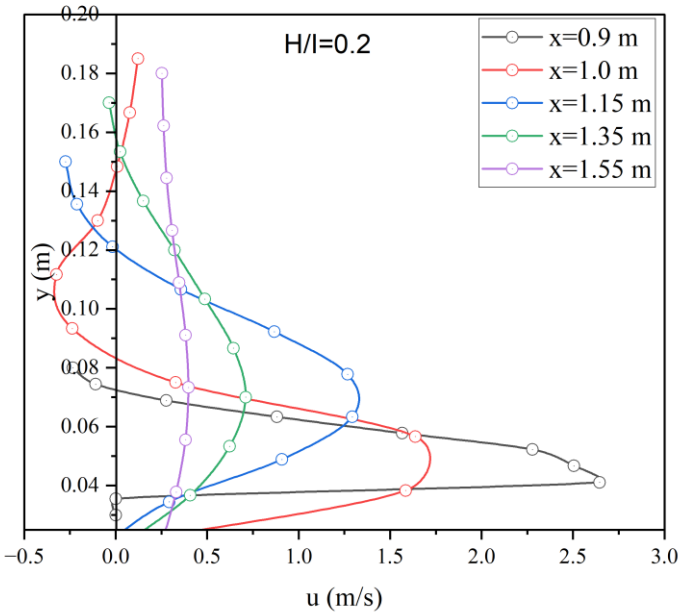

(d)

Figure 4.30 (a-d) Graphical representation of longitudinal velocity variation of free hydraulic jump for H/I i.e., height to wavelength ratio of macroroughness

4.3.7.2 Flow profiles and velocity variation in case of submerged hydraulic jump

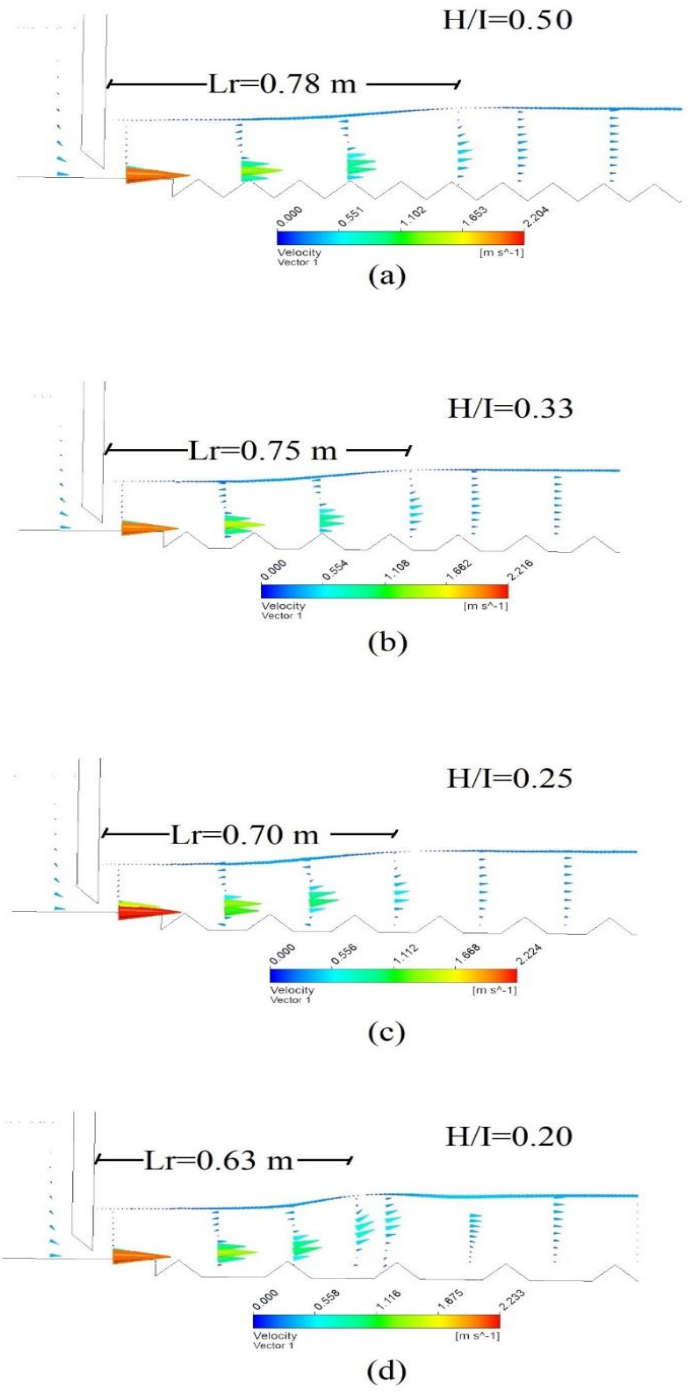

Figure 4.31 (a-d) Numerically generated flow profile with longitudinal velocity variation of submerged hydraulic jump for H/I i.e., height to wavelength ratio of macroroughness

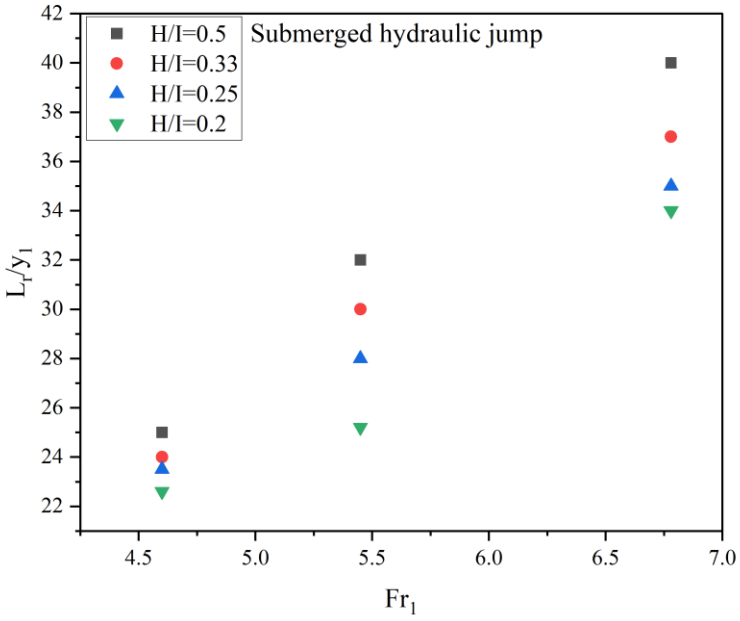

Figure 4.32 Graphical representation of length of jump ratio versus initial Froude number of submerged hydraulic jump for H/I i.e., height to wavelength ratio of macroroughness

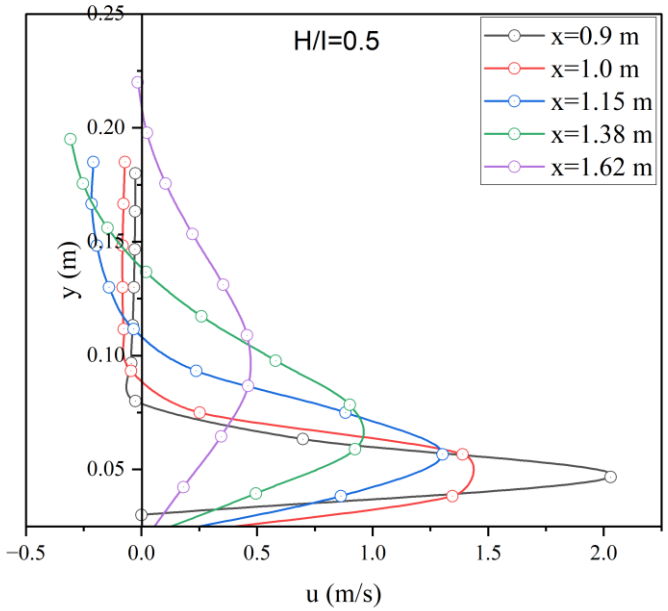

(a)

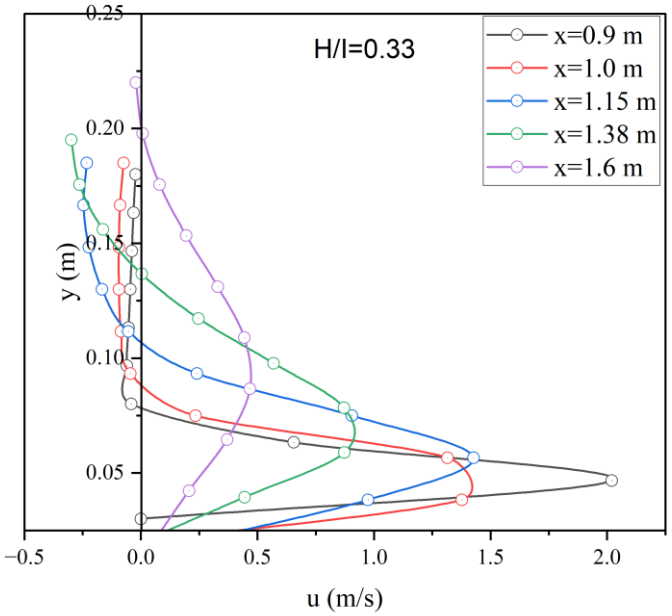
H/l=0.33
x=0.9 m
x=1.0 m
x=1.15 m
x=1.38 m
x=1.6 m
y (m)
u (m/s)
0.25
0.20
0.15
0.10
0.05
−0.5
0.0
0.5
1.0
1.5
2.0

(b)

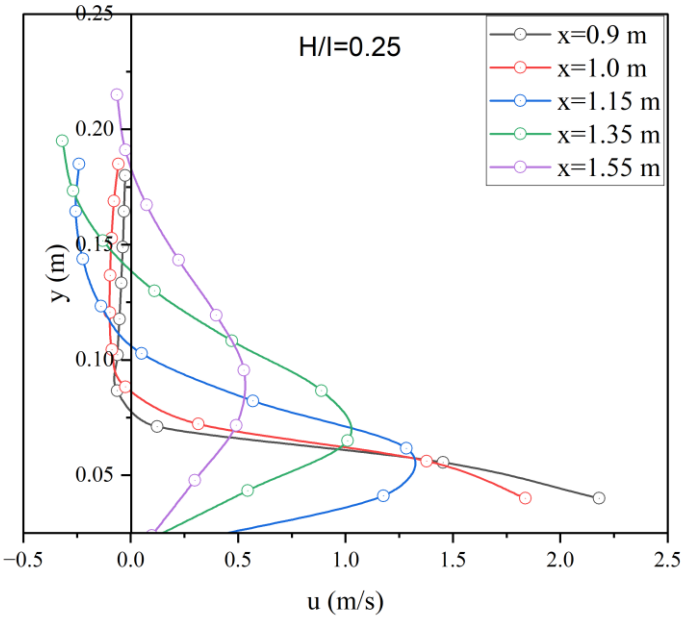
H/l=0.25
x=0.9 m
x=1.0 m
x=1.15 m
x=1.35 m
x=1.55 m
y (m)
u (m/s)
0.25
0.20
0.15
0.10
0.05
−0.5
0.0
0.5
1.0
1.5
2.0
2.5

(c)

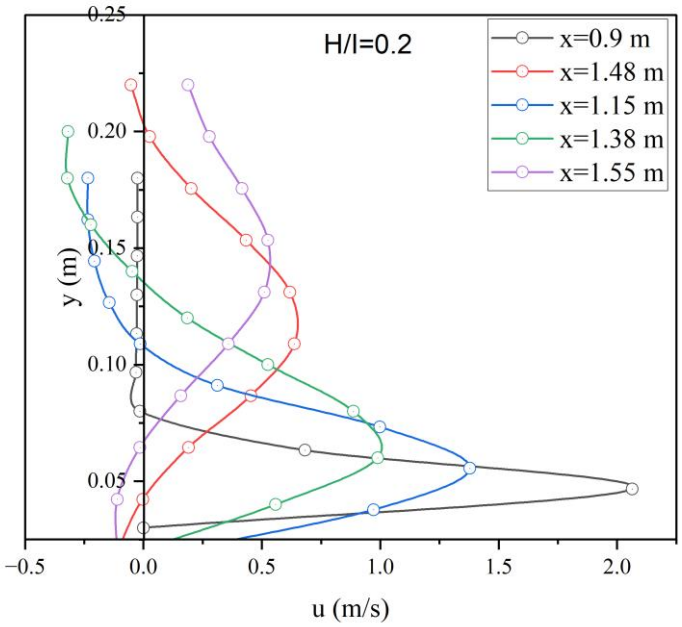

(d)

Figure 4.33 (a-d) Graphical representation of longitudinal velocity profile of submerged hydraulic jump for H/I i.e., height to wavelength ratio of macroroughness

On varying the H/I ratio the spacing between two consecutive strip macroroughness increases and the effect of these are indirectly related to the characteristics of hydraulic jump such as roller length of jump. Figure 4.28 & Figure 4.31 illustrate the pictorial representation of free and submerged hydraulic jump respectively for differen H/I ratio i.e., height to wavelength ratio. In Figure 4.28 & Figure 4.31 four values of H/I ratio *i.e.,* 0.5 , 0.33, 0.25, 0.2 are considered to investigate the hydraulic jump characteristics.

From the pictorial presentation, it is clear that when the length of the strip macroroughness is more, the velocity distribution function has regained an equilibrium state by the time the flow gets to the subsequent roughness. However for short distance, flow reaches the next macroroughness without sufficient recovery of velocity distribution.

Figure 4.29 & Figure 4.32 represents the dimensionless parameter roller length of jump ratio for free hydraulic jump and for submerged hydraulic jump, respectively. From Figure 4.29, it can be reported that the H/I=0.5 & H/I=0.33 has similar results. Whereas, H/I=0.20 is capable in reducing roller length of jump than other combination. Quantitatively, roller length of jump ratio for H/I=0.20 is 3.38% shorter than H/I=0.25, 8.6% shorter than H/I=0.33 or H/I=0.5.

From Figure 4.32 it can be reported that the H/I=0.20 is capable in reducing roller length of jump than other combinations. Quantitatively, roller length of jump ratio for H/I=0.20 is 5.56% shorter than H/I=0.25, 11.28% shorter than H/I=0.33 and 18.8% shorter than H/I=0.5.

4.3.8 Practical challenges in implementing engineered bed features for hydraulic jump control in real-world systems

The present study underscores the effectiveness of strip-type macrorough beds in enhancing hydraulic jump characteristics, notably in improving energy dissipation, reducing jump length, and increasing turbulence for better aeration and mixing. However, practical implementation in real-world river engineering and hydropower systems poses several challenges. Structural integrity and durability are major concerns, as constructing precise geometries like triangular or trapezoidal strips is technically demanding and susceptible to long-term wear from sediment transport, cavitation, and high-velocity flows necessitating the use of high-strength or abrasion-resistant materials. Additionally, closely spaced roughness elements can trap sediment and debris, alter flow behaviour and reduce efficiency, which in turn increases maintenance requirements. Compatibility with existing hydraulic structures may also be limited, particularly in aging infrastructures where retrofitting is constrained by geometry or structural stability.

Moreover, the performance validated under controlled laboratory conditions may vary under real-world flow regimes, including flood events and seasonal discharge changes, thus requiring site-specific customization. Finally, a thorough cost-benefit analysis is crucial to determine the viability of these complex macroroughness shapes compared to traditional energy dissipators like baffle blocks or end sills. Despite these limitations, the study offers valuable design guidance, suggesting that with proper material selection and robust structural design strip-type macrorough elements, especially triangular forms, hold promise for applications in controlled environments such as hydropower tailraces, irrigation outlets, and urban stormwater channels. Further pilot-scale field studies are essential to validate their long-term performance under variable hydraulic and environmental conditions.

4.3.9 Engineering strategies for bed roughness design in energy dissipating structures

The design of the channel bed in hydraulic jump type stilling basins plays a crucial role in controlling flow behaviour and enhancing energy dissipation through turbulence generation. This study highlights several key engineering considerations for optimal design. Macroroughness elements, especially strip-type protrusions, effectively modify the post-jump flow field, with triangular strip macroroughness demonstrating superior performance in promoting energy dissipation, roller formation, and turbulence development, particularly under submerged jump conditions. While the height-to-base width ratio (H/B) has minimal impact on jump characteristics, a lower height-to-wavelength ratio (H/I) enhances energy dissipation by increasing flow resistance and interaction zones. The spacing and arrangement of macrorough

elements significantly influence flow structure, with varied configurations inducing asymmetric turbulence beneficial for submerged jumps.

Elements oriented perpendicular to the flow generate maximum resistance, strong wake zones, and facilitate flow deceleration and reattachment, making this orientation preferable in standard rectangular channels. For numerical simulations, the RNG k-ε turbulence model provides the most reliable predictions of turbulence intensity, energy loss, and jump length over rough beds. Additionally, omitting the upstream reservoir in simulations can halve computational effort without affecting jump formation when the focus is on post-jump behaviour. In summary, careful consideration of macroroughness geometry, spacing, orientation, arrangement patterns, and appropriate turbulence modelling ensures efficient stilling basin design, reduces erosion risk, and improves hydraulic jump stability across various flow regimes.

CHAPTER 5

CONCLUSION, FUTURE SCOPE AND SOCIAL IMPACT

Overall, this research aimed to enhance the understanding of free and submerged hydraulic jumps by exploring various flow characteristics such as sequent depth ratio, tailwater depth ratio, roller length of jump ratio, relative energy loss including longitudinal velocity profile, and flow pattern in the cavity region over different shapes of macroroughness. Based on the numerical investigation, the key findings of the present study are summarised below:

To predict the sequent depth ratio of a hydraulic jump using Computational Fluid Dynamics (CFD), four different turbulence models such as standard k- ε, realizable k- ε, RNG k- ε, and SST k-ω were compared for coarse to fine mesh element sizes i.e., 50 mm, 30 mm, 20 mm, 10 mm, 9 mm, and 7 mm t. It is noted that relative error in predicting the sequent depth ratio reduces with reduced mesh element size. Further, the sequent depth ratio was predicted with an accuracy of more than 98% using RNG k- ε model followed by realizable k- ε, SST k-ω and standard k- ε model for 9 mm mesh element size. Therefore, it can be stated that the complex fluid flow phenomenon such as hydraulic jump can be well investigated by CFD using RNG k- ε turbulence model at finer mesh.

Four flow domains with two different approaches for the analysis of classical hydraulic jump were studied and found that the jump characteristics such as flow profile, and longitudinal velocity profiles do not change by applying different approaches on different flow domains as discussed in the present study. However, the computational time can be saved up to 50 % by reducing the flow domain.

Eight geometrically different strip macroroughness namely triangular, rectangular, trapezoidal, semicircular, and four irregular shapes were used to investigate the effect of shape on the characteristics of hydraulic jump such as sequent depth ratio, tailwater depth ratio, roller length of jump ratio, and relative energy loss, longitudinal velocity profile. The result showed that the average value of the length of the roller for trapezoidal and triangular macroroughness is found to be 23 % and 46.06 % shorter than the smooth bed in the case of a free hydraulic jump. However, these values reduce to 17.85 % and 36.33 % in the case of submerged hydraulic jumps. It is also reported that the triangular model is more capable of reducing the sequent depth ratio up to 7.25%, tailwater depth ratio up to 18.61 %, and increasing the relative energy loss up to 11.04 % as compared to smooth bed. This implies that the macroroughness is effective in enhancing the jump characteristics downstream of the hydraulic structure.

Velocity vector variations are plotted for all eight different macroroughness in which clockwise circulation was noticed in the cavity regions. The magnitude and direction of circulation of fluid mainly depend on the shape of macroroughness. The reduction in the roller length of the jump may be due to

clockwise circulation. Thus, a properly designed macroroughness can improve the jump characteristics and maximize the relative energy loss.

Two values of the height-to-base width ratio *i.e.,*0.72 and 1.43 were considered to determine its effect on the roller length of jump ratio. Negligible variation in roller length of jump ratio was reported in the case of free hydraulic jump whereas roller length of jump ratio reduced up to 7 % on increasing the height to base width ratio in the case of submerged hydraulic jump. This signifies that on varying the height to base width ratio the roller length of jump ratio reduces for submerged hydraulic jump.

Four different models having values of the height-to-wavelength ratio *i.e.,* 0.2, 0.25, 0.33, and 0.5 were considered to study its effect on the roller length of the jump. Results showed that the model having a ratio equal to 0.20 was capable of reducing the roller length of jump ratio up to 8.6 % in the case of free jump and 18.8 % in the case of submerged jump when compared with other models. This signifies that on increasing the spacing between two consecutive macroroughness the roller length of the jump reduces.

In the future, macrorough beds may be used to reduce sediment transport and prevent scouring downstream of hydraulic structures. The study and application of hydraulic jumps on macrorough beds using CFD have significant implications for water management and hydraulic engineering. Ongoing research and interdisciplinary collaboration will be critical in realizing these benefits and overcoming the challenges associated with their implementation. Computational Fluid Dynamics (CFD) has a wide range of social impacts in a variety of industries, including environmental sustainability, public safety, and healthcare. CFD eliminates the need for physical prototypes and extensive trial and error testing, saving time and money in product development across a variety of industries.